


Summer 7-22-2019

# SYSTEM INTEGRATION OF C-ARM ROBOTIC PROTOTYPE USING MOTION CAPTURE GUIDANCE FOR ACCURATE REPOSITIONING

Alireza Yazdanshenas  
*University of Texas at Tyler*

Follow this and additional works at: [https://scholarworks.uttyler.edu/me\\_grad](https://scholarworks.uttyler.edu/me_grad)

 Part of the [Acoustics, Dynamics, and Controls Commons](#), [Biomechanical Engineering Commons](#), [Computer-Aided Engineering and Design Commons](#), [Electro-Mechanical Systems Commons](#), [Manufacturing Commons](#), [Other Mechanical Engineering Commons](#), [Surgical Procedures, Operative Commons](#), and the [Systems and Integrative Engineering Commons](#)

---

## Recommended Citation

Yazdanshenas, Alireza, "SYSTEM INTEGRATION OF C-ARM ROBOTIC PROTOTYPE USING MOTION CAPTURE GUIDANCE FOR ACCURATE REPOSITIONING" (2019). *Mechanical Engineering Theses*. Paper 6.  
<http://hdl.handle.net/10950/1569>

This Thesis is brought to you for free and open access by the Mechanical Engineering at Scholar Works at UT Tyler. It has been accepted for inclusion in Mechanical Engineering Theses by an authorized administrator of Scholar Works at UT Tyler. For more information, please contact [tbianchi@uttyler.edu](mailto:tbianchi@uttyler.edu).

SYSTEM INTEGRATION OF C-ARM ROBOTIC PROTOTYPE USING MOTION  
CAPTURE GUIDANCE FOR ACCURATE REPOSITIONING

by

ALIREZA YAZDANSHENAS

A thesis submitted in partial fulfillment of  
the requirements of the degree of  
Master of Science in Mechanical Engineering  
Department of Mechanical Engineering

Chung Hyun Goh, Ph.D., Committee Chair

College of Engineering

The University of Texas at Tyler  
June 2019

The University of Texas at Tyler  
Tyler, Texas


This is to certify that the Master's Thesis of

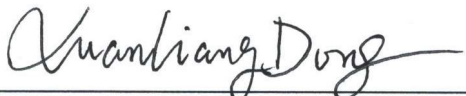
ALIREZA YAZDANSHENAS

has been approved for the thesis requirement on  
May 4<sup>th</sup>  
for the Master of Mechanical Engineering degree

Approvals:

  
Thesis Chair: Chung Hyun Goh, Ph.D.

  
Member: Fredericka Brown, Ph.D.

  
Member: X. Neil. Dong, Ph.D.

  
Chair, Department of Mechanical Engineering

  
Dean, College of Engineering

© Copyright by ALIREZA YAZDANSHENAS 2019  
All rights reserved

## **Acknowledgments**

First, I must thank my parents for supporting me through my college career. I hope that one day I can pay them back for all their hard work and sacrifice. Next, I want to thank my fiancé Stephanie Tutt for always being patient with me while I spent many hours apart working on my academic goals. Now it is time that I put us first. I would also like to express my special thanks and gratitude to my thesis advisor Dr. Chung Hyun Goh for helping and guiding me through my college career. Dr. Goh has always been there for us, through sickness and health, no matter what. His work ethic and dedication are unmatched. Thank you. In addition, I want to thank my brother Armin Yazdanshenas for being a good research partner, teammate and roommate. I also want to express my explicit gratitude to my thesis committee members Dr. X. Neil Dong and Fredericka Brown. Without their help and without the skills they have taught me, my research would have been impossible. My deepest appreciation also goes to Dr. Nael Barakat he has done a lot for my brother and me. We will never forget that. Without hesitation, I thank Dr. Michael McGinnis for always guiding the students into the right direction and for being a great mentor to us all. My respect and appreciation also go to Dr. Javier Kypuros for always trussing in me and helping us all move in the right directions. Finally, I want to thank Kirill Safrin, Joseph Oyedele, Emilli Morrison, Steven Auzenne, and Andrew Hernandez for being good friends and for helping me achieve this goal.

## Table of Content

List of Tables .....	v
List of Equations .....	vi
List of Figures .....	vii
Abbreviations & Nomenclature .....	x
Abbreviations .....	x
Nomenclature .....	xi
Abstract .....	xii
Chapter 1: Frame of Reference .....	1
1.1 Background and Motivation .....	1
1.2 Limitation Factors .....	5
1.3 Innovative Approach .....	6
1.3.1 Motion Capture Integration .....	6
1.3.2 Motion Capture Integration Key Advantages .....	6
1.3.3 C-Arm Kinematics, Programing, and GUI .....	7
1.3.4 Robot Prototype Development .....	8
1.4 Overview / Scope .....	8
1.4.1 Objective .....	8
1.4.2 Research Questions .....	8
1.4.3 Hypothesis .....	9
1.4.4 List of Tasks .....	9
1.4.5 Thesis Outline Description .....	10
Chapter 2: Literature Review .....	11
2.1 Literature Introduction .....	11
2.2 C-Arm Virtual Reality Repositioning .....	11
2.2.1 The C-Arm .....	11
2.2.2 C-Arm Local Vision Dependent Repositioning .....	13

2.2.3 C-Arm Global Vision Dependent Repositioning .....	16
2.2.4 C-Arm Training for Surgical Personnel .....	23
2.3 Kinematics and Robotics .....	24
Chapter 3: Methodology .....	28
3.1 Objective Overview .....	28
3.2 Virtual Prototype and Virtual Platform .....	31
3.2.1 C-Arm Virtual Prototype .....	31
3.2.2 Virtual Platform .....	33
3.2.2.1 Virtual Platform Physical Setup .....	33
3.2.2.2 Virtual Environment Visually Generated Computer Model .....	35
3.2.3 Virtual Platform GUI .....	36
3.2.4 Virtual Platform Advantages and Results .....	37
3.2.5 Comment .....	41
3.3 Kinematic Modeling of C-Arm .....	41
3.3.1 Kinematics Approach .....	41
3.3.2 Forward Kinematics .....	42
3.3.3 MATLAB Script for C-Arm Forward Kinematics .....	44
3.3.4 Inverse Kinematics.....	45
3.3.5 Comment .....	48
3.4 C-Arm Physical Prototype Design and Manufacturing.....	48
3.4.1 Requirements of the C-Arm Physical Prototype .....	48
3.4.2 Hardware Development .....	49
3.4.2.1 Standard Parts .....	50
3.4.2.2 Custom Machined Parts .....	50
3.4.2.3 Motor Selection .....	51
3.4.3 Comment .....	52
3.5 Integration of Vicon Motion Capture with the C-Arm Physical Prototype .....	53

3.5.1 Vicon Motion Capture.....	53
3.5.2 Vicon Integration with C-Arm Prototype.....	54
3.5.3 Comment .....	55
Chapter 4: Testing and Validation.....	56
4.1 Vicon Testing Expectations.....	56
4.2 Vicon Testing Procedure.....	57
4.2.1 Testing Setup.....	57
4.2.2 Vicon Data Acquisition .....	59
Chapter 5: Results and Discussion .....	61
5.1 Key Results.....	61
5.1.1 Vicon Raw Data .....	61
5.1.2 Data Comparison and Analysis .....	65
5.2 Discussion .....	66
5.2.1 Task 1: Virtual Platform and GUI.....	66
5.2.2 Task 2: Kinematic Modeling .....	66
5.2.3 Task 3: Physical Prototype.....	67
5.2.4 Task 4: Integration with Vicon .....	67
5.2.5 Testing Results .....	68
Chapter 6: Concluding Remarks.....	69
6.1 Closure .....	69
6.2 Implications and Expected Outcomes .....	70
6.3 Future Work.....	70
References .....	72
Appendix A: C-Arm Virtual Prototype & Virtual Platform CAD Models.....	76
Appendix B: Simulink Models .....	81
C-Arm Virtual Platform Simulink Subsystems .....	81
C-Arm Physical Prototype Simulink Subsystems .....	83



Appendix C: MATLAB Computer Code .....	86
User defined function block “Vertical Axis- Stepper Motor Control Loop” .....	86
User defined function block “Denavit Hartenberg Parameters” .....	87
User Defined Block IDK for the calculation of the Inverse Kinematics .....	89
Vicon Data Processing MATLAB Code .....	90
Wig-Wag Test .....	90
Tilt Test.....	91
Orbital Test .....	91
Appendix D: G-Code Used in CNC .....	93
Appendix E: Purchased Standard and Stock Parts .....	95
Appendix F: C-Arm Prototype Engineering Drawings.....	99

## List of Tables

Table 1. Vicon Cartesian Test Points Comparison to Theoretical Kinematic Values .....	65
Table 2. Average Repositioning Error .....	66

## List of Equations

Denavit & Hartenberg Matrix (1).....	44
Denavit & Hartenberg Transformation (2).....	45
Midpoint Formula (3) .....	55

## List of Figures

Figure 1. C-Arm X-ray System [1].....	1
Figure 2. Translational Degrees of Freedom.....	2
Figure 3. C-Arm Wig-Wag Movement.....	2
Figure 4. C-Arm Tilt and Orbital Movement.....	3
Figure 5. Current Method of C-Arm Maneuvering [2].....	3
Figure 6. Research Questions and their Task Relevance (Section in the Thesis).....	9
Figure 7. The BV 20 First Surgical C-Arm [6].....	12
Figure 8. Kinematics and Behavior of Beam Cone in C-Arm [7].....	13
Figure 9. Planning of Needle Trajectory [8].....	14
Figure 10. X-ray Overlay for Surgical Accuracy [9].....	15
Figure 11. Double Mirror Modification for the CAMC [10].....	15
Figure 12. RGBD Integration with CAMC [9].....	16
Figure 13. Schematic Representing the Detection of IR-Markers [12].....	17
Figure 14. Surgical Tools with Integrated IR-Markers [13].....	17
Figure 15. C-Arm Reposition Using IR-Marks on the Patients body [14].....	18
Figure 16. Point Cloud Augmentation using VR Googles [15].....	19
Figure 17. C-Arm X-ray System with Vicon Motion Capture IR-Markers [16].....	21
Figure 18. Process of 3D Rendering form Multiple X-ray Imaging [16].....	21
Figure 19. ToF Coin Calibration for Human Body Part Detection [17].....	22
Figure 20. Body Segments Recognized and in Space Using ToF Integration [17].....	22
Figure 21. Scattering of X-rays during C-Arm use [18].....	23
Figure 22. Elements of Radiation Free C-Arm Training for Spine Surgery [19].....	24
Figure 23. Programable Universal Machine for Assembly [20].....	25
Figure 24. Relationship of Forward and Inverse Kinematics [21].....	25
Figure 25. Cable-Driven Parallel Robot [22].....	26
Figure 26. Robotic Hip Joint Testing [25].....	27
Figure 27. First Method of C-Arm Repositioning.....	29
Figure 28. Two Step C-Arm X-ray System Repositioning System.....	30
Figure 29. Isometric View of C-Arm Virtual Prototype.....	31
Figure 30. Different Views of the C-Arm Virtual Prototype.....	32
Figure 31. C-Arm Virtual Prototype with Visible Degrees of Freedom.....	33
Figure 32. Surgical Room Setup for the Virtual Platform.....	34
Figure 33. Virtual Environment of the C-Arm X-ray System.....	34

Figure 34. Simulink Block Diagram of the Visual System and CAD Model Interaction....	35
Figure 35. Virtual Platform GUI (all joints set to zero) .....	36
Figure 36. Simulink Virtual Platform Simulation .....	37
Figure 37. Position vs Time Graph using P Controller [12].....	38
Figure 38. Position vs Time Graph using PI Controller [12].....	38
Figure 39. Position vs Time Graph using PID Controller [12] .....	39
Figure 40. Torque vs Time Graph using P Controller [12] .....	39
Figure 41. Torque vs Time Graph using PI Controller [12] .....	40
Figure 42. Torque vs Time Graph using PID Controller [12].....	40
Figure 43. Common Types of Robot Design [26] .....	41
Figure 44. Denavit Hartenberg Joint Parameters [27] .....	42
Figure 45. C-Arm Kinematic Model .....	43
Figure 46. Inverse Kinematics Model for Case 1.....	46
Figure 47. Inverse Kinematics Model Case 2.....	47
Figure 48. Inverse Kinematics Model Case 3.....	47
Figure 49. Inverse Kinematics Model Case 4.....	48
Figure 50. C-Arm Physical Prototype CAD Model and Robot.....	49
Figure 51. C-Arm Comparison: Virtual Prototype, Physical Prototype and Actual C-Arm .....	50
Figure 52. Computer Aided Marching using Inventor HSM .....	51
Figure 53. Nema 23 Manufacturer Torque Curve.....	52
Figure 54. Autonomous Drone Equipped with Reflective Motion Capture Markers [36]..	53
Figure 55. Vicon Video Overlay onto Detected Markers with Labels .....	54
Figure 56. Four-Factor Validation of Motion Capture Testing.....	56
Figure 57. Testing Setup and Procedure for Revolute Joints .....	57
Figure 58. Wig-Wag Test Positions and Procedure .....	58
Figure 59. Tilt Test Position and Procedure .....	58
Figure 60. Orbital Test Positions and Procedure .....	59
Figure 61. Vicon Data Acquisition of Markers Placed on Prototype.....	59
Figure 62. Wig-Wag Testing Coordinates of the Camera Lens .....	61
Figure 63. Wig-Wag Testing Coordinates of AOI .....	62
Figure 64. Tilt Testing Coordinates of Camera Lens .....	62
Figure 65. Tilt Test Coordinates of AOI.....	63
Figure 66. Orbital Test Coordinates of Camera Lens .....	64

Figure 67. Orbital Test Coordinates of AOI .....	64
Figure 68. Motion Planning Algorithm Example Problem [38] .....	70
Figure 69. Second Step of Automatic C-Arm Repositioning Goal.....	71
Figure 70. Virtual C-Arm Base .....	76
Figure 71. Vertical Translation Joint.....	76
Figure 72. Horizontal Translational Joint.....	77
Figure 73. Wig-Wag Link .....	77
Figure 74. Tilt Link .....	78
Figure 75. Orbital Link .....	78
Figure 76. Humanoid Shape .....	79
Figure 77. Operation Table .....	79
Figure 78. Vicon Motion Capture Camera.....	80
Figure 79. GUI Virtual Model Background Calculations .....	81
Figure 80. GUI Signal Input Conversion.....	82
Figure 81. GUI for C-Arm Prototype (all joints set to zero).....	83
Figure 82. C-Arm Prototype GUI Background Computations .....	83
Figure 83. Stepper Motor Control Loop (vertical axis used as an example) .....	84
Figure 84. Signal Output Subsystem to Arduino .....	84
Figure 85. Inverse Kinematics Subsystem.....	85

## Abbreviations & Nomenclature

### **Abbreviations:**

**AOI**-Area of Interest

**CAMC**- Camera Augmented Mobile C-Arm

**CAP**- C-Arm Physical Prototype

**C-Arm**- C-Arm X-ray System

**CVP**- C-Arm Virtual Prototype

**CBCT**- C-Arm cone beam computer tomography

**CAD**- Computer Aided Design

**CAM**- Computer Aided Machining

**CGI**- Computer Generated Imagery

**CNC**- Computer Numeric Control

**CT**- Computer Tomography

**DC**- Direct Current

**DH**- Denavit and Hartenberg

**DOF**- Degree of Freedom

**GUI**- Graphic User Interface

**HSM**- High Speed Machining

**IR**- Infra Red

**Mocap**- Motion Capture System

**MRI**- Magnetic Resonance Imaging

**P**- Proportional

**PI**- Proportional and Integral

**PID**- Proportional, Integral and Derivative

**PPS**- Pulse Per Second

**PUMA**- Programable Universal Machine for Assembly

**RGB-D**- Red, Green, Blue and Depth

**ROI**- Region of Interest

**ToF**- Time of Flight

**VP**- Virtual Platform

**VR**- Virtual Reality

**XML**- Extensible Markup Language

## Nomenclature:

a- distance create by wig-wag angle in the x direction  
a- joint x axis translational offset  
 $A(x_o, y_o, z_o)$ - cone beam origin coordinate  
 ${}^{j-1}A_j$ - Denavit & Hartenberg joint transformation  
 $\vec{a}$  - first translation vector of cone beam  
b- distance created by the wig-wag in the y direction  
 $\vec{b}$ - second translation vector of cone beam  
 $d_j$ - joint “z” axis offset  
 $H$ - reference point for cone beam  
 $M$ - margin of cone beam  
 $Mid$ - midpoint between Camera lese and detection plate  
 $N$ - normal point in cone beam  
 $\vec{n}$ - normal translation vector of cone beam  
 $O(x_c, y_v, z_c)$ - cone beam center coordinate  
 $r$ - radius of cone beam  
 $R_n$ - reference coordinate system  
T- horizontal translation value  
 ${}^0T_E$ - transformation of end effector relative to origin  
 ${}^0_nT$ - cartesian space point or robot  
 $x_j$ - joint reference x axis  
 $x_t$ - target marker x global coordinate  
X- inverse kinematic x coordinate  
 $y_j$ - joint reference y axis  
 $y_t$ - target marker y global coordinate  
Y- inverse kinematic y coordinate  
 $z_c$ - camera height offset  
 $z_j$ - joint reference z axis  
 $z_t$ - target z global coordinate  
 $\alpha_j$ - joint x axis angle offset  
 $\delta$ - target marker horizontal angle offset to camera  
 $\theta$ - wig-wag joint angle  
 $\theta_j$ - joint actuated angel



## Abstract

One of the important surgical tools in spinal surgery is the C-Arm X-ray System also known simply as the C-Arm. The C-Arm is a large “C” shaped and manually maneuvered arm that provides surgeons and X-ray technicians the ability to take quick quality X-rays during surgery. Because of its five degrees of freedom, the C-Arm can be manually maneuvered around the patient to provide many angles and perspectives, ensuring surgical success.

This system works fine for most surgical procedures but falls short when the C-Arm must be moved out of the way for complicated surgical procedures and later repositioned with accuracy for validation X-rays. The manual repositioning accuracy is a challenge for surgical personnel, because there are too many movements and joint combinations to keep track of. Unsuccessful efforts by X-ray technicians to reposition the C-Arm manually have many downsides, such as excessive radiation exposure to the patient and staff, longer surgery time, higher surgery cost, increased risk of infection, and increased risk of anesthesia complications.

The aim of this thesis is to develop an accurate repositioning method with the use of motion capture technology. This will be a novel approach to creating a repositioning integrated system. While other repositioning methods for the C-Arm exist, most require constant calibration, only work in specific ranges or are too slow to be used effectively. All those downsides can be overcome by integrating the C-Arm with motion capture systems that are already deployed in high accuracy spine surgery centers. By using motion capture as a repositioning feedback, we remove the need of separate and repeated calibrations for the surgical tools and the C-Arm since both will be using the same system for accurate maneuvering.

To develop a motion capture repositioning integrated system, a set of research tasks needed to be completed. A virtual prototype and a virtual platform were developed that quantified the dynamics of the C-Arm maneuvering. The virtual platform proved critical for understanding the nature of C-Arm movement during surgery. In addition, the virtual platform became the basis for developing a Graphic User Interface for automatic repositioning. Next, a complete kinematic model of the C-Arm was developed. The kinematic model created the relationship of C-Arm joint angles with the respective Cartesian coordinates for critical points on the C-Arm. Automatic maneuvering of the C-Arm relies on a proper kinematic model. Third, a fully automatic robotic C-Arm prototype

was designed and manufactured to serve as a replacement for the actual C-Arm. Since the C-Arm is a radioactive and expensive piece of equipment, access to it is limited. The development of the C-Arm prototype allowed for physical validation of new repositioning ideas. Finally, the robotic prototype, the virtual platform, and the kinematic model were all systematically integrated using Vicon motion capture system to perform the automatic repositioning of the C-Arm.

Testing of the newly developed repositioning system was completed with successful results. The C-Arm prototype was able to be repositioned using the Vicon system with an average position error value of less than  $\frac{1}{2}$  inches cubed. This error is in part due to imperfect marker placement and the physical size of the markers. With the development of such a simple, effective, reliable, and fast repositioning system of the C-Arm, it is expected that professional interest in motion capture-based repositioning grows. With committed use of this kind of systems, repositioning will be done faster and with greater accuracy. This will not only reduce the excessive radiation exposure of patients due to repositioning but also significantly reduce surgery time. This reduced surgery time will in turn also reduce surgery cost, risk of infection, and anesthesia complications.

## Chapter 1: Frame of Reference

### 1.1 Background and Motivation

One of the most common health complaints amongst American adults is back pain. The source of back pain has many origins, and sometimes the pain cannot be traced back to a specific root. Usually, spinal surgery is a last resort for the treatment of back pain. Spinal surgery is also used to treat a host of other spine related issues such as scoliosis which might not be accompanied with pain at all.

Like all surgeries, spinal surgery comes with possible complications. These complications include bacterial or fungal infections that can become fatal. Other complications can range from excessive loss of blood to tissue damage. Sometimes, even without any surgical complications, the surgery is not successful in accomplishing the final surgical result of relieving the patient's pain.

One of the most important elements of surgery, especially spinal surgery, is radiography. In simpler surgeries, an X-ray or an MRI is usually taken before the surgical procedure to aid in the diagnosis. After the surgical procedure is completed, doctors might recommend further X-rays to ensure surgical success. However, in more complicated surgeries, such as spinal surgeries, X-rays must be taken during the procedure to ensure proper outcome. One of the few X-ray systems that allow for imaging during surgery is the C-Arm X-ray System (C-Arm) shown in Figure 1 below.



Figure 1. C-Arm X-ray System [1]

The C-Arm is a large 'C' shaped robotic arm with five degrees of freedom (DOF). The C-Arm can move up, down, back, and forth for two translational DOF. In addition, the C-Arm has three rotational DOF: tilt, wig-wag, and orbital movement. These DOF are visually represented in Figures 2-4.

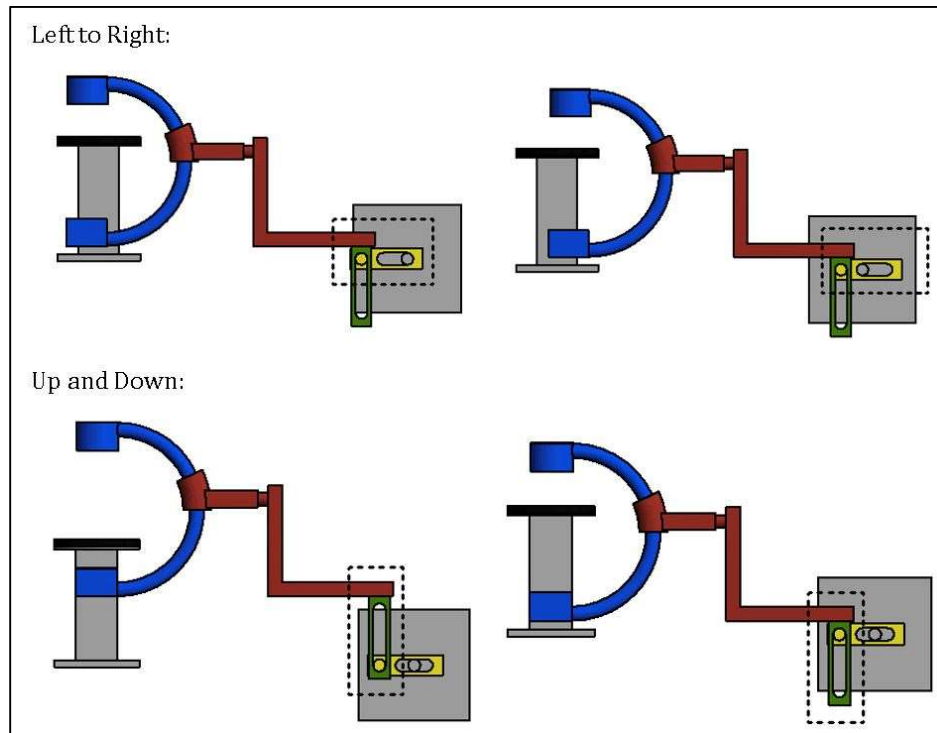


Figure 2. Translational Degrees of Freedom

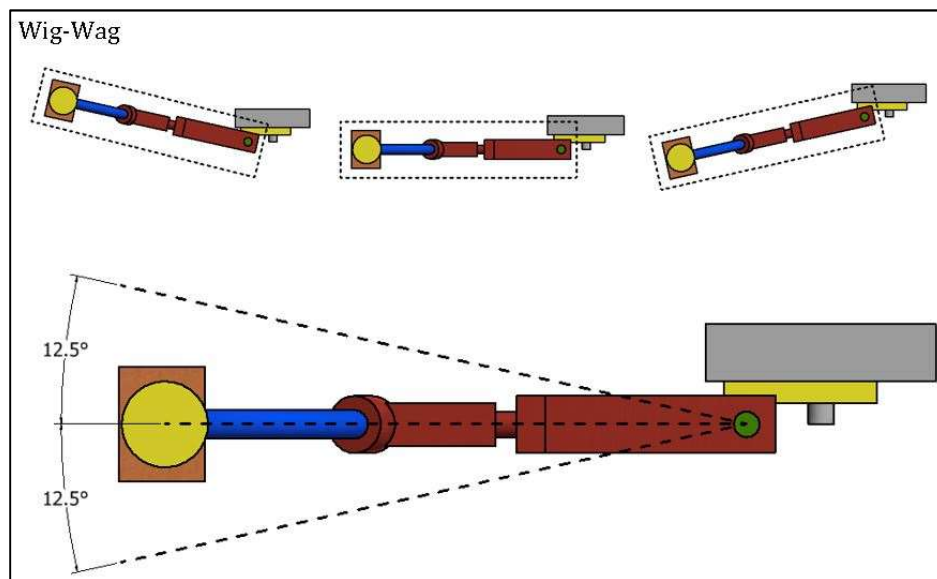


Figure 3. C-Arm Wig-Wag Movement

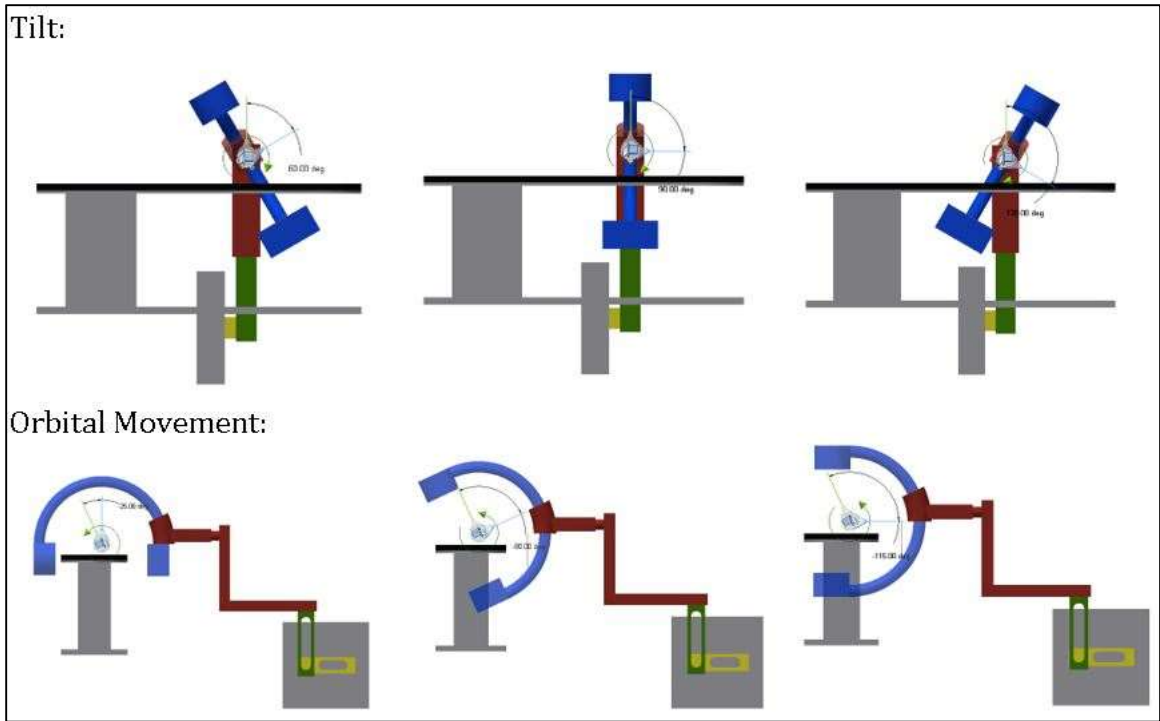


Figure 4. C-Arm Tilt and Orbital Movement

This robot arm is moved through its ranges of motion manually by the X-ray technicians. Manual repositioning is currently one of the fastest ways of repositioning and can be seen in Figure 5. New models of the C-Arm have been developed to allow X-ray technicians to move the C-Arm by motor control. Even when the movement of the C-Arm is motorized, the positions of each joint are still manually handled by the X-ray technicians. The C-Arm provides substantial advantages for the surgeons, allowing them to perform surgical maneuvers and to validate these maneuvers immediately.



Figure 5. Current Method of C-Arm Maneuvering [2]

However, the C-Arm still has weaknesses and limitations. One of the biggest weaknesses is the exact repositioning of the C-Arm. For most surgical procedures, the C-Arm does not have to move and can take multiple images from the same position. Even if the C-Arm must move for proper X-ray imaging, the X-ray technicians are very competent in providing quality imaging.

Some surgical procedures are more complicated and require the C-Arm to be moved or rolled completely away from the operating table. This is done to allow for more room for other equipment and procedures. Once those procedures are completed, the C-Arm is manually repositioned by the X-ray technicians. Manual repositioning of the C-Arm by the X-ray technician is usually not a problem. Although the manual repositioning is not exact, it gets the job done rapidly and with enough accuracy. In certain cases, the repositioning needs to be extremely accurate, and this is where the limitation of the current models arise. In cases where repositioning accuracy is of the essence, much time and effort are spent trying to reposition the C-Arm so that the post-operation and pre-operation X-ray images are aligned and taken from the same references.

By spending valuable operating time on C-Arm repositioning, medical professionals can cause an increase in surgical risks. Because the patient is laying exposed on the operating table, the risk of infection increases with time. In addition to infections, every minute spent to reposition the C-Arm for X-ray imaging is another minute under anesthesia. Therefore, this means that the risk of anesthesia complication also rises.

Often, X-ray technicians must take multiple X-ray images to ensure proper repositioning. Sometimes X-ray videos known as fluoroscopes must be used to ensure proper repositioning of the C-Arm. By using multiple X-rays and taking real time fluoroscopes, the patient and the medical professionals are exposed to excessive and harmful X-ray radiation [3]. In extreme cases, patients may suffer from radiation poisoning brought on by excessive use of X-ray imaging.

The increased health risk of long C-Arm repositioning time is also accompanied with large cost increases. Everyone involved in the surgery must get paid, meaning the cost of surgery increases as more time is spent repositioning the C-Arm for accurate imaging. The increased time cost is split amongst surgeons, nurses, X-ray technicians, and hospital fees. Any less minute in the operating room reduces the cost by a significant amount.

So far, companies like SIEMENS and General Electric, who are the top manufacturers of the C-Arm, have been attempting to develop a solution to the C-Arm repositioning problem. Thus far, no cost-effective solutions have been proposed that are commercially available and meet the strict demands of effective repositioning for surgical purposes. Therefore, the overarching goal is to develop a C-Arm maneuvering system that is sufficiently accurate for even the most complicated surgeries and faster than current repositioning methods.

## **1.2 Limitation Factors**

To improve the accuracy and efficiency of the current C-Arm repositioning during critical surgery procedures, a system needs to be developed that will reposition the C-Arm quickly and reliably. To solve this problem, certain factors need to be considered that limit the options in developing a solution to this problem. The first limiting factor is the cost of the C-Arm itself. Because a C-Arm costs the hospital about \$70,000-\$100,000, nobody is willing to make significant modifications to their C-Arm at the risk of having a malfunctioning machine [4]. Any proposed solution to the C-Arm repositioning cannot be invasive to the C-Arm hardware. Because the C-Arm is used in a surgical and radioactive environment, certain materials are not suited for use. Materials or methods used must also adhere to sterile surgical standards. In addition, any solution proposed to improve the C-Arm repositioning must be implemented in a timely manner. Hospital rooms are reserved for days to months ahead of time, meaning that any implemented solution cannot delay the use of surgical rooms or the C-Arm for an extended amount of time. Propositions that would interfere significantly with surgery schedules are not out of the question but are highly discouraged. Lastly, because the C-Arm works just fine in most surgical procedures, any new updates should not interfere with the current model of use of the C-Arm.

## **1.3 Innovative Approach**

### **1.3.1 Motion Capture Integration**

There already exist a handful of C-Arm repositioning methods all with their pros and cons. This thesis, however, proposes the novel idea of integrating the C-Arm with motion capture technologies that are already deployed in operating rooms. This approach has its distinct advantages and overcomes a set of limitations that hinder most repositioning ideas.

Because C-Arms are expensive instruments, any major or minor modification to the hardware is usually out of question. However, using motion capture as a sensing system for the C-Arm only requires a handful of reflective IR markers to be placed on the C-Arm. This approach, discussed further in Chapter 3, avoids the need of making any hardware modifications. Using already deployed motion capture systems to reposition the C-Arm also has a significant time advantage. Any proposed method to improve the C-Arm's performance should be implemented in a timely manner because any C-Arm or operating room out of commission for an extend amount of time is out of question. Therefore, the implication of a motion capture system should not take up any significant amount of time and should not delay any surgeries, especially if motion capture is already used. An additional advantage of integrating the C-Arm with motion capture is the fact that the normal use of the C-Arm is not changed at all. This means that once a C-Arm is integrated with a motion capture system, it can immediately be used in a traditional way, allowing the C-Arm to still be useful for simple surgeries that don't require any special repositioning. Finally, this proposed method is also able to adhere to the sterile hospital surgery room standards while still performing in radioactive X-ray environments.

### **1.3.2 Motion Capture Integration Key Advantages**

There can be many advantages that will improve the repositioning of the C-Arm; however, those advantages might not be important or significant to the end-users. The key advantages that will make the integration of the C-Arm with a motion capture system marketable in the healthcare community are as follows: First, the proposed system does not need repeated calibration. While similar solutions have been proposed in the past, they have not been put into practice because of repeated calibration. When the Vicon motion capture (Vicon) system is calibrated once, it can work for days and hours without needing to be recalibrated. Although periodic recalibration is required to ensure quality, it



is nothing like other propositions that need recalibration with every surgical procedure. Second, the reposition system developed here is modular, meaning that it can be applied to all C-Arms no matter the size or brand. While some propositions in the past work well with certain models of C-Arm, they have fallen short to be applied to all brands and models of the C-Arm. This repositioning system was intentionally designed to be compatible with all models, including small scale prototypes. In addition, this reposition method can be deployed for all surgical procedures. While other repositioning methods are limited to only a hand full of repositioning ranges, this method can be used throughout all extreme ranges of the C-Arm. Finally, other proposed solutions require extensive training of the surgical staff to understand and operate their rather complicated repositioning systems. The proposed integrated repositioning system of this thesis is intended to be very simple and easy to learn, removing the need for long and expensive staff training.

### **1.3.3 C-Arm Kinematics, Programming, and GUI**

One of the current setbacks of C-Arm repositioning is that developed methods are too specialized and not as versatile as they could be. Most methods of repositioning have refrained from creating a method that works for all kinds of surgery and all surgical procedures. The lack of a method that works in a broad range of C-Arm applications is mostly due to the limitations mentioned in the “Limitation Factors” subsection and due to the high cost that such a working system would have. Proposed methods that do work for most C-Arm applications do exist but need constant recalibration and are too slow to be considered ideal.

The tasks in this project aim to overcome these hurdles by creating an original kinematic model, developing a repositioning program that is accurate and versatile enough without needing constant calibration, and easily learned by the development of an intuitive Graphical User Interface (GUI). The original kinematic model will be a model that can be applied to any C-Arm no matter the size. This kinematic layout will allow offsets that can be changed based on the specific dimensions of the C-Arm in use. The kinematic model will then be programmed to work in all scenarios of C-Arm use without needing constant calibration. The program should consider multiple scenarios of repositioning and be able to select the correct method. Finally, an intuitive GUI must be developed that allows for users with limited C-Arm experience to master the repositioning using the proposed method of this project. By creating an original kinematic

model and a versatile program that is maneuvered with an intuitive GUI, this project will set itself apart from previously created methods.

### **1.3.4 Robot Prototype Development**

Since access to a real C-Arm is limited, testing and validating proposed ideas to improve the C-Arm is also limited to the public. However, by designing a cost effective and functioning C-Arm prototype that can be easily recreated with little cost, will help eliminate the need of having full access to a real C-Arm, therefore, welcoming further improvements to the current models and techniques of C-Arm operation and maneuvering at a much lower cost. Thus, the original design and manufacturing of a fully functioning C-Arm prototype is also a major contribution of this project.

## **1.4 Overview / Scope**

### **1.4.1 Objective**

The objective of this thesis is to develop a system or a method in which the C-Arm can maneuver itself automatically, quickly, and more reliably than X-ray technicians and current methods of automatic repositioning.

### **1.4.2 Research Questions**

To reposition the C-Arm automatically, faster, and more reliably than current ways of accurate repositioning, this thesis lays out the following research questions (RQs):

- 1) RQ 1: Will a virtual platform of a C-Arm aid in the design of a C-Arm prototype, and will it help evaluate the performance of a developed C-Arm custom GUI? This first question will be investigated in section 3.2 and directly relates to Task 1.
- 2) RQ 2: How can we develop a feasible kinematic model that will apply to any C-Arm, and potential prototypes? The development of a kinematic model, modular enough to be applied to any C-Arm will be conducted in section 3.3 by Task 2, directly answering the second research question.
- 3) RQ 3: Is it possible to develop a fully functioning robotic C-Arm Prototype that will have the same movements and joints as the real C-Arm? This question will be answered by Task 3 in section 3.4, where the development of a fully functioning C-Arm Prototype is discussed.

4) RQ 4: Can the C-Arm prototype be reliably integrated with currently used motion capture system, such as Vicon, for fast and accurate repositioning ? The answer to this final research question is investigated in depth in section 3.5. which marks Task 4. This section discusses the integration of the C-Arm porotype with Vicon.

A diagram showing the order and the chapter sections in which these reach questions are investigated in is shown in Figure 6 below.

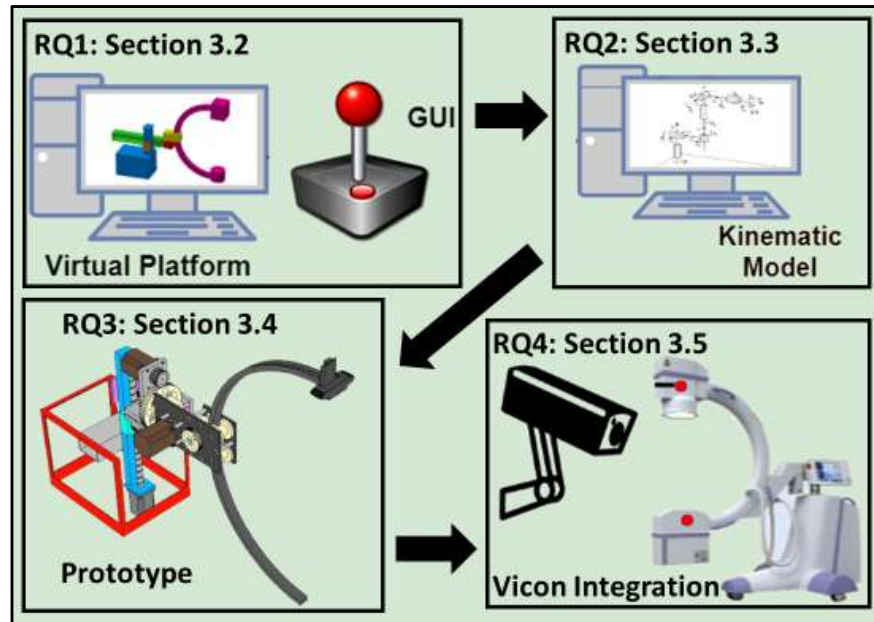


Figure 6. Research Questions and their Task Relevance (Section in the Thesis)

### 1.4.3 Hypothesis

By integrating the C-Arm with Vicon, a virtual platform, an appropriate kinematic model, and a custom GUI, we can automatically reposition the C-Arm accurately for surgery.

### 1.4.4 List of Tasks

To accomplish a reliable integration of the C-Arm and Vicon system for the use of C-Arm repositioning, a list of tasks needs to be addressed. These prerequisites include the following:

- 1) Task 1: Design and develop a virtual prototype and virtual platform development with an intuitive Graphic user interface.

- 2) Task 2: Develop the mathematical forward and inverse kinematics models of the C-Arm physical prototype, and integrate the kinematics with the GUI using MATLAB programming.
- 3) Task 3: Design and manufacture a fully functional small-scale prototype model of the real C-Arm.
- 4) Task 4: Systematically integrate the C-Arm prototype with Vicon motion capturing system.

By completing these prerequisites, the analysis of integration of the C-Arm prototype with the Vicon system can be properly performed. Once the C-Arm prototype is integrated with Vicon motion capture testing and validation procedures will be conducted to ensure quality.

#### **1.4.5 Thesis Outline Description**

This thesis consists of six chapters. Chapter 1 covers the background of this project and aims to help the reader understand the motivation behind this research and why this research is needed. Chapter 2 consist purely of a literature review. This literature review is split into two sections; the first section is dedicated to the current standing and advancements made specifically to the C-Arm, and the second section is solely about the current approaches of kinematic modeling. The third chapter, named Chapter 3 Methodology, is a collection of the methods used to complete all four research tasks and, thereby, answering all four research questions. Section 3.2, 3.3, 3.4 and 3.5 are the individually completed research tasks for research questions 1-4, respectively. Chapter 4 is dedicated to the testing procedures and validation methods performed in the system integration testing of the C-Arm repositioning. This section also explains the dependencies of all subsystems with one another. In Chapter 5, the results are revised and discussed in detail. Finally, Chapter 6 wraps up the thesis with concluding remarks and the discussion of needed future work.

## Chapter 2: Literature Review

### 2.1 Literature Introduction

The C-Arm has become one of the most favorite mobile X-ray systems available for surgery, especially for minimally invasive spine procedures. With its versatility and quick manual maneuverability, surgeons and X-ray technicians have had much success in operating the C-Arm for surgical procedures.

Accurate repositioning of the C-Arm is crucial for surgical success, and much effort has been brought on by the scientific community to reposition the C-Arm with efficient speed and proper accuracy. So far, different approaches and suggestions to accurate reposition have been made, all with their own strengths and weaknesses. The most popular trend in repositioning the C-Arm is integrating the C-Arm with a virtual reality (VR) platform. This integration, being the most popular option, also has its own strengths and shortcomings.

With the advancements in medical science, surgeries have naturally become more complicated. Surgical procedures often require special equipment designed for specific surgical procedures only designated for one function at a time. In addition, surgical procedures have also modernized in the recent years with the help of motion capture. This modernization includes the use of motion capture systems integrated with surgical equipment, allowing surgeons to perform difficult and precise maneuvers previously known to be too risky or unreliable.

With the advancements of robotics, especially those advancements made by the automobile industry, automation using robotics is becoming more and more common. Simple tasks can be allocated to robots, thereby cutting costs and improving efficiency. Robotic arms are one type of robot that have shown great potential in many industries. These days, robotic arms are also trusted to conduct complicated tasks such as welding or moving fragile objects at a fast pace.

### 2.2 C-Arm Virtual Reality Repositioning

#### 2.2.1 The C-Arm

Prior to 1955, all X-ray systems were stationary and did not provide many options for surgeons to take customized images during surgery. It was then when Philips developed the first C-Arm. This system was in shape of a half moon, or “C” shaped, and allowed, with its new maneuverability, for better and faster imaging during surgeries.

This design not only improved surgical quality but also improved patient comfort by removing the need of the patient to maneuver him or herself for imaging [5].



Figure 7. The BV 20 First Surgical C-Arm [6]

One of the largest downsides the C-Arm presented was the high dose of radiation exposure to the patient and to the surgical staff. Since the first C-Arm did not include image intensifiers, the radiation intensity was increased for proper imaging. Not too long after the first C-Arm was developed, image intensifiers were intergraded to reduce radiation exposure. It is important to note that C-Arm radiation is still a concern and remains a problem that has not been solved completely. The first ever developed C-Arm, shown in Figure 7 above, received additional DOF to improve its work quality. Currently most C-Arms have five DOF or arguably 6, if one includes the wheels as an additional DOF.

Since the C-Arm made its debut in 1955, not much has changed. The simple-to-use physical design has stayed virtually the same except for the change in material selection and color. While most other equipment has been modernized with automatic moving joints, C Arm manufactures have not had much interest in integrating automatic positioning to the C-Arm. Because the C-Arm itself is expensive, additional automation is not desired since it marginally adds utility to the handling of the equipment. Only a small fraction of surgeries requires extreme accurate repositioning of the C-Arm. Therefore, surgeons who rely on accurate repositioning of the C-Arm have had to resort to aftermarket customization for reaching their goal of accuracy.

### 2.2.2 C-Arm Local Vision Dependent Repositioning

The general kinematics of the C-Arm have been developed and studied to understand the X-ray imaging better. One area of large interest is the behavior of the cone beam during translation and rotation of the C-Arm. By understanding the cone beam of the X-ray radiation better, developers and users of the C-Arm have been able to better estimate C-Arm position and reposition. Figure 8 shows the behavior of the cone through both rotation and translation for two selected DOF. It is important to note that ROI in Figure 8 stands for region of interest and represents an infinitely thin cross section of the patient's body.

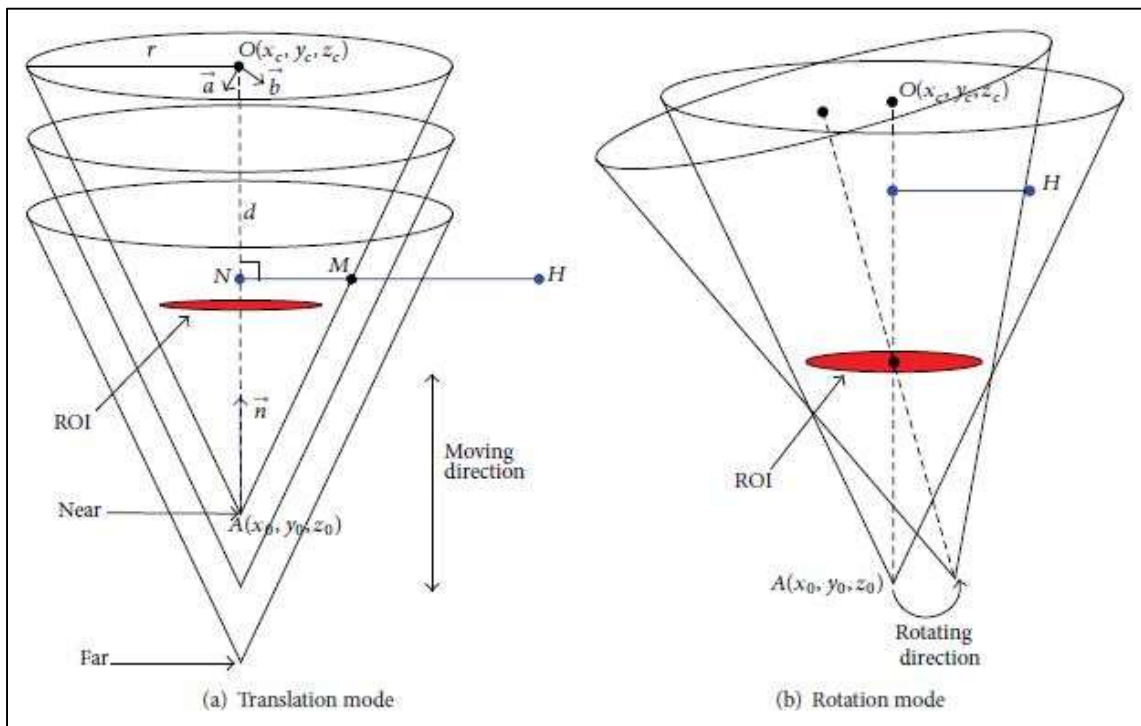


Figure 8. Kinematics and Behavior of Beam Cone in C-Arm [7]

With a complete understanding of the cone beam, fluoroscopy guided biopsies became a real possibility during surgery. Fluoroscopy guided biopsies are surgical procedures where the images of the C-Arm are collected and combined with the understanding of the cone beam model. Image-guided procedures based on C-Arm cone beam computer tomography (CBCT), combined with real-time fluoroscopy for preoperational procedures of the spine and pelvis, became technically feasible and safe. In one study, target lesions were reached in 11 of 12 patients on the planned trajectory

with an error margin of <5 mm [8]. However, procedures like this require two images from two different plane axes to develop a proper path model, meaning that C-Arm positions are constants and always accurate. In other words, these developed tomography methods do not work if the C-Arm base is moved. Once the C-Arm is moved away from the patient, the calibration needs to be redone every single time. One example of the use of CBCT procedure can be seen Figure 9 below.

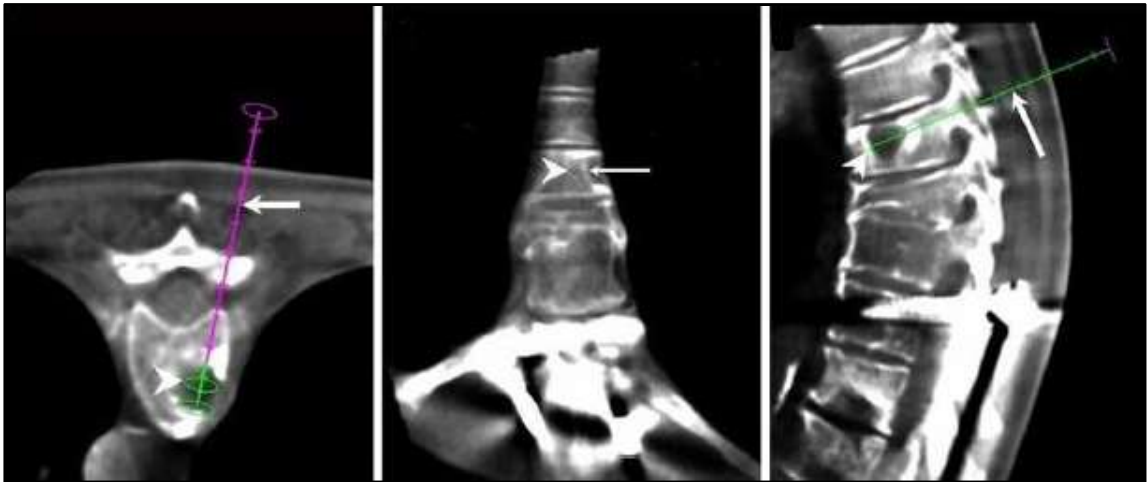


Figure 9. Planning of Needle Trajectory [8]

In the recent years, it has been discovered that useful modifications can be made to the C-Arm without jeopardizing its functionality by much. In addition, these modifications have managed to stay subtle enough to not hinder the traditional manual use of the C-Arm. A certain type of modification to the C-Arm allows for the use of augmented reality during surgery. A C-Arm augmented reality consist of overlaying X-ray images over a live feed to give surgeons a better positional awareness. One such augmentation can be seen in Figure 10, where the surgeon can essentially see the bones of the patients arm and the joint of the elbow before making the first incision. Because the overlay of the X-ray is exactly calibrated with the live feed of the camera, the surgeon knows exactly where to place the instruments, thereby improving surgical performance.



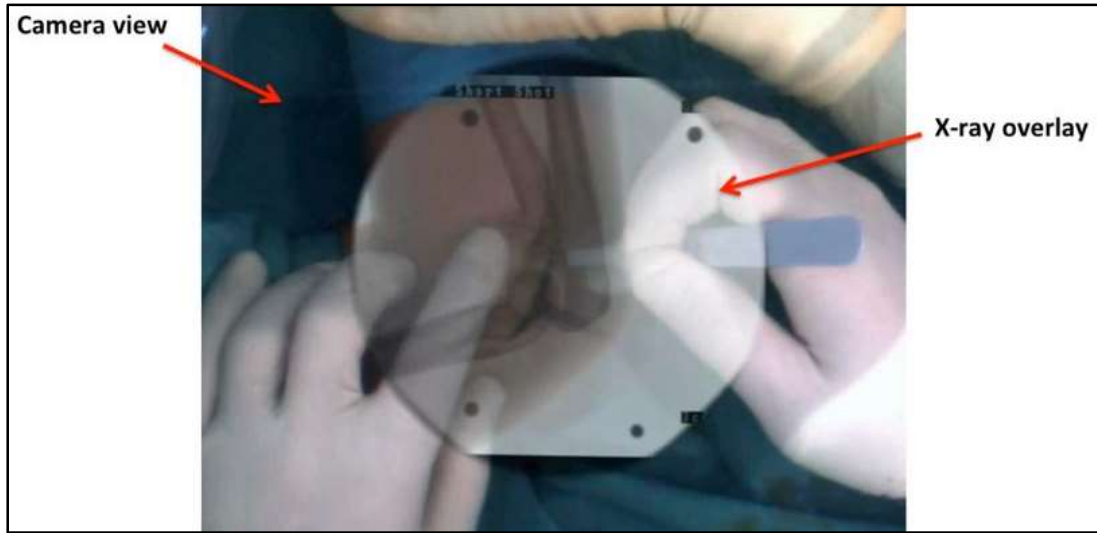


Figure 10. X-ray Overlay for Surgical Accuracy [9]

To achieve such an augmentation, a camera mirror system has been added onto the traditional C-Arm. Using the mirrors, the camera view is calibrated to exactly match the X-ray cone beam. The live feed of the camera therefore allows surgeons to see from the view of the C-Arm. The modification for a camera augmented mobile C-Arm (CAMC) is shown in Figure 11 below.

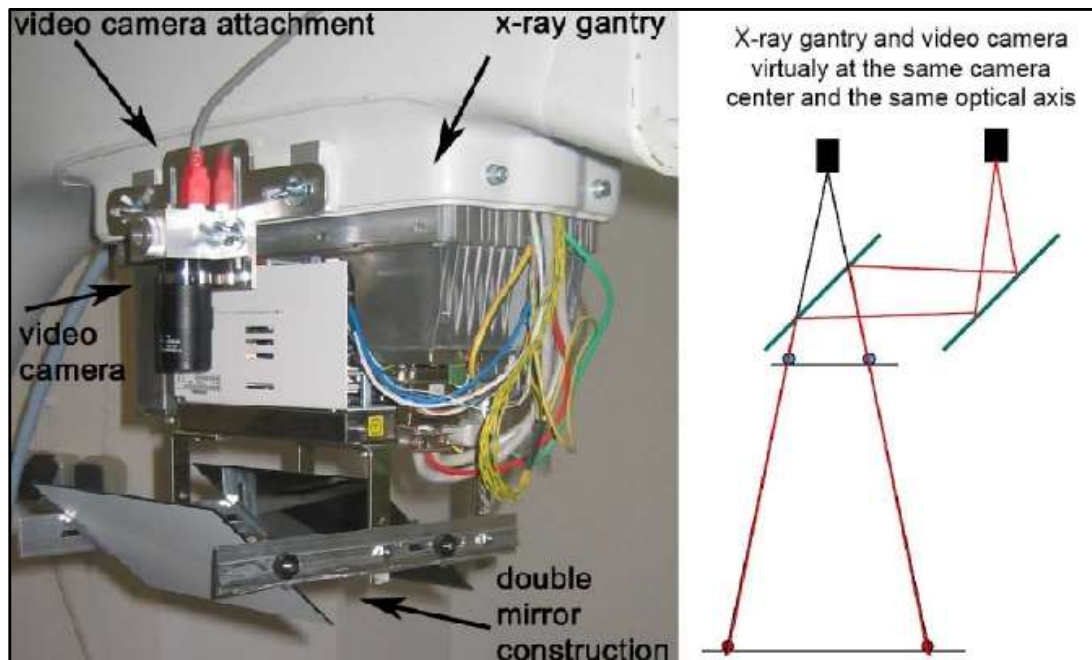


Figure 11. Double Mirror Modification for the CAMC [10]

In addition to camera augmentation, further modifications have been proposed and successfully implemented to enhance the augmented reality dynamics. For instance, RGB-D sensor, cameras that can perceive all color and depth, such as the Kinect sensors, have been added to further improve augmentation quality. The usual overlay is based on 2D-3D vision calibration. The usual CAMC system is not able to tell the spatial relationships between surgeon's hands, tools and targets due to the lack of depth information in the image. As a result, surgeons' hands and tools are partly covered by the X-ray overlay. The Kinect sensor can then segment hands and tools according to depth data and create an enhanced X-ray overlay that will not block hands and tools. This would provide a more intuitive view of spatial relationships between targets, hands, and tools [9]. In other words, ideas of integrating the X-ray images with the body patient have been done successfully only if the C-Arm nor the patient are moving.

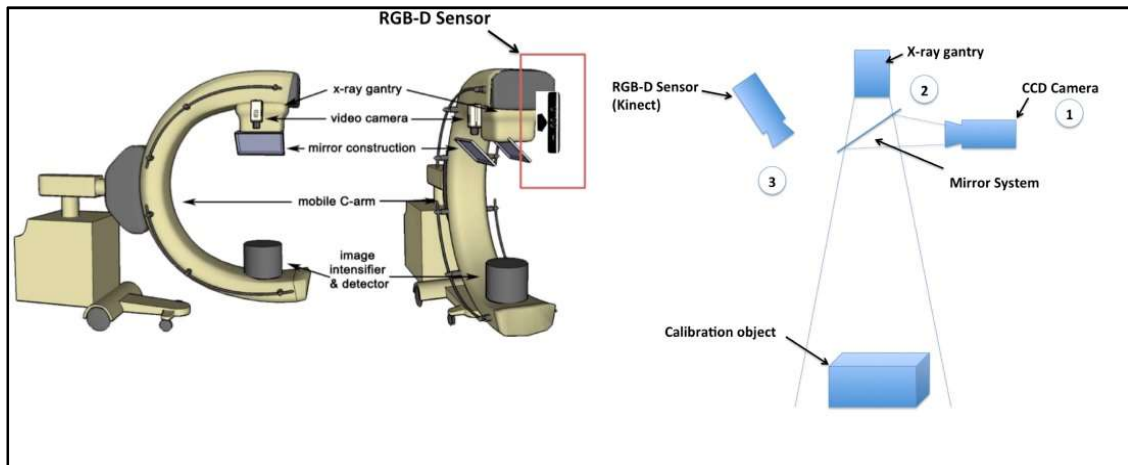


Figure 12. RGBD Integration with CAMC [9]

### 2.2.3 C-Arm Global Vision Dependent Repositioning

Naturally, after the progress of visual alignment with modified cameras reached the point of demising returns, the focus changed to finding the orientation and position of surgical tools in space. By the integration of optical tracker-based navigation systems, such as motion capture systems, reflective markers attached to surgical instruments became the next natural step in improvement of surgical utility. These tracker systems work by emitting IR light to spherical reflectors. The reflected light is then recorded by a set of fixed cameras, usually 6-12 cameras. Through careful image processing and

calibration, the exact position of each spherical reflector can be known about the stationary cameras. Using such models, the starting and end points of lines can be projected very efficiently into the image plane, allowing real-time tracking of objects with relatively low computational effort [11]. Figure 13 shows the theory of acquiring the location of a reference point using a system of cameras.

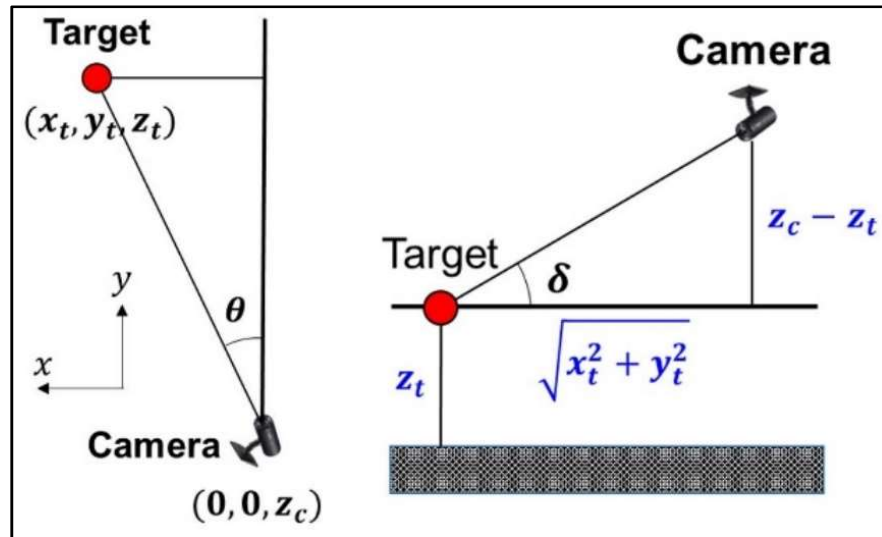


Figure 13. Schematic Representing the Detection of IR-Markers [12]

Using a motion capture system (mocap) such as the Vicon system to model position of surgical tools in space has distinct advantages. Since the mocap cameras are always stationary, there is no need to recalibrate the system if the C-Arm is moved during the surgery. Usually, the mocap system is calibrated before the surgery, and this calibration lasts throughout the entire procedure, no matter how long the surgery is to last. This cannot be said about any other C-Arm integration since those need to be recalibrated every time the C-Arm or the patient is moved.



Figure 14. Surgical Tools with Integrated IR-Markers [13]

For example, in Figure 14 above, a modular marker system is shown that integrates most surgical tools to be detected by the mocap system. If three or more markers are designated to an object, this object can be defined as rigid. The rest of the rigid objects can be defined with computer drawings if and only if the distance between markers do not change. This detection system allows for surgeons to know the exact position and angle of rotation of the surgical instruments modified with these modular markers. This information can then be combined with the cone beam data to aid for more exact surgical processes. Although the mocap marker system only needs to be calibrated once, the cone beam of the C-Arm needs to be recalibrated every time the C-Arm is moved by its base platform.

Since the markers on the surgical equipment only need to be calibrated once before the surgery, suggestions have been made to place markers on the patient's body. By placing markers on the patient's body, surgeons have been able to not only find the orientation of their surgical equipment but also the orientation of the patient's body. With this technique, surgeons have been able to reposition the C-Arm successfully using CAMC. However, the success of this repositioning method depends on the kind of surgery that is conducted. Surgery on distal body parts are ideal for this repositioning technique. Since the markers are placed on smaller body parts, the markers can be in proximity, allowing for better orientation derivation. In addition to the proximity of markers, the markers can be placed on far sides of a single body part and still be visible to the mocap cameras, allowing for the 3D shape estimation. Such an example can be seen in Figure 15 where surgery on the ankle of a cadaver was performed with successful repositioning.

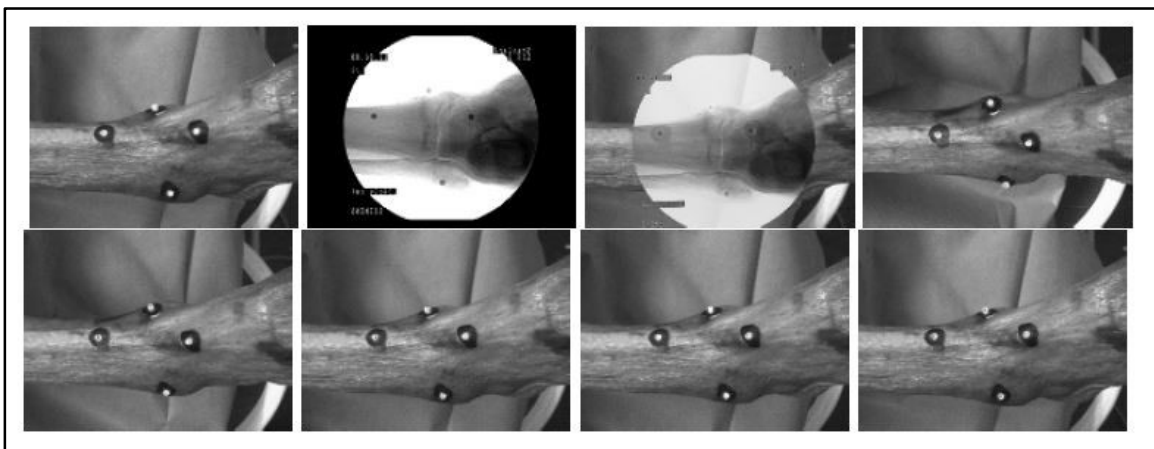


Figure 15. C-Arm Reposition Using IR-Marks on the Patients body [14]

One of the downsides of using a repositioning system that places markers on the patient's body is that it cannot be used for all kinds of surgeries or procedures. For example, during spine surgery, these markers would have to be placed on the back of patient, but these areas are supposed to be covered by surgical sheets, meaning that the CAMC cameras cannot see the sensors. The surgical sheets could be removed at the risk of reducing hygiene, or the markers could be placed on surgical sheets prone to movement. A second downside of this marker to skin system is the fact that the markers could get in the way of surgical procedures. Simple joints such as an elbow or ankle could be relocated using a few markers, but something as complicated as the spine would require either many markers or the marker system would not be accurate enough. In other surgeries like knee surgeries, the knee joint is moved in its ranges of motion, causing markers to fall off or worse, get lost. Because of these reasons, the marker to skin repositioning system is limited to distal body parts and minimally invasive surgeries, making it unsuitable for more complicated spine procedures.

In 2018, large efforts have been made to solve the C-Arm repositioning problem for once and for all. One of the more promising solutions to reposition the C-Arm once again makes use of augmented reality base feedback. However, this time, instead of the augmentation coming from the origin of the cone beam camera, the augmentation comes from VR goggles worn by the X-ray technicians. Cameras overseeing the surgery room generate a point cloud, shown in Figure 16, over a certain position of the C-Arm that is saved. Once the C-Arm is moved from that saved position, X-ray technicians can use VR goggles to see an augmentation of this saved point cloud. The process of saving C-Arm positions is repeated for every desired X-ray view such that point clouds of the C-Arm device in every pose are available [15]. By seeing the virtual point cloud, X-ray technicians can reposition the C-Arm over this previously saved point cloud, resulting in an accurate repositioning maneuver.

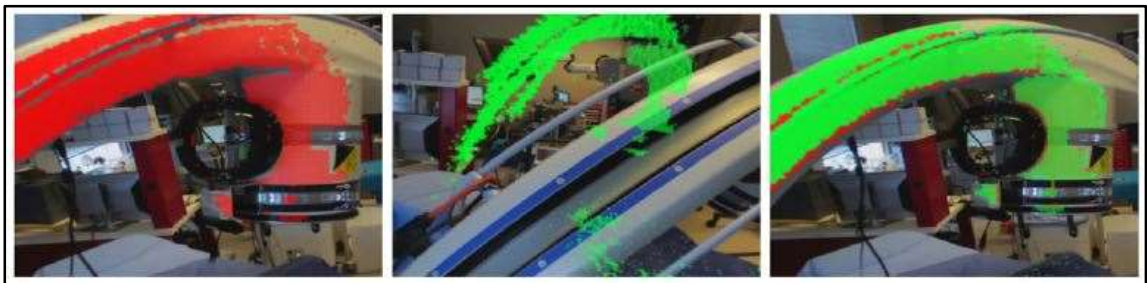


Figure 16. Point Cloud Augmentation using VR Goggles [15]

The downside of the point cloud VR repositioning methods lies with the additional hardware and software that needs to be integrated into the surgery room. For example, the X-ray technician needs to wear VR goggles through the entire duration of the surgery to see the point cloud generation. This could become tiring during long surgeries and could be a source of additional hardware maintenance. On the other hand, the surgeon who does not have the convenience of wearing VR goggles is completely out of the loop when it comes to repositioning the C-Arm. This means if there ever is a dispute between the surgeon and the X-ray tech in terms of repositioning the C-Arm, both cannot see the same screen or data in order to reach a quick consensus. In short, the accuracy and reliability of vision-based simultaneous localization and mapping seem yet insufficient to warrant immediate clinical deployment [15].

Simpler ways of repositioning have also been proposed by adding additional robotic movements to the C-Arm. The mobile C-Arm is modeled as a redundant robot by adding three more DOF onto the base. It significantly increases the flexibility and mobility in the congested operating room [16]. However, the installation of a second maneuvering system is time intensive and makes the five DOF of the original C-Arm completely redundant. Such a solution is acceptable for a short-term solution, but the cost and space associated with this addition is no long-term solution.

The best lead in repositioning was developed by the University of Tennessee in the end of the year 2013. Researches adopted the mocap system that uses IR-markers on surgical tools or on the patient's skin to trace the movement and position of the C-Arm. This method is the most promising thus far because these marker systems already exist and are deployed in the surgery rooms. By also considering the C-Arm as a surgical instrument itself and placing markers on key points of the C-Arm as shown in Figure17, surgeons and X-ray technicians use mocap systems such as Vicon to trace the exact kinematic position when X-rays are taken.

Using the known locations of each image operators would take a multitude of X-ray images at different C-Arm positions to create a 3D rendering of the area of interest. This newly developed 3D rendering would then be combined and calibrated with previous MRI or CT images allowing for better repositioning.

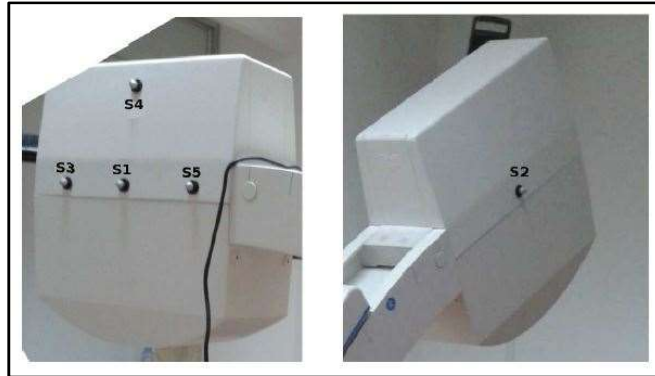


Figure 17. C-Arm X-ray System with Vicon Motion Capture IR-Markers [16]

This method of reposition is of high accuracy, but it is not without significant downsides. The biggest downside is the radiation required to develop a 3D rendering from a multitude of X-ray images. To develop a proper 3D rendering from 2D X-ray imaging, a larger set of 40 images is required as shown in Figure 18. The high number of X-rays produce a significant amount of radiation at the benefit of simpler repositioning.

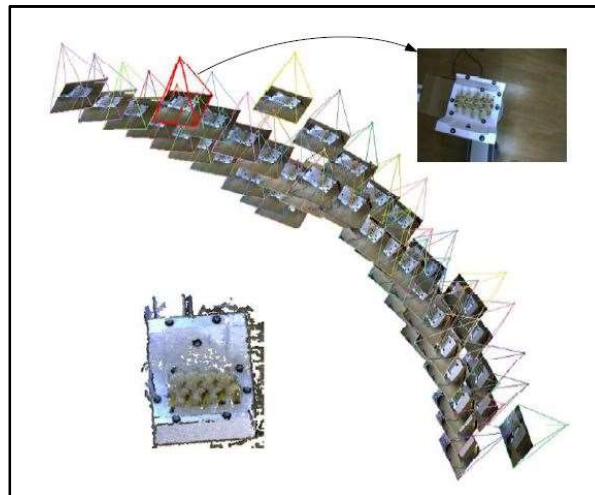


Figure 18. Process of 3D Rendering from Multiple X-ray Imaging [16]

Interestingly, German researchers have developed an inverse kinematic system of the C-Arm that allows for automatic repositioning. This system works by extracting camera footage that are integrated with a Time of Flight (ToF) sensors that recognize individual body parts of a patient [17]. This camera is placed on the ceiling of the operating room right above the patient to allow for proper viewing of the patient's body. Next, the system is calibrated using a coin as shown in Figure 19.

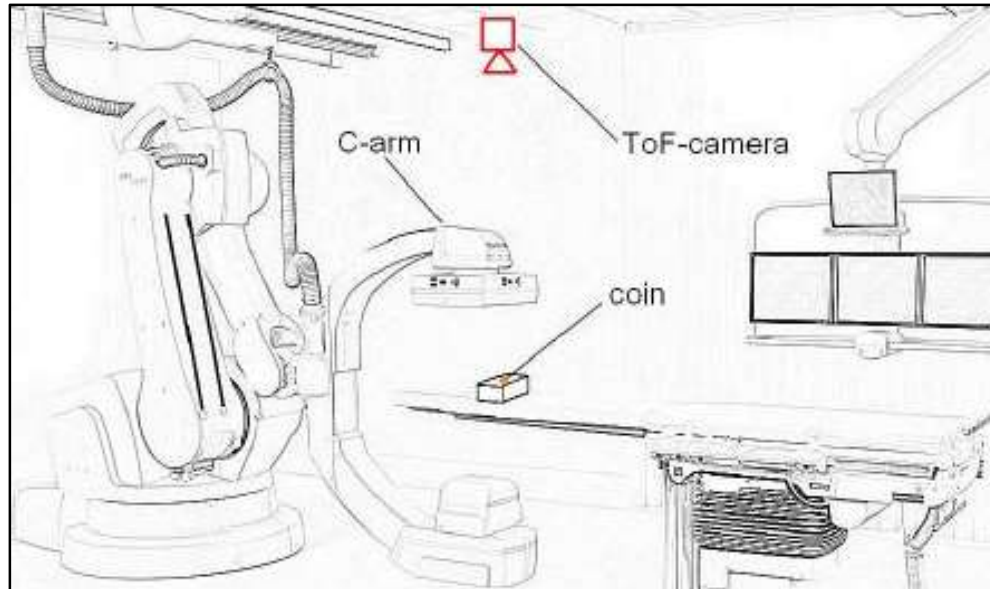


Figure 19. ToF Coin Calibration for Human Body Part Detection [17]

Once the calibration is completed, the integrated ToF system allows for the C-Arm to recognize the patient's body parts and their respective position, thereby allowing the C-Arm to automatically position itself to the patient. This ToF system, however, cannot see the outline of the patient with enough accuracy to be useful during surgery. Once a body part is detected, a rectangular area is designated as the region for that body part, meaning that the accuracy is severely limited. The view of the ToF system and each rectangular body part segment can be seen in Figure 20. It is important to note that the accuracy of repositioning with this system is too low and that each body part has a large area designated to it.

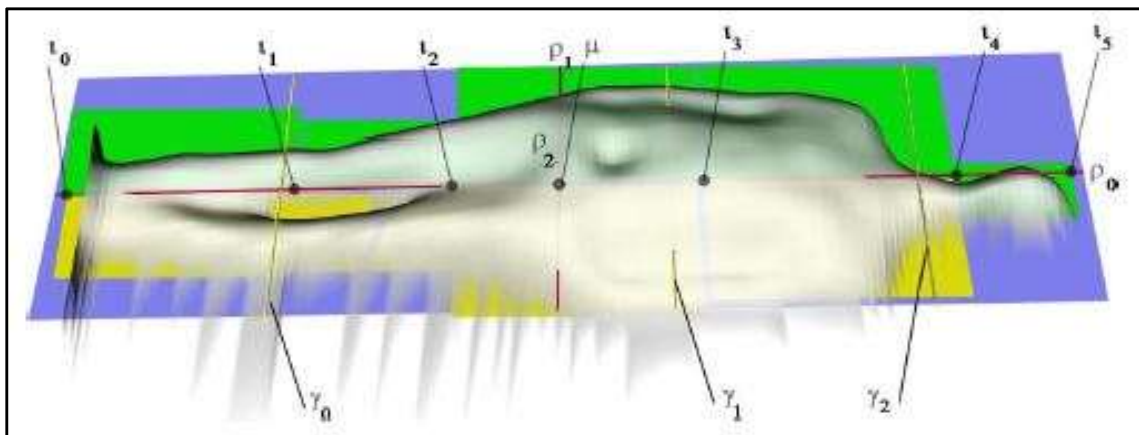


Figure 20. Body Segments Recognized and in Space Using ToF Integration [17]



### 2.2.4 C-Arm Training for Surgical Personnel

To improve image quality surgeons and X-ray technicians undergo extensive training. This training is to foremost familiarize the surgeons and technicians with the operation of the C-Arm and therefore improving efficiency. Proper training of the surgeon is the best way of reducing radiation exposures to the patients. However, the more time surgeons and X-ray technicians spend in training, the more time they must spend under radiation themselves. In order to battle this problem, radiation free methods of training have been developed that still provide quality experience to surgery personnel.

C-Arm fluoroscopy simulators have been developed to ensure radiation free training for surgery. To improve training in C-Arm operation, the Virtual X-ray computer-based training system was developed by an interdisciplinary team of medical informatics specialists, trauma surgeons, and radiologists [18]. This new system, much like other systems of its kind, use an integrated or custom GUI. The shift to use computer simulations and graphics for training has become more popular not only because it reduces radiations but also because it shows improved training results.

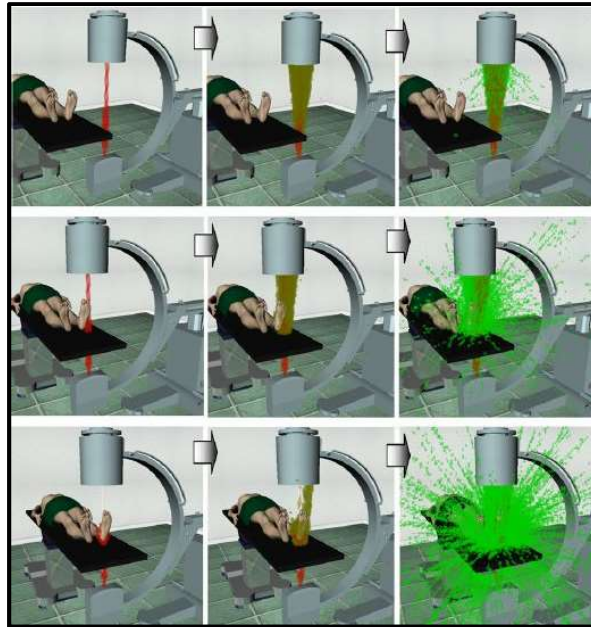


Figure 21. Scattering of X-rays during C-Arm use [18]

The use of computer-based simulation seems to be an especially important factor in the success of radiology training efforts [18]. In addition to improved none radioactive learning, these simulation training systems show surgeons and X-ray

technicians a visual representation of the X-ray radiation during C-Arm fluoroscopy. These visual effects, shown in Figure 21, are not essential to learning the operation of the C-Arm but show surgeons and X-ray technicians the scattering and intensity of X-ray imaging. By understanding the radiation dynamics of the C-Arm better, it is hypothesized that surgeons will develop a bigger respect for X-ray imaging and thereby reduce the radiation exposure to patients and the surgery personnel.

In addition to VR supplementation, hands on and radiation free methods of training have also emerged. These hands-on radiation free training programs have come to use as a byproduct of radiation free C-Arm reposition systems. So called Mixed-Reality training systems make use of camera augmentations in combination with IR-marker based positioning to provide a radiation free yet interactive surgery environment for training. Simply explained, by prior knowledge of the 3D printed spine parts, the kinematics of the cone beam, and IR-marker calibrated tools, the surgeons can receive pseudo X-ray images from any position they place the training C-Arm in. Images of such training can be seen in Figure 22 below; however, it is important to note that such accurate positioning without the use of X-ray is only possible because the 3D rendering, and the 3D printed spine segments are fully known and exactly placed on the operating table. This cannot be done with an actual human body, reverting surgeons back to less accurate and more radiation intensive reposition during actual surgery.

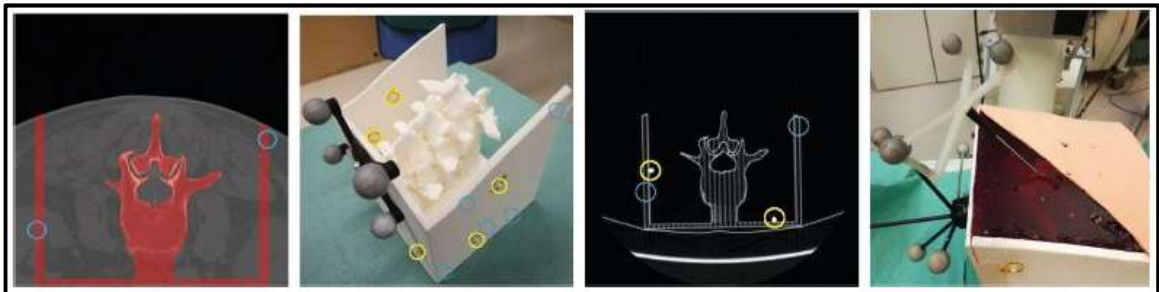


Figure 22. Elements of Radiation Free C-Arm Training for Spine Surgery [19]

### 2.3 Kinematics and Robotics

The word 'robot' came into existence sometime between 1920 and 1940. The first robots were very simple and had at most 3 or 4 DOF. The push to improve robotics came from the executive branch of government. This push originated mostly from the arms and the space race where problems needed to be solved in space crafts or on satellites without human access. The solution to these problems led to the first

Programable Universal Machine for Assembly (PUMA), a robot arm capable of maneuvering and solving problems by the application of different programs shown below in Figure 23. However, the application of robotics for medical and surgical use is relatively new in the last 30 years [20].



Figure 23. Programable Universal Machine for Assembly [20]

To manipulate and move the robots, new and faster methods of kinematics had to be developed that would predict the robot's movement as accurately as possible. Robot kinematics is separated into two main sections, the forward kinematics and inverse kinematics. Forward kinematics, being the easier one of the two to calculate, concerns with the movements of the robotic joints to predict the exact location and movements in Cartesian space, whereas the inverse kinematics attempts to model the joint movements of the robot base on imported Cartesian values. Inverse kinematics problems are split into two branches, the ones that can be solved analytically, and those that need to be solved numerically. [21] The relationship between the forward and inverse kinematic modeling is represented in Figure 24.

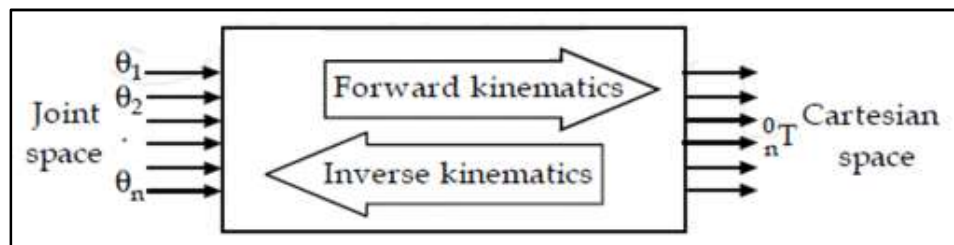


Figure 24. Relationship of Forward and Inverse Kinematics [21]

These forward and inverse kinematics modeling systems have been further improved to include Cable-Driven Parallel Robots. Parallel robots are robots in which the actuation occurs from cables that change their lengths and thereby pull an interest point or object into different directions. This results in the ability to maneuver in cartesian space based on stationary motors. This method shown in Figure 25 has the advantage of low settling time since each DOF uses the dampening of two motors at once. Other advantages include accurate maneuvering since the mechanical slack is significantly reduce by the tension proved in the cables.

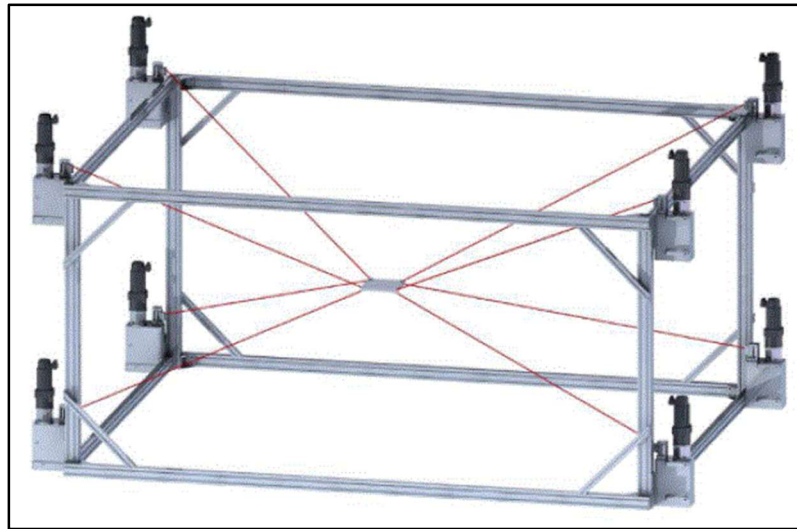


Figure 25. Cable-Driven Parallel Robot [22]

To further expand, each set of kinematics, forward or inverse, comes with its own specialized kinematic formulations. These formulations consist of the mathematical model, position kinematic model, differential kinematic model and the dynamic model. The mathematical models are subdivided into two further distinct groups called the geometric and the dynamic models. The geometric models are mainly concerned with positions of the robot, and dynamic models are concerned more with the movement vectors in space. Position kinematic models establish mathematical relation between joint angles and position whereas the differential kinematic models produce the velocity vectors of selected regions. Finally, dynamic modeling uses the position and the differential models to produce acceleration and force requirements for the selected robots. The dynamic models, which concern themselves with inertia and force, can be used to determine the optimal motor and power requirements for each robotic joint [23].

Traditionally, the solution to kinematics has always been solved through referencing stationary points or through using accurate sensors. However, in the recent years with the development of higher computer powered artificial intelligence programs, successful attempts have been made to train robotic arms to perform [24][<sup>obj</sup>]. Currently the Artificial Intelligence Laboratory of Massachusetts Institute of Technology is developing ways to apply forwards and inverse kinematics to artificial intelligences and thereby removing the need for constant robot calibration.

Kinematics have also been combined with sensitive force sensors to provide independently moving components which allow for testing mechanisms through ranges of motion. This combination allows not only for testing various mechanism and joints but also for accurate acquisition of force and stress through the movements of those mechanism. For example, a 6 DOF robot was created in combination with force sensors to test the interaction of the ball and socket joint of the hip. The data gathered by this robotic system can in term can be used to design better hip joint prosthetics because users will have a more realistic force to position curves in real time [25]. This method has significant advantages and can be used as validation of dynamic finite element modeling. In turn, it can be seen how important robotics is becoming for the medical field. Figure 26 is the configuration of such robot systems developed to test forces in the hip joint during movement.

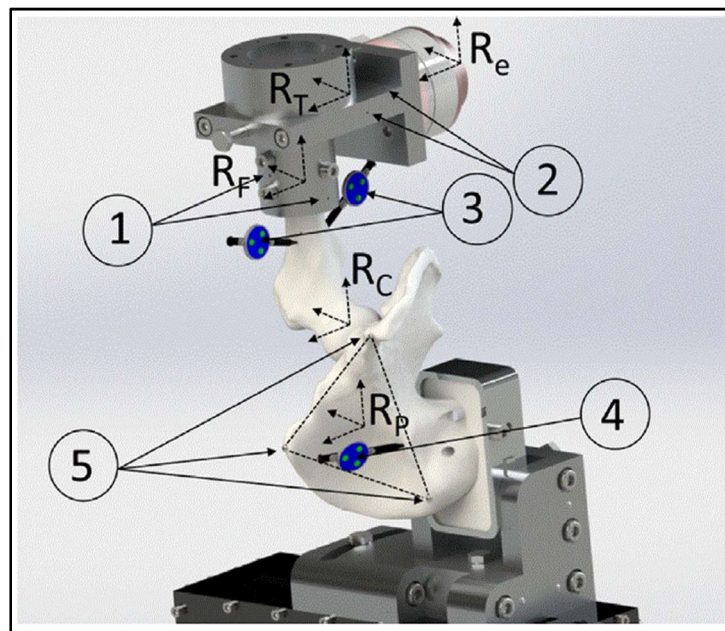


Figure 26. Robotic Hip Joint Testing [25]

## Chapter 3: Methodology

### 3.1 Objective Overview

During certain surgeries the C-Arm must be completely moved out of the way to make room for other equipment and surgical procedures. Next, the C-Arm needs to be repositioned to its previous position to take a validation X-ray image with the same exact reference to the patient. In most cases the reposition of the C-Arm is not a problem, but in certain surgeries accurate repositioning is crucial. In those cases, much time and effort are spent to accurately reposition the C-Arm to acquire a validation X-ray with the same reference frame as the preprocedural X-ray. To resolve this repositioning problem, this thesis proposed integrating the C-Arm with Vicon System.

In Figure 27, highlighted in green, it can be seen how the Vicon system will use IR markers placed on the C-Arm to acquire cartesian coordinates of each marker in the global coordinate space. These cartesian coordinates will be sent to the developed kinematic model of the C-Arm. The kinematic model will then output angles and translation vectors for the C-Arm joints to reposition the C-Arm accurately for the validation X-ray. In addition to sending the rotation and translation vectors to the physical C-Arm, the kinematic model will also send the same values to a developed virtual platform. The developed virtual platform will aid as a validation for the repositioning. Finally, a developed GUI will also provide the ability to manual repositioning of the C-Arm. This repositioning method will be the first step of accurate repositioning.

If the first step of repositioning is not accurate enough, a second step of repositioning can be used to further move the C-Arm into the correct position. This second step, shown in Figure 28 and highlighted in orange, uses deep learning and image processing to calculate further movements that need to be taken by the C-Arm to reposition it further. The blue highlighted region in Figure 28 shows the shared sections between both repositioning methods.

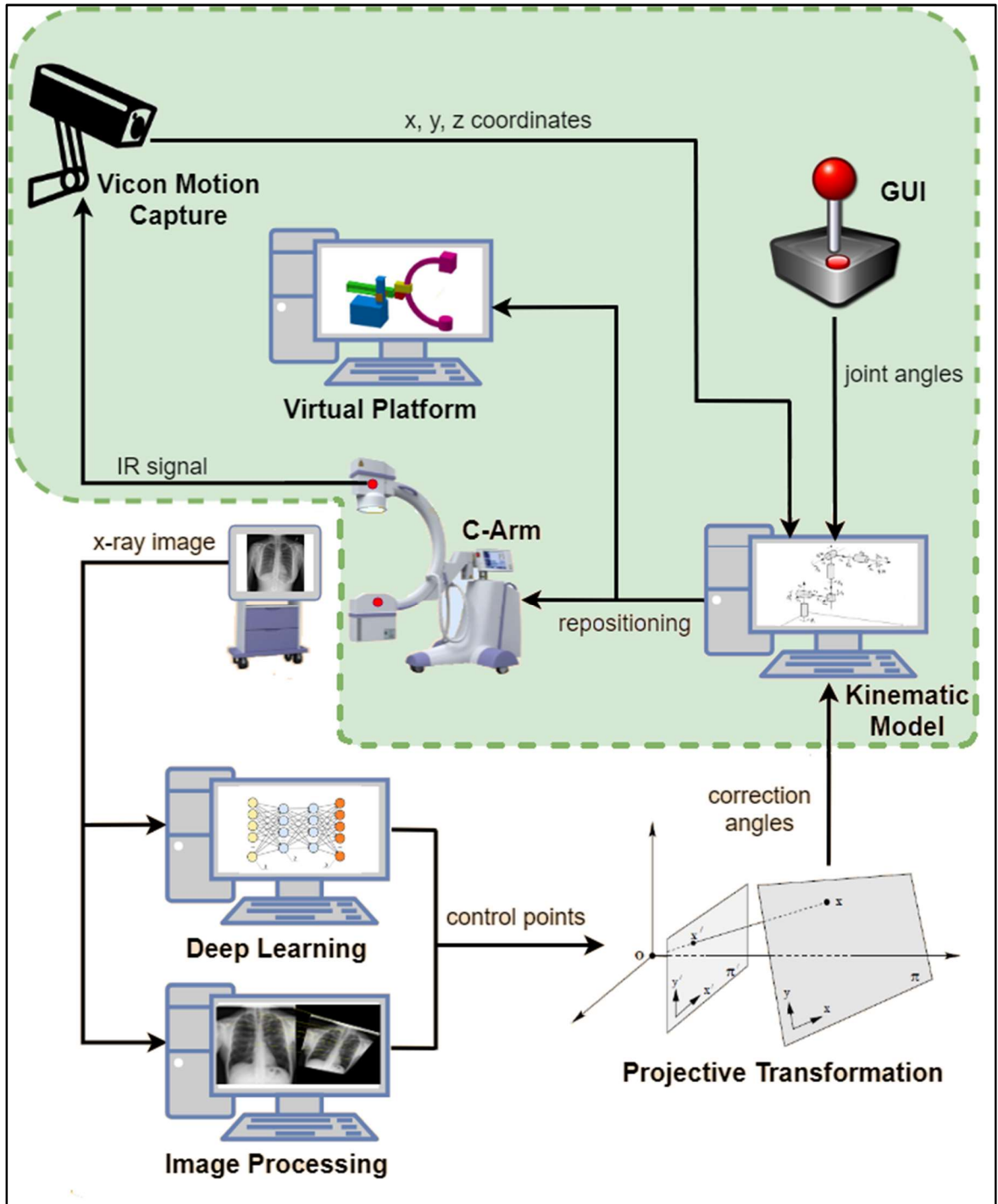


Figure 27. First Method of C-Arm Repositioning

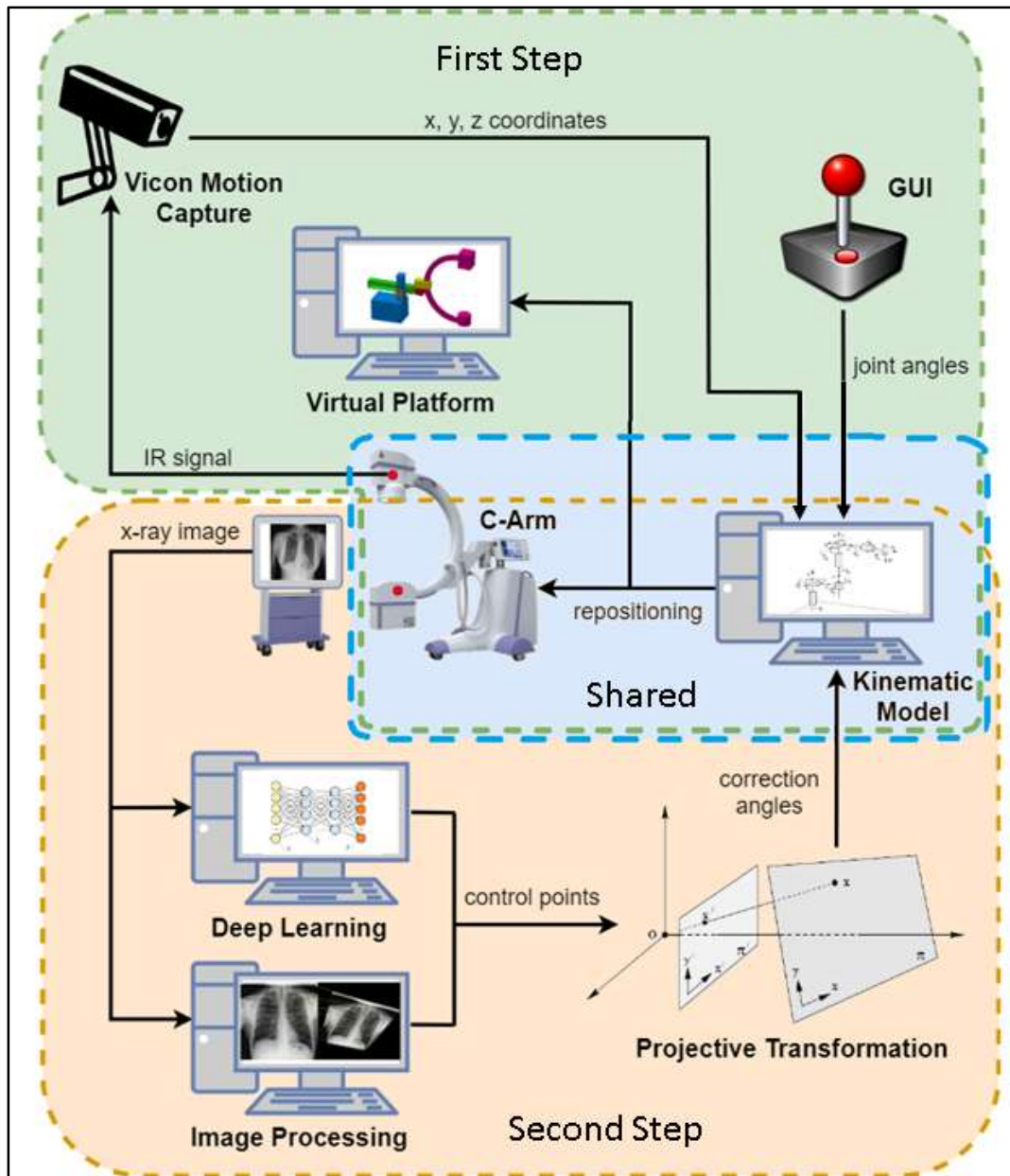


Figure 28. Two Step C-Arm X-ray System Repositioning System

This thesis will focus on the development of first step in repositioning, while the second step of repositioning will be further explained in Chapter 6, the future work. To successfully implement the first step in C-Arm repositioning a set of tasks need to be completed. These tasks include the following: development of the Virtual Prototype and Virtual Platform (VP), development of the C-Arm Kinematic Model, design and manufacturing of a C-Arm Physical Prototype (CAP), and finally the Integration of all these subsystems with Vicon system.



## 3.2 Virtual Prototype and Virtual Platform

### 3.2.1 C-Arm Virtual Prototype

Virtual simulations have changed the pace of design realization significantly for the faster. By using computer programs to model design ideas, engineers can estimate feasibility of future design with greater confidence. In addition to future design estimation, virtual modeling can help engineers better understand the problems they are trying to overcome or design problems they are trying to communicate to others.

For the case of the C-Arm, the virtual model became the first natural step in developing and proposing a better solution than current available models. The virtual model would provide an accurate description of the functions and demands of the C-Arm. These functions include the physical demands of joints and possible modeling for the control system.

First, using standard computer aided design (CAD) software, the general shape and functions of the C-Arm were developed. The virtual model consists of general and simple geometric shapes. Since the C-Arm Virtual Prototype (CVP) is not used for the actual manufacturing of the physical prototype, it is, therefore, beneficial to keep the components as simple as possible. Simple components are easier to draft in CAD programs and allow for faster processing time during virtual simulations, giving further reason in keeping the virtual model as simple as possible. The Autodesk Inventor assembly of the CVP can be seen in Figure 29 below through the isometric view. All other views can be seen in Figure 30.

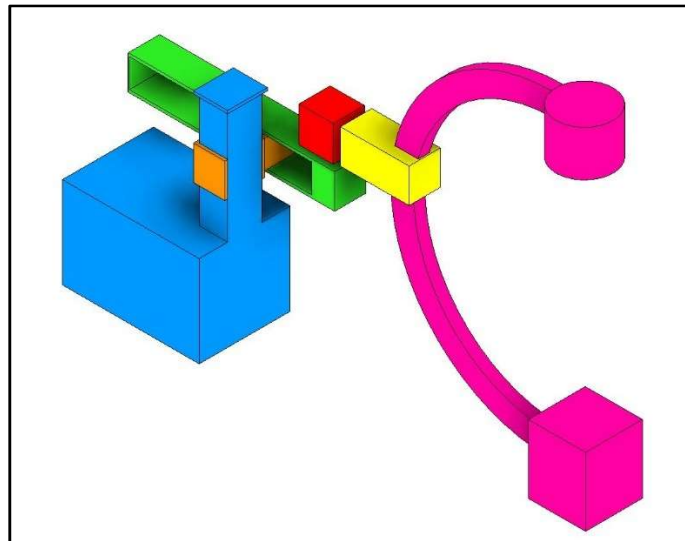


Figure 29. Isometric View of C-Arm Virtual Prototype

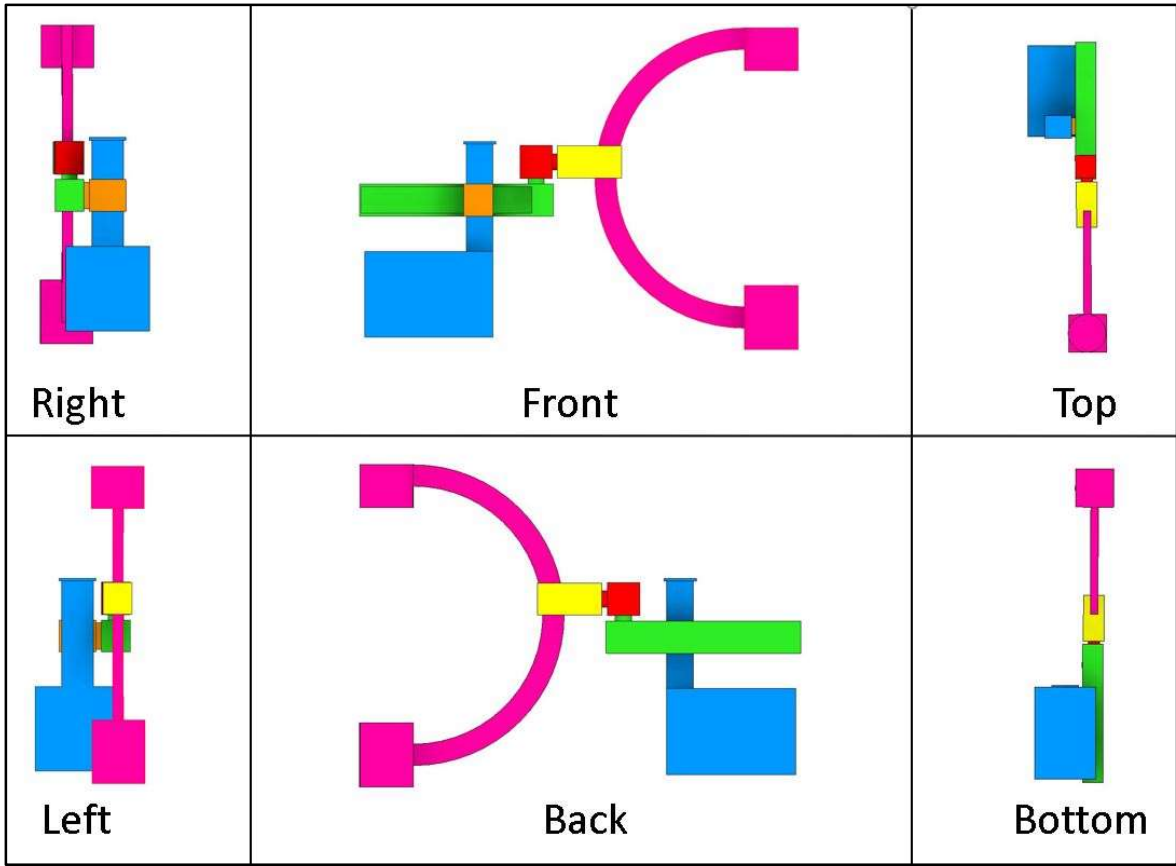


Figure 30. Different Views of the C-Arm Virtual Prototype

It is important to note that the CVP has as few components as possible. This is also a key factor in the simplicity of the model. The total number of parts for this model is six components, and these six components allow for a total of five DOF. Two translational DOF and three rotational. All DOF were adapted from currently used C-Arms to provide realistic feedback of the mechanics and kinematics. The virtual model will be the key component in the extended development of the VP; therefore, the correct use of each joint and feedback are important. The DOF of the C-Arm virtual model can be seen in Figure 31. The small green and red arrows show how the individual joints move in space. This visualization allows not only for better understanding of the C-Arm kinematics but also allows for quick visual inspection in case one of the joints does not follow a realistic model or DOF.

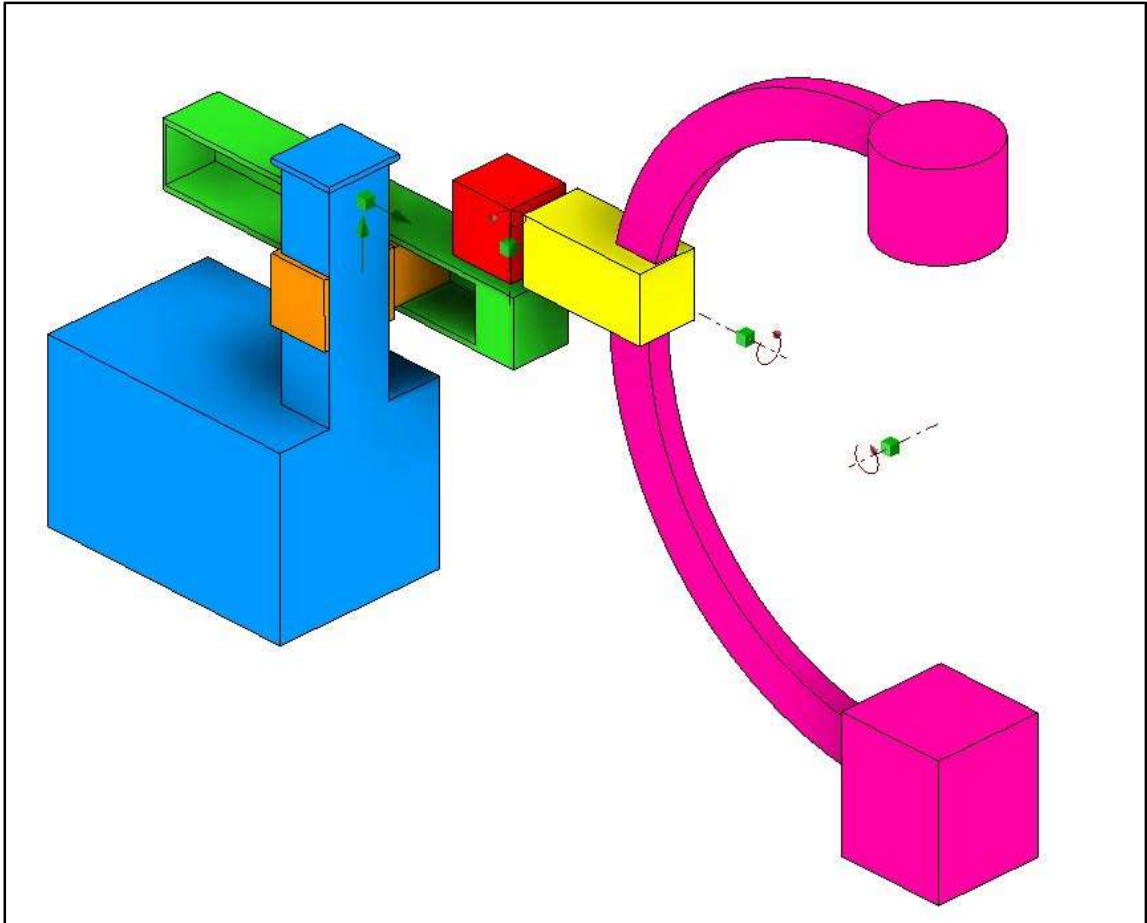


Figure 31. C-Arm Virtual Prototype with Visible Degrees of Freedom

### 3.2.2 Virtual Platform

#### 3.2.2.1 Virtual Platform Physical Setup

The VP is to represent how an actual C-Arm would behave in an operating room during surgery. The more realistic the VP, the more insight to the real scenario can be obtained, however, after a certain threshold the margin of returns is reached. This means that no significant gain will be provided after a certain level of detail is reached in the VP.

For this project, it was decided that the VP should include a surgery room with a fixed operating table. In addition, a human manikin placed on the operating table will aid in how the real C-Arm maneuvers around a person in surgery. Lastly, six cameras are fixed around the surgery room to represent the aid of a motion capture system in the repositioning of the C-Arm. The virtual set up of the room can be seen in Figure 32.

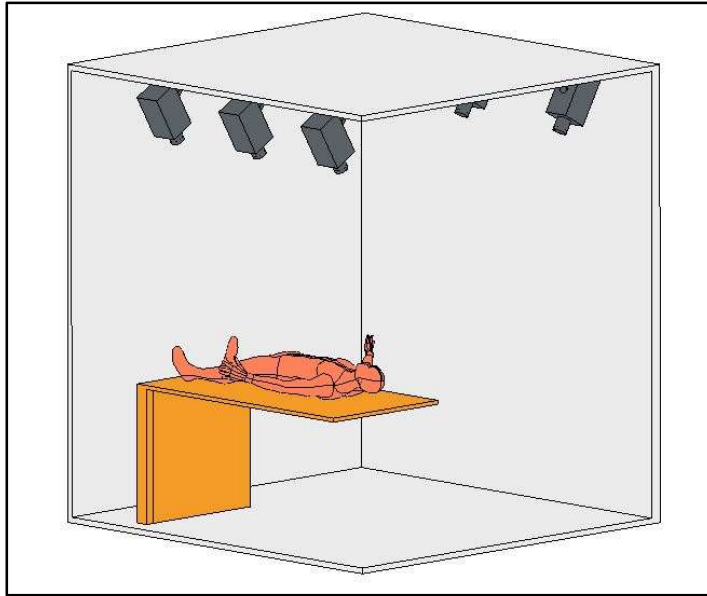


Figure 32. Surgical Room Setup for the Virtual Platform

The full set up of the VP includes a physically accurately surgical environment and a fully mechanically functioning virtual C-Arm. This combination can be seen in Figure 33, where the surgical room and its components are completely stationary, and the CVP is a movable and dynamically realistic model.

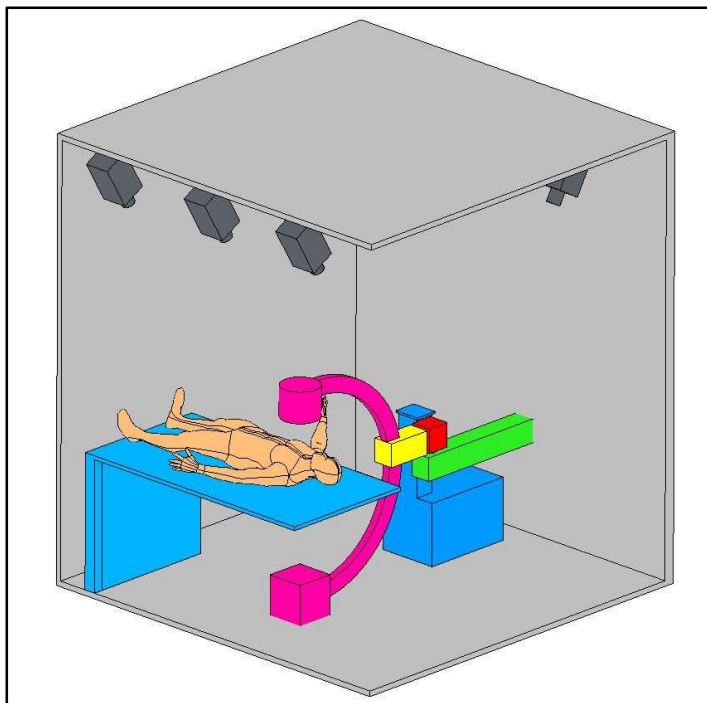


Figure 33. Virtual Environment of the C-Arm X-ray System

### 3.2.2.2 Virtual Environment Visually Generated Computer Model

In the VP, specific rules and equations govern the interaction of individual components and joints to provide a realistic feedback to the user. For example, limits in the joints need to be specified or else users might get a wrong impression of the way the real C-Arm behaves during operation. Additionally, each joint is given a mathematical function to ensure proper mechanical function that translates to a visual representation in the VP.

To generate the VP, visual coding was used in MATLAB/Simulink. First, the CAD assembly of the surgery room and the CVP were given appropriate mating constraints that would be automatically recognize by Simulink. Then, by using Simscape Multibody, a MATLAB/Simulink extension package, the CAD assembly was converted into an Extensible Markup Language format (xml) file. This extension is a conversion of a CAD model to a mathematical/numeric matrix system, allowing for custom programming in MATLAB/Simulink. Finally, the xml file is uploaded into Simulink, allowing for a block diagram representation of the generated code and allowing for easy user input to change variables in the code. Below, in Figure 34 is the MATLAB/Simulink subsystem block network diagram of the virtual system and CAD model interaction.

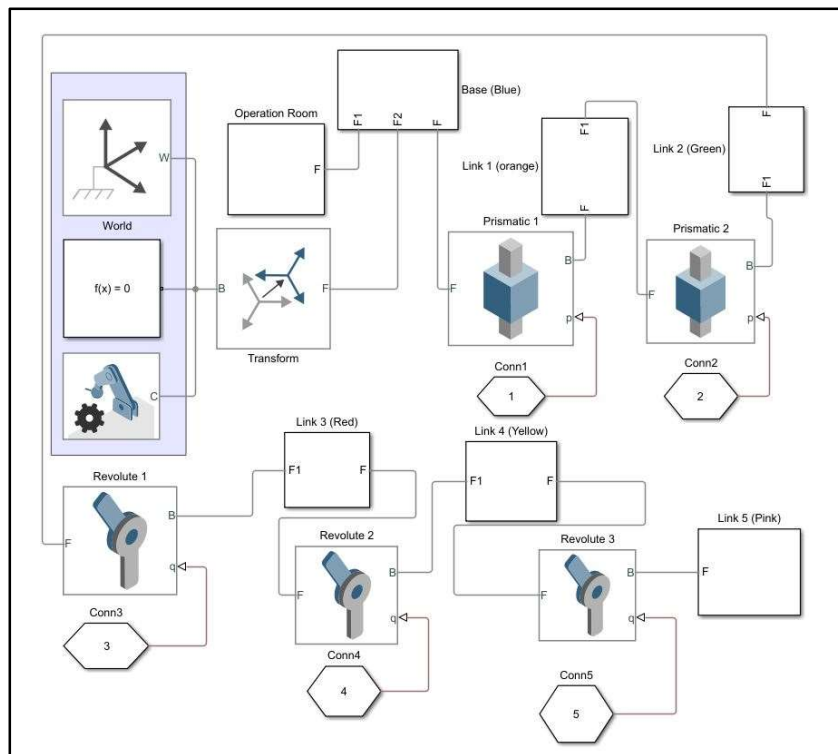


Figure 34. Simulink Block Diagram of the Visual System and CAD Model Interaction

In this visual code, the two translational linkages and the three rotational joints can be seen. The digital input to each joint is represented by five individual hexagonal blocks. The three blocks in the highlighted region represent the 3D world frame, MATLAB solver, and mechanical configuration block. All other blocks are block diagram representations of the six CAD components that make up the virtual C-Arm and the operation room. The rest of the Simulink modeling can be found in Appendix B.

### 3.2.3 Virtual Platform GUI

To acquire quality results from the VP, the C-Arm virtual model needs to be maneuvered by a human user. This led to the development of a GUI for the VP. The GUI will allow users to input desired translational locations and desired angular vectors to the virtual model. This input will allow the Simulation to react to the desired user input and maneuver the C-Arm virtual model through the VP.

It was chosen that the best way for a user to input their desired data is through manual sliders. These sliders will be actuated through the click and drag of the mouse with tick marks showing the graduated values that the user is selecting into the program. Once an input is made, the program runs and mechanically moves the virtual C-Arm through the VP with the appropriate force, acceleration and position predictions. These results can then be fed back to the user through the GUI. In the developed GUI for the VP the X, Y, and Z coordinates of the origin of the hypothetical X-ray cone beam and the coordinates of the region of interest are given. Below is a screenshot view of the VP GUI with labeled sliders and coordinate outputs.

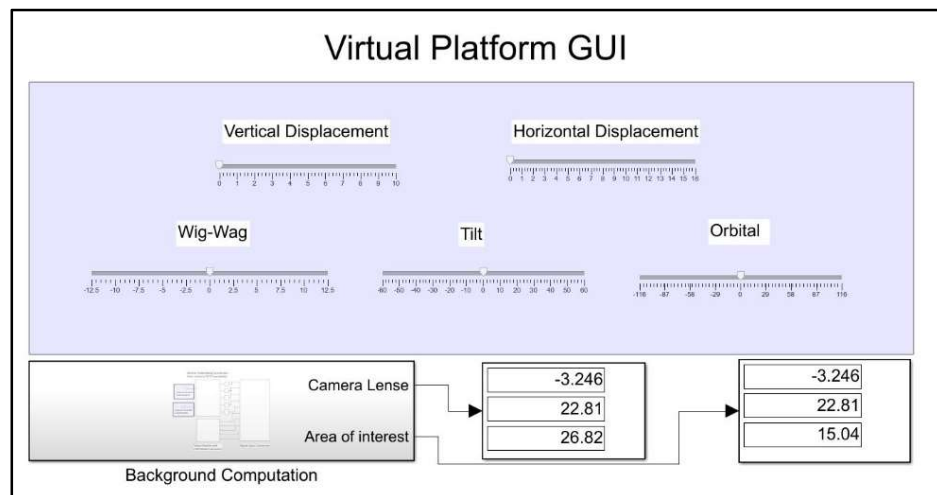


Figure 35. Virtual Platform GUI (all joints set to zero)

Finally, when the user maneuvers the GUI, Simulink produces a simulation of the C-Arm movement in real time. This simulation in addition to the virtual data allows for users, experienced or unexperienced, to understand what the strengths and weaknesses of the design are. Figure 36 shows the visual simulation results of the program according to the GUI input values. Four views are automatically generated to show in detail how the GUI input values move the CVP.

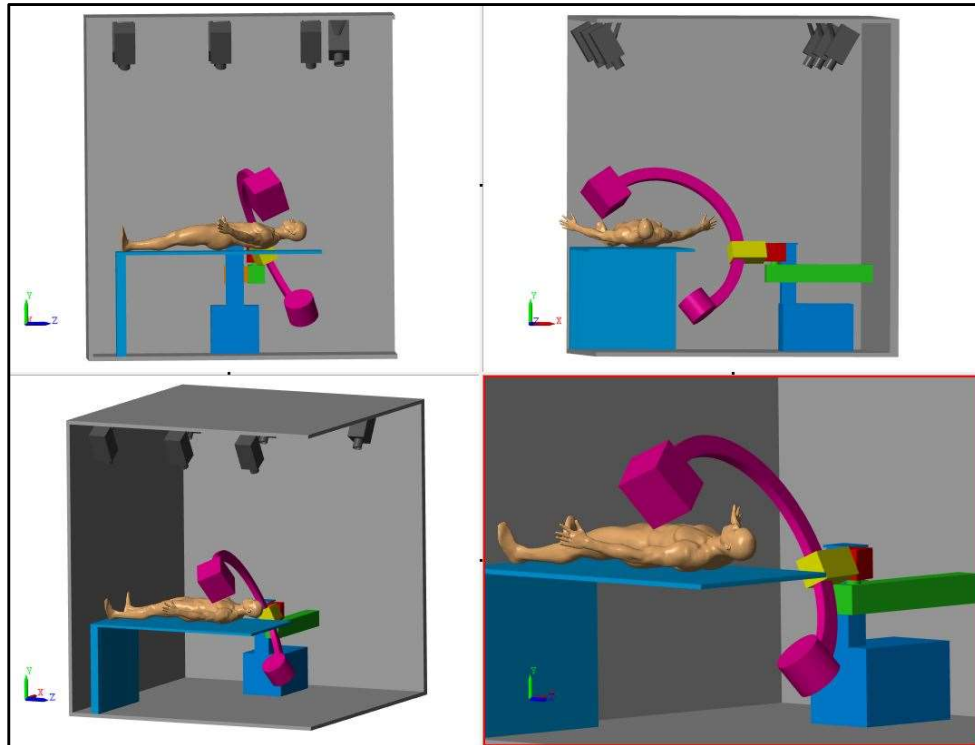


Figure 36. Simulink Virtual Platform Simulation

### 3.2.4 Virtual Platform Advantages and Results

Much useful information can be derived with the configuration of the VP. For example, by applying a general mass values to each virtual component in the Simulink modeling, the required torque or force for the actuation of each joint can be estimated. In addition, these results can be used to determine the appropriate motor size for prototype development and material selection. Foremost, the Simulink modeling can aid in the development of a feasible control system for any kinematic control model. As a preliminary study, various control system blocks were applied to the CVP to determine what kind of control system would best suit for the future development of a possible physical prototype.

The preliminary study considered applying three different controllers to the CVP. These included a proportional (P) controller, a proportional and integral (PI) controller, and a proportional, integral & derivative (PID) controller. In a virtual experiment, the CVP was maneuvered and its mechanical behavior analyzed to determine what kind of controller would best suit a physical prototype of the C-Arm. The results concluded that a PID controller would best suit the movement of the CAP because of its small settling time only if fast mechanical reposition is priority. The comparison results of the position vs time are in Figures 37-39, while the torque vs time comparison results are in Figures 40-42.

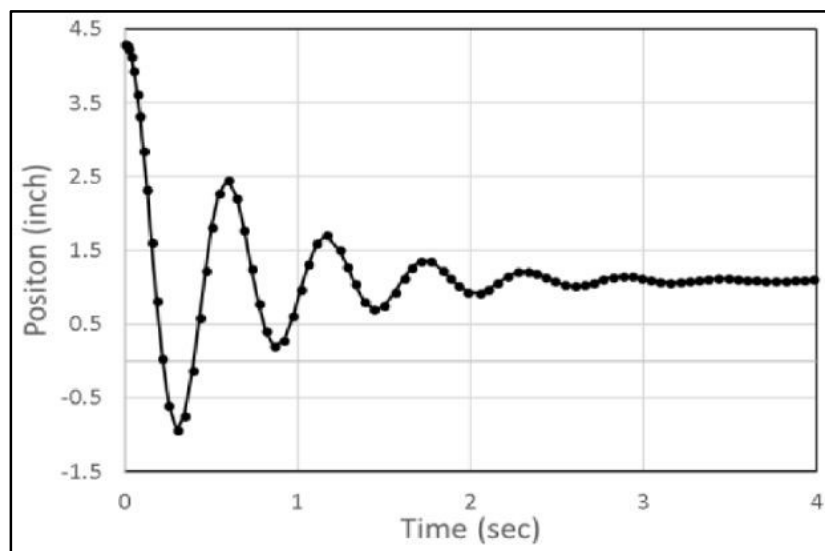


Figure 37. Position vs Time Graph using P Controller [12]

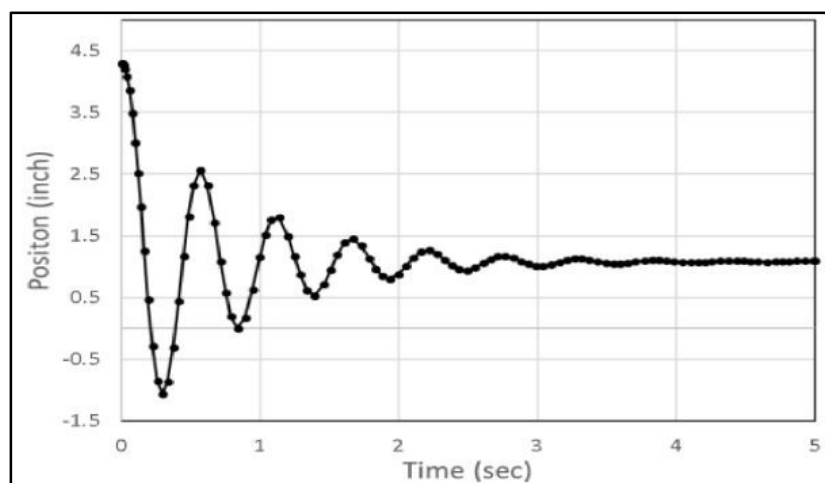


Figure 38. Position vs Time Graph using PI Controller [12]



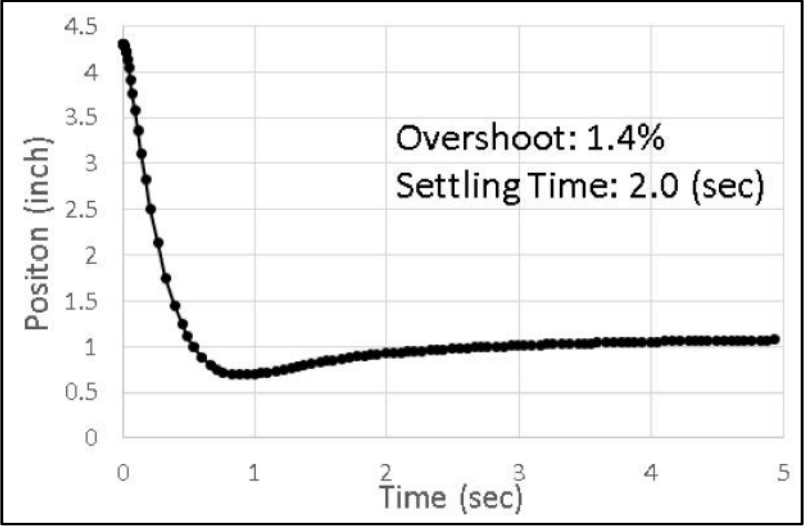


Figure 39. Position vs Time Graph using PID Controller [12]

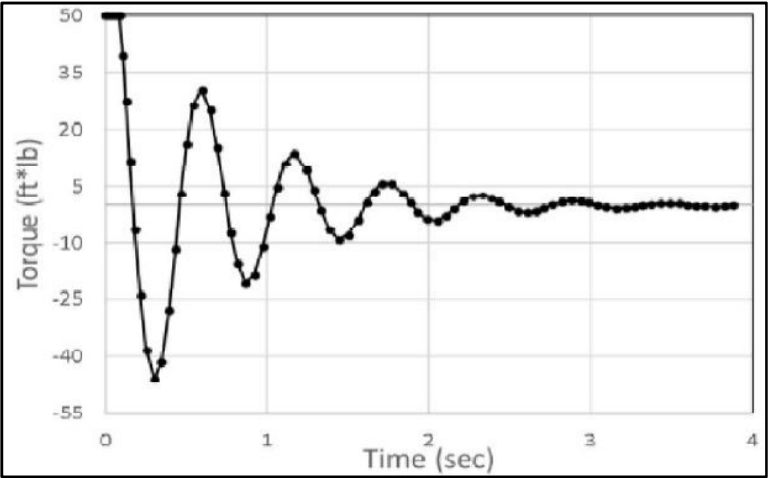


Figure 40. Torque vs Time Graph using P Controller [12]

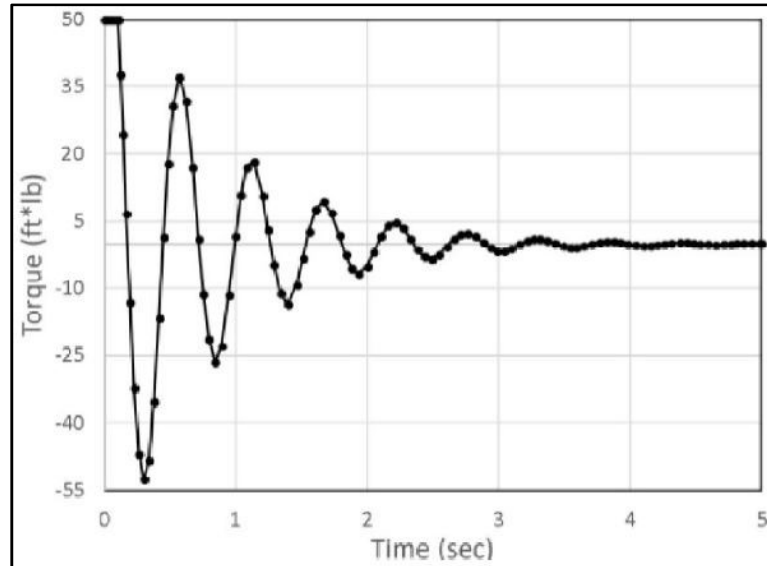


Figure 41. Torque vs Time Graph using PI Controller [12]

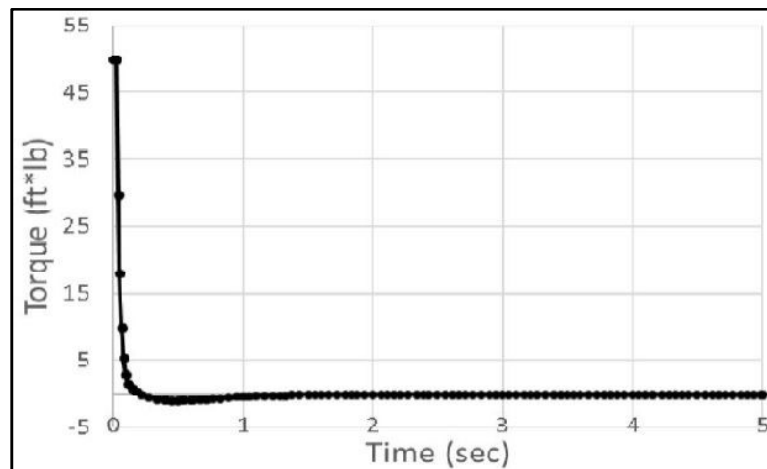


Figure 42. Torque vs Time Graph using PID Controller [12]

The results of the preliminary study showed that the PID controller would have the fastest results in repositioning the C-Arm; however, the PID controller did not provide any torque values that are significantly lower than other control options, meaning that either a gear system or a pulley system needs to be used to increase torque output from the motors to actuators and joints. This information turned out to be a significant factor in developing the CAP.

### 3.2.5 Comment

By completion of this first task it is obvious that the C-Arm VP does in fact help enormously with the upcoming design process decisions. In addition, it can be inducted that the VP is indeed a reasonable method to test and validate a custom-built GUI for the purpose of robotic C-Arm manipulation.

## 3.3 Kinematic Modeling of C-Arm

### 3.3.1 Kinematics Approach

To reposition the C-Arm accurately, C-Arm movements in space must first be established. Because the C-Arm is essentially a robotic arm, the kinematics of the C-Arm can be generalized as the kinematics of a robotic arm. Kinematics is defined as the study of possible movement and configurations of a system [26]. The C-Arm only uses translational and rotational joints, something typical for most robotic arms. However, a closer look at the most common type of robotic arms shows that the C-Arm is not the typical robotic arm. Figure 43 shows the common types of robotic arm. These common robotic arms can be compared to the CVP in Figure 31.

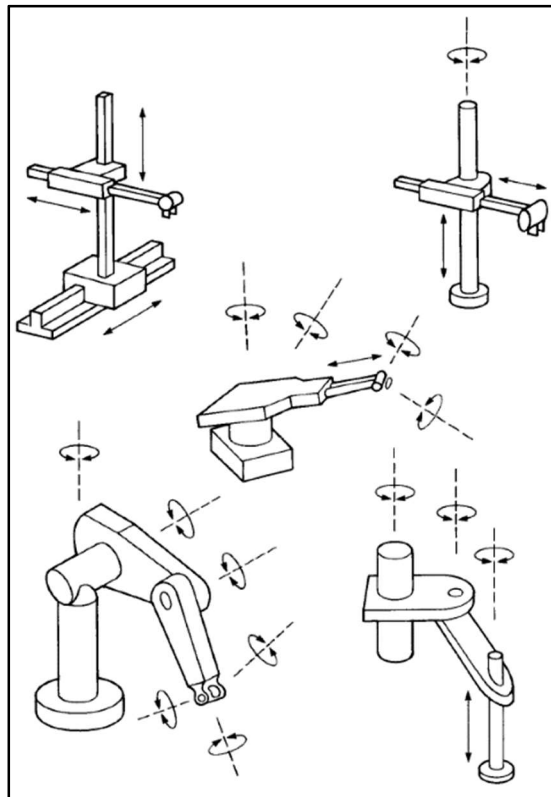


Figure 43. Common Types of Robot Design [26]

No matter how complicated the geometry of a robot, the links can always be generalized by the Denavit and Hartenberg (DH) link parameters. The DH link parameters and simple serial joints by applying a hand full of simple parameters. The first parameter is the angle of the joint of interest. This angle is always expressed about the local Z-axis or axis of rotation of the joint. The second parameter is determined by the length of the interested joint form its previous link along the Z-axis. Finally, the angle and length offsets about the respective X-axis determine the radius offset and altered orientation for the joint. Figure 44 below shows how the parameters for the joint  $j$  are obtained and represented, where joint  $j-1$  is the previous joint and  $j = 1$  is the following joint. Link  $j$  is assigned to be the link for joint  $j$ . Theta represents the joint angle and alpha shows the rotational offset of a joint form its previous link. The distance  $d_j$  and  $a_j$  show the offset of the Z- and X-axis, respectively.

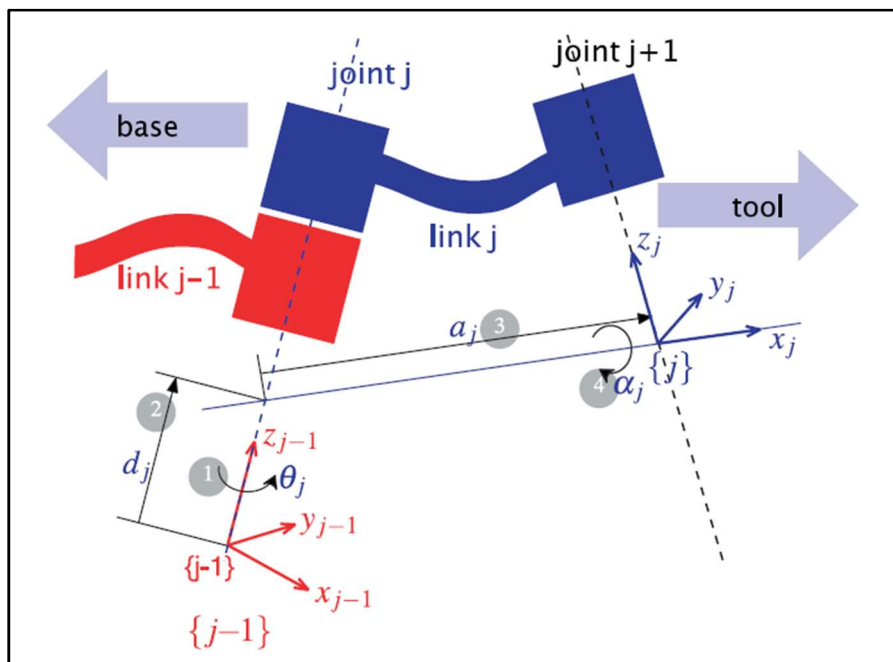


Figure 44. Denavit Hartenberg Joint Parameters [27]

### 3.3.2 Forward Kinematics

After developing the CVP and observing the movements in MATLAB Simulink, the forward kinematic model of the C-Arm was developed by applying the DH joint parameters. Thus, this kinematic model enabled the C-Arm to simulate 5 DOF of its movement, which include two prismatic and three revolute joints.

The prismatic joints move the C-Arm vertical and horizontally. The three revolute joints provide roll, pitch and yaw for the C-Arm camera X-ray source. In colloquial terms, those three revolute joints perform wig-way, tilt, and orbital rotations. Wig-way corresponds to the yaw, tilt for the roll, and orbital movement for the pitch.

To develop the kinematics, first a reference point was selected to be the origin for the C-Arm local coordinate system. From there on, all subsequent joints were modeled as shown in Figure 45.

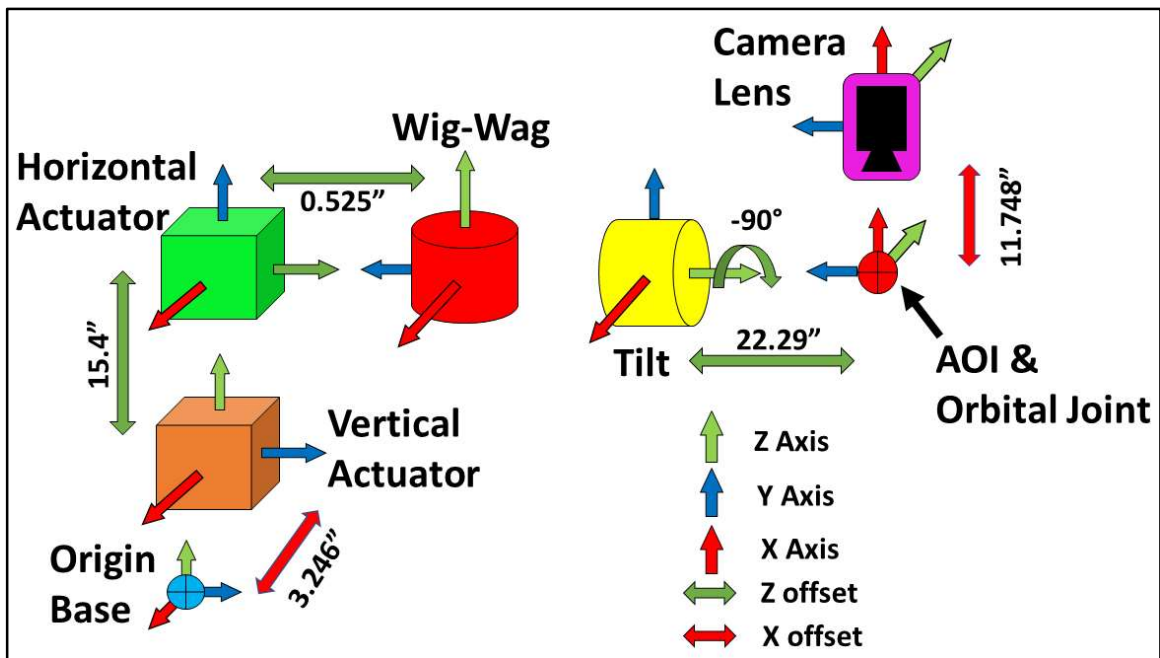


Figure 45. C-Arm Kinematic Model

Because access to a real C-Arm for a graduate student is extremely limited, the offset and length values used in the kinematic model are based on the CAP. This prototype will be further introduced in the subsequent sections. To keep the kinematic model as intuitive as possible, the same colors as the CVP were used to represent each kinematic section. A reminder for these colors is available in Figure 31.

In the kinematic model depicted above, just like the traditional DH parameters, the Z-axis is the line of action either by rotation or translation. The cubes represent prismatic joints and the cylinders represent revolute joints. It is important to note that the orbital joint does not exist in a physical manner and is represented by a hypothetical joint location at the center of the orbital movement [28]. The orbital joint is also naturally the

center of the “C” shaped orbital link, making it the desired focal point for X-ray imaging or the Area of Interest (AOI). Lastly, the end effector of this robotic arm kinematic model is the tip of the beam cone discussed in the literature review shown in Figure 8.

At this point, it is good to remember that the whole purpose of the repositioning the C-Arm accurately is to take an image of the same point with the same orientation as the pre-procedural image. With this in mind and with a good look at the kinematic model, it can be concluded that the only two points that need to be accurately repositioned for the purpose of X-ray imaging are the AOI/orbital joint and the camera lens/ end effector. In other words, if the C-Arm camera lens and the AOI are properly positioned, a quality repositioned X-ray can be taken. This reasoning is also exactly why the GUI for the CVP, shown in Figure 35, and the GUI for the CAP, shown in Appendix B, in Figure 81, only output the coordinates of the camera lens and the AOI.

### 3.3.3 MATLAB Script for C-Arm Forward Kinematics

Once the critical requirements of the kinematic model were identified, a mathematical model using the DH parameters was developed. This, in turn, was used to calculate the critical coordinates of the camera lens and the AOI. A MATLAB script was written that uses the input vales of joint translations and joint rotations from the GUI and calculates the final cartesian positions of critical points. The full MATLAB script can be found in Appendix C, where GUI joint values, selected by the user, are combined with the DH parameters in the DH transformation matrix, giving an output of desired cartesian coordinate points.

The DH transformation matrix, shown in Equation 1, makes use of the DH parameters to extract cartesian position and orientation of subsequent joints based on GUI manipulations. This extraction is symbolized as  ${}^{j-1}A_j$ , where  $A$  is the transformation of joint  $j$  relative to the previous joint  $j - 1$ .  $\theta_j$  represents the actuated angle of a joint based on the GUI input.  $d_j$  is the length offset combined with the translational movement along the Z-axis for the respective joint, and  $\alpha_j$  is the perpendicular offset along the X-axis for that same joint, respectively.

$${}^{j-1}A_j = \begin{bmatrix} \cos\theta_j & -\sin\theta_j\cos\alpha_j & \sin\theta_j\sin\alpha_j & a_j\cos\theta_j \\ \sin\theta_j & \cos\theta_j\cos\alpha_j & -\cos\theta_j\sin\alpha_j & a_j\sin\theta_j \\ 0 & \sin\alpha_j & \cos\alpha_j & d_j \\ 0 & 0 & 0 & 1 \end{bmatrix} \quad (1)$$

With the establishment of the DH matrix for all the C-Arm joints, a forward kinematic model can be produced using Equation 2. By multiplying all joint transformations, generally denoted by  ${}^{j-1}A_j$ , from the origin to the end effector, the forward kinematic model transpires.  ${}^0T_E$  is the final transformation from the origin to the end effector.

$${}^0T_E = {}^0A_1 {}^1A_2 {}^2A_3 \dots {}^{j-1}A_j \quad (2)$$

Once the forward kinematic model reaches the end effector or an important point, the cartesian coordinates can be extracted from the final product. The translational values are stored in the fourth column from the first to the third row, where x, y, and z are in order from top to bottom. The rotational transformations or orientation are stored in the first to third column and the first to third row. These values were extracted in the MATLAB script and then sent back to the GUI for the user to see the exact coordinates of the movements.

### 3.3.4 Inverse Kinematics

Unlike forward kinematics, inverse kinematics does not have a general formulation/method. Whereas in the forward kinematics the DH parameters and matrix can be used to model any robot, the inverse kinematics are still solved with more primitive mathematics [29]. Because of the lack of more ideal mathematical models, inverse kinematics are still solved by using a combination of simple algebra and simple trigonometry. This is also true for even the most versatile robotic arms and autonomous drone applications [30]. For example, even the best of industrial robotic arms still needs six joints to provide six DOF. Usually, the first three larger joints are responsible for providing the exact cartesian coordinates while the last three smaller joints provide the orientations with respect to each axis. However, if there existed a better inverse kinematic model approach, the position and orientation of the robotic end effects could be accomplished with far fewer joints. In general, the more joints a robot has, the more difficult the inverse kinematics will be.

To develop an inverse kinematic model for the C-Arm and the CAP, a similar approach to other robotic manipulators with five DOF was taken [31]. The inverse kinematics for the CAP was developed from the local origin on the base to the AOI,

using the same elements as shown in Figure 45. A hierarchy of operation was set to acquire the correct joint angles based on the coordinate input of the AOI. This hierarchy consists of calculating the joint positions to reach the Z-coordinate first. Then, the program calculates the wig-wag angle needed to reach the expected X-coordinate value. Based on the proscribed joint positions to reach the Z- and X-coordinates, the joint positions to find the Y-components are derived and implemented.

To solve the inverse kinematic in the full robotic range, the inverse kinematic model had to be broken into four sperate sections. The sections were created based on the geometric limits of the physical prototype. All four cases are shown in Figures 46-49.

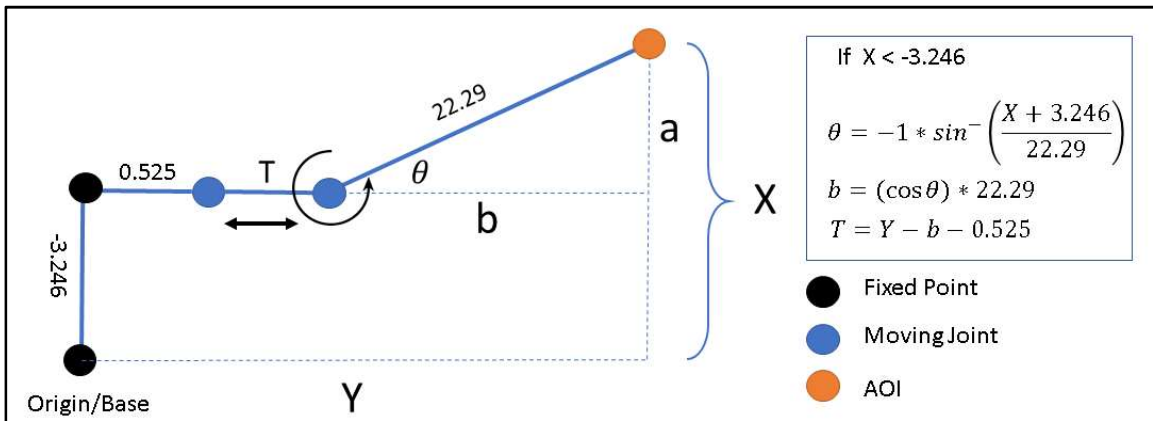


Figure 46. Inverse Kinematics Model for Case 1

For the first case, the AOI is rotated into any positive wig-wag angle. This means that the X-components of the AOI is a sum of the X offset and the value of “a”. Once the angle theta is found, the length of “b” can be calculated, added to the Y offset, and subtracted from the total Y value, resulting in the horizontal translation of “T”.



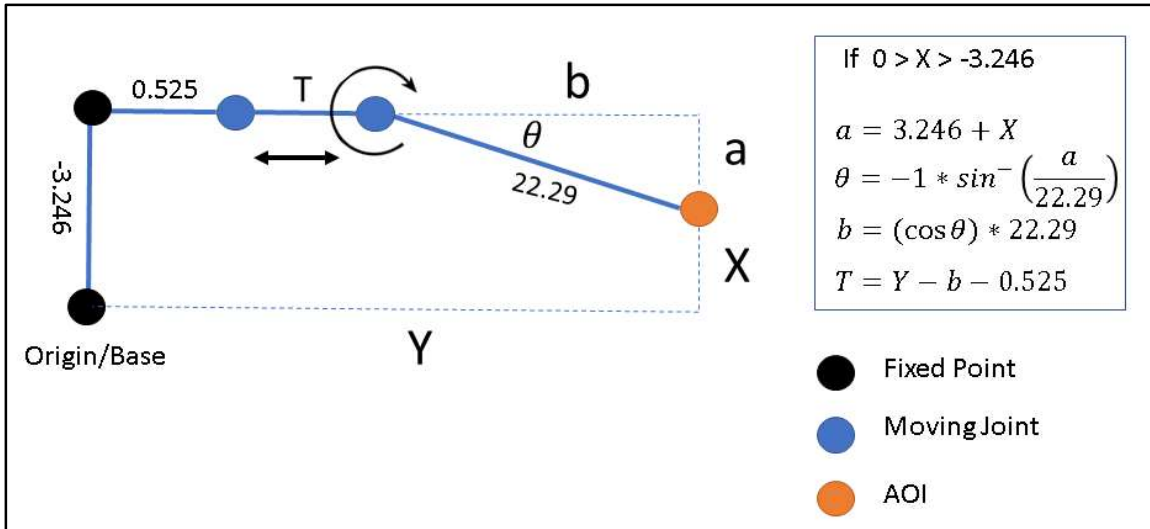


Figure 47. Inverse Kinematics Model Case 2

In the second case, the AOI lies in a negative wig-wag angle. However, the X-component is smaller than zero and yet larger than the X offset of -3.246. Therefore, the “a” value is the difference between the X-component and the total X offset. With this information, the angle theta and length “b” can be found. Finally, the horizontal offset “T” can be found as shown in Figure 47.

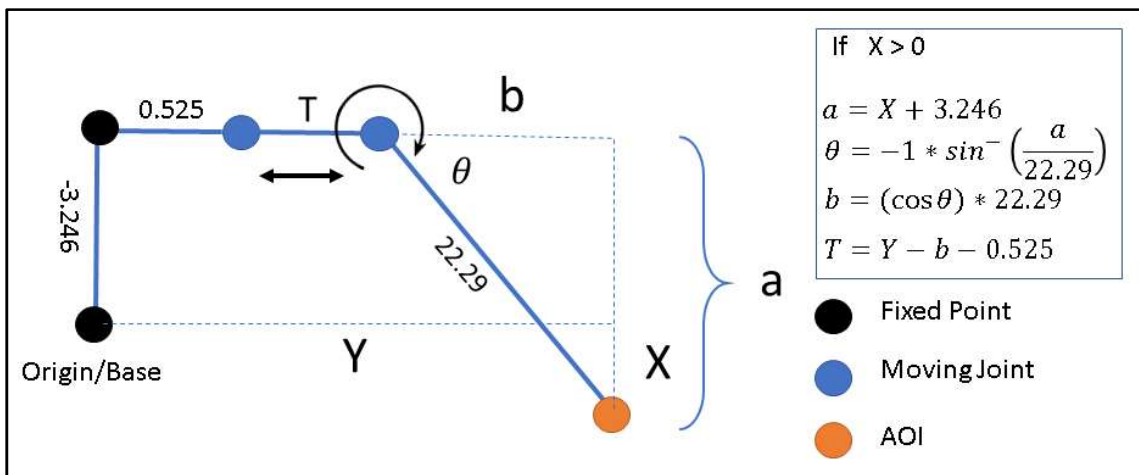


Figure 48. Inverse Kinematics Model Case 3

The third kinematic case exists when the AOI has a positive X-component. This means that the value for “a” is a combination of the X-component and the X offset - 3.246. Once again, after finding the value for “a” theta and “b” can be calculated. Finally, using “b” and the Y offset, the horizontal translation “T” can be found.

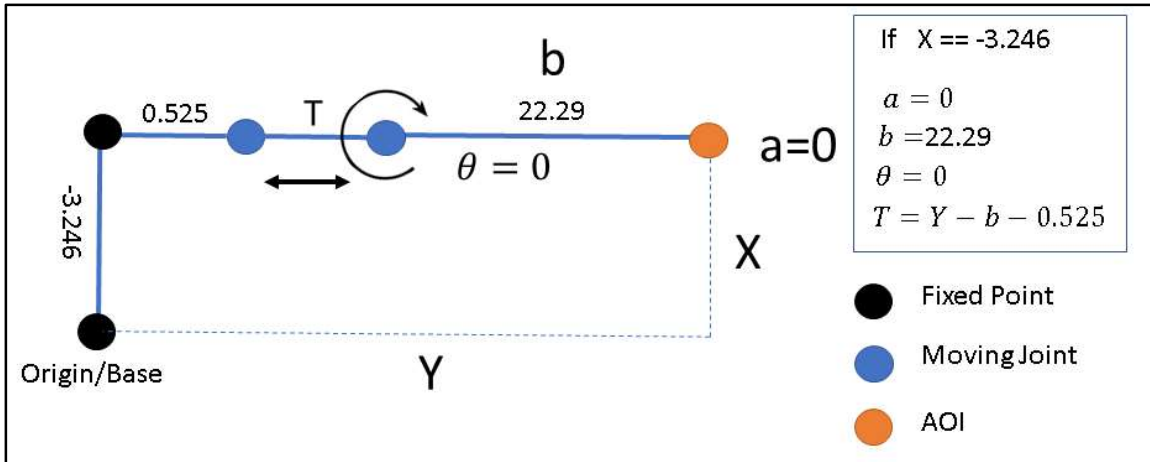


Figure 49. Inverse Kinematics Model Case 4

The fourth and final case for the inverse kinematics is the simplest to solve because the X-component for the AOI is the same exact value as the -3.246 X offset. This leads to a theta of zero and an automatic “b” value of 22.29. With this information, the last possible value of “T” can be calculated and implemented.

All these four possible scenarios for the inverse kinematics have been written in MATLAB script using multiple “if loops” and converted into a Simulink block. This Simulink block was integrated with the forward kinematics, leading to a complete kinematic modeling of the CAP that can all be used with a single GUI. The inverse kinematic MATLAB script can be found in the appendix.

### 3.3.5 Comment

After completion of the second task, it can be confidently said that a full kinematic model of the C-Arm was successfully developed. This kinematic model can therefore be adjusted to various C-Arm models and even small-scale C-Arm prototypes. In addition, the kinematic modeling was converted into computer code, allowing it to be used by any GUI. The developed kinematic model computer program is also easily modified for physical robot manipulation.

## 3.4 C-Arm Physical Prototype Design and Manufacturing

### 3.4.1 Requirements of the C-Arm Physical Prototype

Ideally the repositioning of the C-Arm using Vicon is tested and validated on a real C-Arm. However, because the C-Arm is an expensive radioactive device, access to

using and maneuvering it is limited to trained professionals. Therefore, in order to have unlimited student access to a C-Arm, a fully functioning prototype had to be built.

This small-scale prototype must fulfill all five degrees of freedom that the C-Arm performs. These include two translational and three rotational DOF. This prototype must be able to maneuver itself in the same maximum ranges as the real C-Arm. These extreme ranges include 25 degrees of yaw, 120 degrees of roll, and 232 degrees of pitch. Because the C-Arm prototype must be as realistic as possible in functionality, the pitch of the prototype must be performed with an orbiting mechanism and thereby adding a higher level of difficulty in design and manufacturing. Finally, the C-Arm prototype must have the ability to maneuver itself as accurately as possible, which is the most important demand of the prototype. All these demands led to the final version and production of the CAP shown in Figure 50 below.

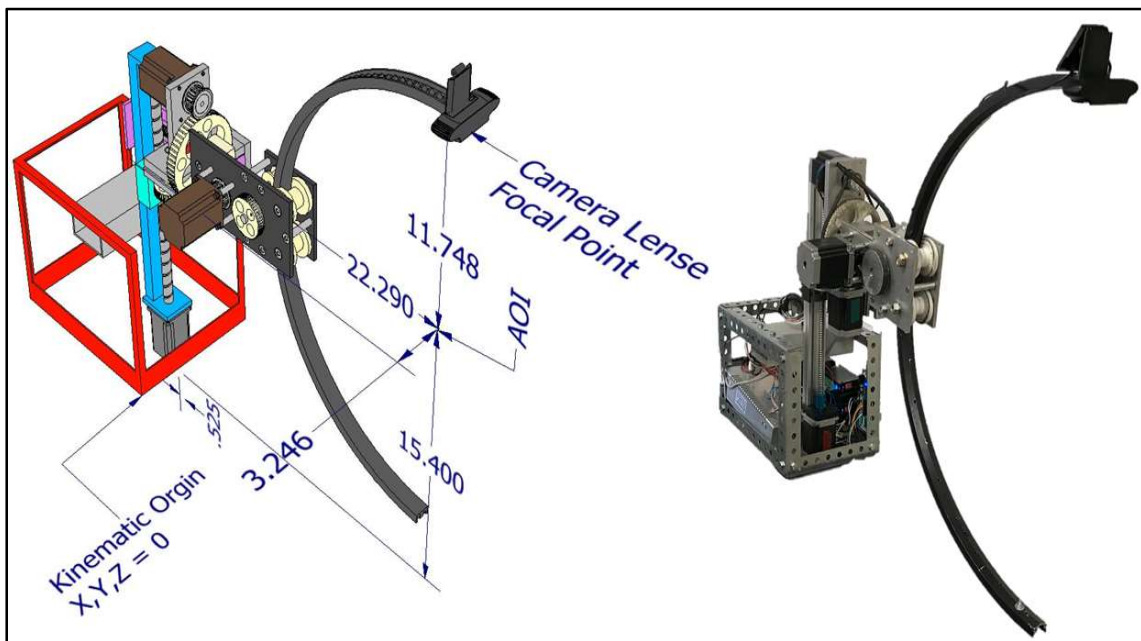


Figure 50. C-Arm Physical Prototype CAD Model and Robot

### 3.4.2 Hardware Development

The CAP was developed as a mixture based on the actual C-Arm and the CVP. The decision to do so was based on the fact that the CVP is much too simple of a design to be real-life applicable and manufacturable and that the actual C-Arm is way too complicated for the scope and purpose of this project. A comparison of all three C-Arm system can be seen in Figure 51 Below.

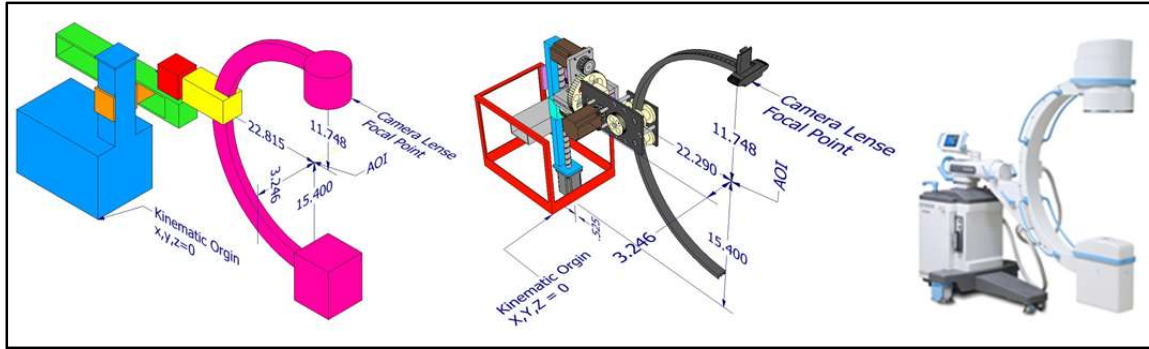


Figure 51. C-Arm Comparison: Virtual Prototype, Physical Prototype and Actual C-Arm

### 3.4.2.1 Standard Parts

To keep the cost of the CAP down, standard parts were used wherever possible. For example, the “C” shaped link is a modified 24” bicycle rim. For the translational joints, stepper motor driven linear actuators were used because of their proven reliability, modularity, and ease of access. All the important standard parts used for the manufacturing of the CAP are listed in Appendix F.

### 3.4.2.2 Custom Machined Parts

The custom parts and mechanisms of the C-Arm prototype were developed with production steps in mind as the first criterion. The approach was to use readily available stock parts and make the least amount of modifications to them in order to develop custom parts. Each part was designed such that the manufacturing would only require a drill press and a lathe for successful completion. A total of 3 aluminum stock types were used to manufacture all custom parts and sections. Load bearing link sections were built by machining 3” x 0.5” 6061 aluminum bars. Non-load bearing sections, mostly found in the orbital mechanism, were made from 3” x 0.25” 6061 aluminum bars. 6061 aluminum round stock of 2.25” was also used to machine out custom sprockets.

However, not all part productions could be limited to just using a drill press and lathe for manufacturing. A total of five parts had to rely on CNC machining for proper manufacturing. These parts included the base frame, the base plate, the tilt base, the large side plate, and the small side plate based. CNC code, known as G-code, was automatically developed using Computer Aided Machining (CAM) in Autodesk Inventor. A High-Speed Machining (HSM) plug-in was used to apply the CAM modeling to custom parts that required machining. All HSM procedure steps were simulated as shown in Figure 52 below.

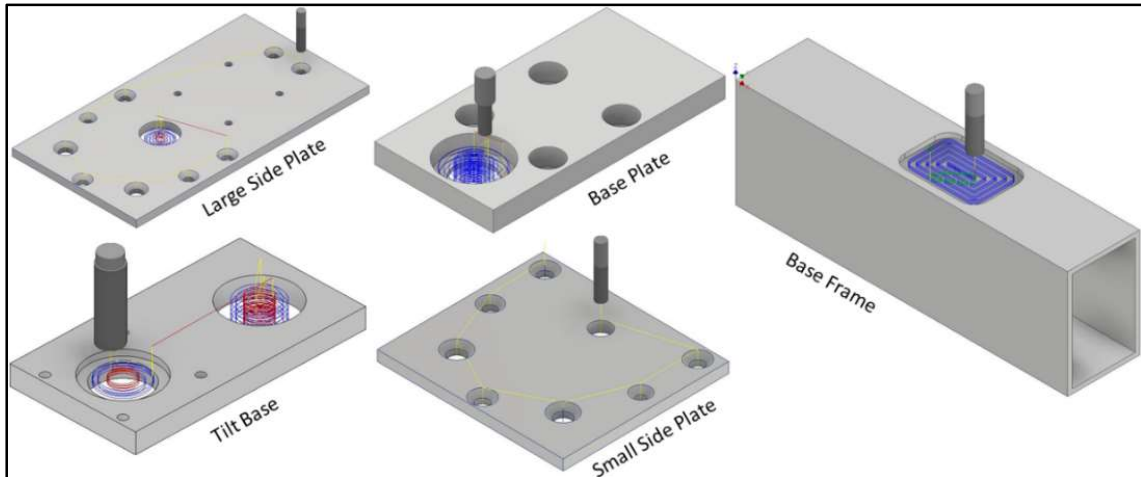


Figure 52. Computer Aided Machining using Inventor HSM

The lines in this figure show the tool path of the entire operation. All yellow line segments are rapid tool movements where the tool is not in contact with the stock. Blue line sections represent tool path sections where the tool is in contact with the stock and actual material is removed. Red lines usually represent plunge sections, where the tool lowers onto the stock to make the first cuts; otherwise, red lines represent tool collisions or tool paths that are prone to collision. Any green line is a path deviation to a new cut where stock and tool contact is maintained continuously. Post processing of the CAM model was converted for the use in Mach3 by Artsoft. Mach3 was chosen because this G-code language is quite universal for most CNC machines, allowing for replication of parts in most machine shops. Dimensions of CNC manufactured parts can be found in Appendix F, and the developed G-Code for all parts can be found in Appendix D.

#### 3.4.2.3 Motor Selection

Motor selection for the CAP was a decision that needed to be considered carefully. There existed three main options for motor choice: DC motors, servo motors, and stepper motors. DC motors produce the most torque and are the most efficient, but because dc motors need additional sensors to detect angular position, the decision was made to exclude them for the design. Next, servo motors were considered as a viable option. Servo motors are relatively easy to program and provide a decent amount of torque compared to their weight. In addition, servo motors do not need additional sensors to detect their angular position. However, two factors led to the decision to move forward with other options. The first factor was the fact that servo motors are

limited in revolution, and in order to use the linear actuators, a constantly rotating motor is needed. The second reason was the fact that most servo motors are limited in resolution to half of a degree. Such resolutions are usually enough for most applications but are not small enough to be trusted in the repositioning of the C-Arm prototype. Although stepper motors have the lowest torque to weight ratio of any motor, stepper motors are the most accurate motors available. The decision was made to move forward with a Nema 23. The low torque output of these motors had to be compensated with pulley systems to allow for proper function. More information about the Nema 23 can be found in Appendix E. Finally, to avoid skipping steps, the motors were set at a speed of 1000 steps per second and a value of 800 steps per revolution. Figure 53 shows the manufacturer's torque curve in terms of torque vs. pulse per second (PPS) for the Nema 23.

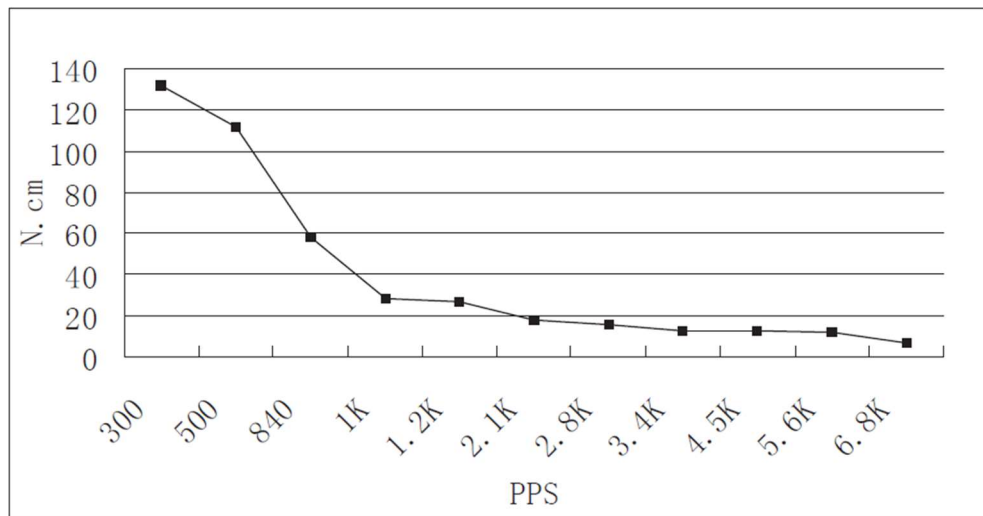


Figure 53. Nema 23 Manufacturer Torque Curve [32]

### 3.4.3 Comment

The CAP was successfully designed, manufactured, and assembled. In addition, all the required DOF and ranges of motion of an accurate C-Arm have been replicated. This prototype also functions as a robotic arm actuated by stepper motors. The use of stepper motors allows for accurate and sensitive maneuvering and repositioning. Lastly, the developed robotic prototype is capable of being integrated and actuated with any GUI and appropriate kinematic models.

### 3.5 Integration of Vicon Motion Capture with the C-Arm Physical Prototype

#### 3.5.1 Vicon Motion Capture

Vicon is a motion capture system that is produced in the United Kingdom. Vicon, like most motion capture systems, uses IR light as a medium to record markers in space. These markers can either be light emitting or can be spherical reflectors. During a motion capture session, Vicon cameras are focused onto the area of action. Because all Vicon cameras are fixed, the location of each Vicon marker can be calculated as shown in Figure 13. This style of motion capture has been used mainly for analyzing biomechanics [33]. In addition to biomechanics, movie producers have also started using motion capture to produce better quality CGI [34].

Recently the use of motion capture has extended its application to the maneuvering of autonomous drones [35]. This means that the Vicon system is also a good tool to validate the movement of robots and kinematic models. Figure 54 shows a drone equipped with reflective markers to provide position and orientation of that drone midflight using a motion capture system. It is important to note that the drone has 3 or more markers attached to it. This is done because modeling a rigid object can only be done with a minimum of at least 3 points/markers [36].



Figure 54. Autonomous Drone Equipped with Reflective Motion Capture Markers [37]

### 3.5.2 Vicon Integration with C-Arm Prototype

To validate and test the CAP and the developed kinematic model, Vicon was used [38]. Essentially, the C-Arm prototype's movement is objectively gathered and compared to the kinematic model. Because the translational joints of the C-Arm prototype are easily validated using traditional measuring methods, only the rotational joints of the C-Arm prototype were tested with Vicon.

First, spherical reflective markers were placed on the C-Arm. One marker was placed on the kinematic origin of the C-Arm prototype. This critical marker will be used to convert the global coordinate values of all markers placed on the C-Arm prototype to local coordinate values relative to the kinematic origin. Second, two other markers are placed on the base to establish a rigid body as the reference for all other movements. Next, a marker is placed on the camera lens to provide the exact coordinates of that point. In addition, a second marker is placed directly opposite of the camera lens onto the detection plate of the C-Arm prototype. Finally, two other markers are placed on the orbital link of the C-Arm prototype to model a ridged object. This set up can be seen in Figure 55. This figure shows an overlay of the detected markers onto the live video feed of the C-Arm prototype.

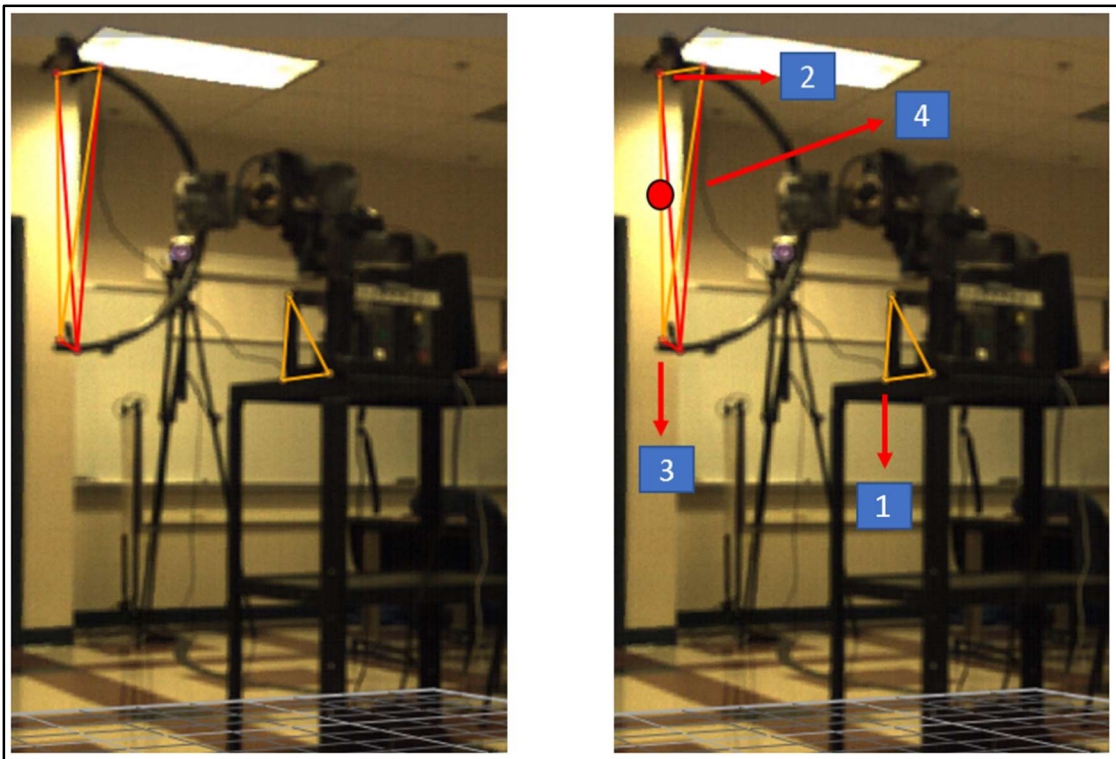


Figure 55. Vicon Video Overlay onto Detected Markers with Labels



To properly reposition any C-Arm for imaging, only two points of the C-Arm need to be properly repositioned as discussed in the Forward Kinematics subsection of this thesis. However, the AOI is not a physical existing point and cannot have a Vicon marker placed on it. To overcome this issue, the AOI point is calculated by applying the midpoint formula, in Equation 3, to the marker placed on the camera lens and the marker placed on the detection plate. Where  $Mid$  is the calculated midpoint and  $x, y, z$  represent the coordinates of the camera lenses and detection plate with the subscripts denoting the order.

$$Mid = \left( \frac{x_1 - x_2}{2} \right), \left( \frac{y_1 - y_2}{2} \right), \left( \frac{z_1 - z_2}{2} \right) \quad (3)$$

Although 7 markers were used in the Vicon model, only 3 markers are critical for the validation of the Kinematic model. Looking at Figure 55, marker number one is the local origin of the C-Arm prototype. Marker number two is the center point of the camera lens. Marker number three is the center point of the detection plate. Finally, point number four is the calculated AOI. With this set up, the C-Arm physical prototype is fully integrated with the Vicon system.

### 3.5.3 Comment

The CAP was successfully integrated with Vicon. By selective IR marker placement, the actual movements of the robotic prototype were extracted from the Vicon global coordinate system relative to the prototype kinematic origin. Since kinematics of the prototype originates from the base of the porotype model, placing a marker in the same exact point will always result in the conversion of local coordinates for any orientation of the prototype. Therefore, this will always allow for the kinematic model to work in any orientation of the prototype within the Vicon working space. This system integration, through selective marker placement, also allows for extraction of points that are not physical, yet crucial to repositioning.

#### 4.1 Vicon Testing Expectations

Once the C-Arm prototype is fully integrated with Vicon by placing markers on key points as explained in the “Vicon Integration with C-Arm Prototype” subsection, testing for validation can begin. Motion capture testing of the C-Arm with Vicon has a four-factor effect, meaning that correct test results will validate all four tasks of this project thereby completing the objective of this research. A successful motion capture test with Vicon would validate the following: correct functioning of the VP and GUI, correct kinematic modeling and programming, successful physical prototype design and prototype manufacturing, and successful integration of the CAP with Vicon technology. In other words, if one or more of the four task/subsystems are not functioning properly Vicon test results will be negative without any exception. Figure 56 visually reinforces the four-factor testing outcomes of successful motion capture testing of the CAP. Successful completion of a task is validated by the successful completion of its dependent tasks. Dependency is shown with a black arrow.

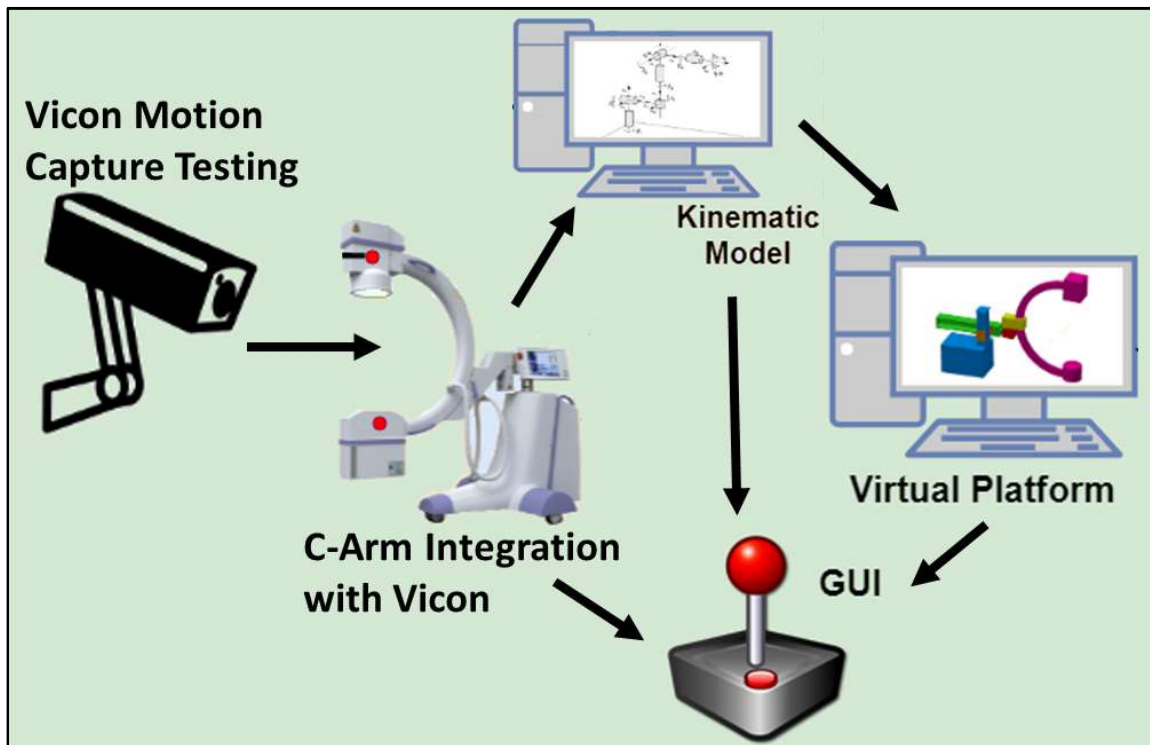


Figure 56. Four-Factor Validation of Motion Capture Testing

A positive Vicon test can only be completed if the CAP performs successfully. A successfully functioning prototype relies on an accurate kinematic model and a properly working GUI. The results of the kinematic model also, in parallel, depend of the GUI performance. In addition, because the kinematic model was validated with the help of the VP, the performance of the kinematic model heavily relies on a properly functioning VP. Finally, because the VP is also maneuvered with the GUI, the VP performance also relies on a properly working GUI.

## 4.2 Vicon Testing Procedure

### 4.2.1 Testing Setup

Motion capture test are time intensive and produce a large amount of datapoints. The resolution of Vicon, for the purpose of C-Arm Physical Prototype, was set to a standard 100 frames per second. This means that 100 datapoints will be produced with Vicon during a test for every single marker used. Because of the high data rate, it was decided that the prototype testing be split up into three short individual tests (one for each revolute joint of the C-Arm). From here, it is assumed that, if each joint is successful in maneuvering itself, the combined/complex movements of all joints at once will also be successful. The two translational joints were tested differently as explained in the subsequent thesis subsections.

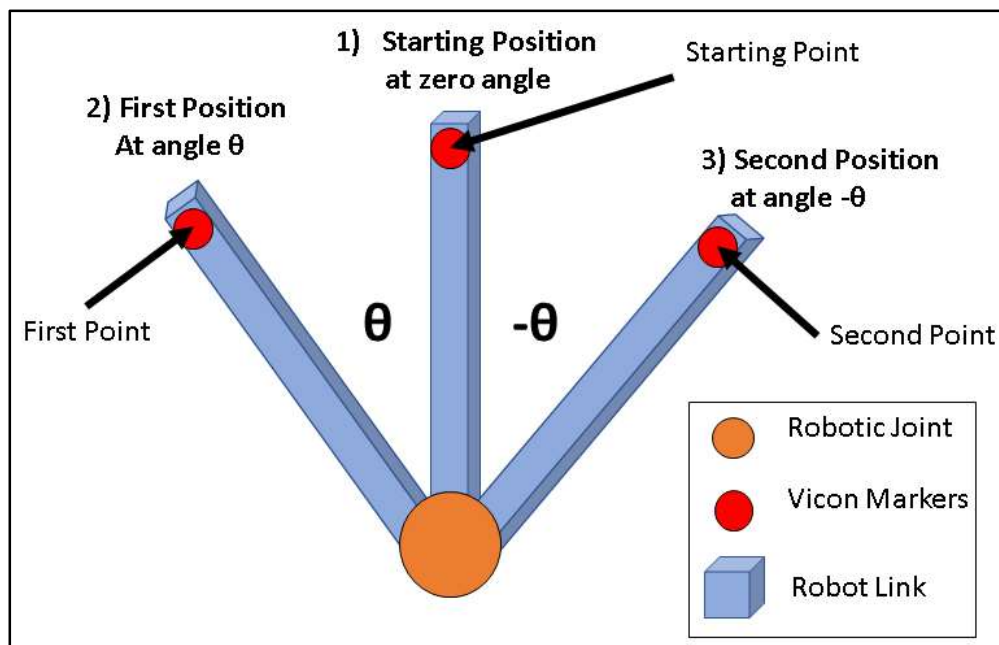


Figure 57. Testing Setup and Procedure for Revolute Joints

The setup of the testing procedure was as follows and can be seen in Figure 57 above. Recording of Vicon is started. First the wig-wag movement was tested and followed by the tilt and orbital movements. Each joint, during its testing, was started at zero degrees; the position of the markers at the start of the test were named the “starting points”. Then using the GUI, the joint is moved to a first specific angle and followed by a second specific angle value. At those specific angle values, the marker points were name “first points” and “second points”. After the joint had reached the second and final angular position, it is then moved back to the zero position. The first and second angle values for the wig-wag and tilt were 10, -10 degrees and 40, -40 degrees, respectively. The orbital, however, was only asked to move from the starting position to the first position of 10 degrees. After each joint had successfully finished the steps, Vicon recording was stopped. Visual representation of the three individual joint tests are shown in the Figures 58-60 below.

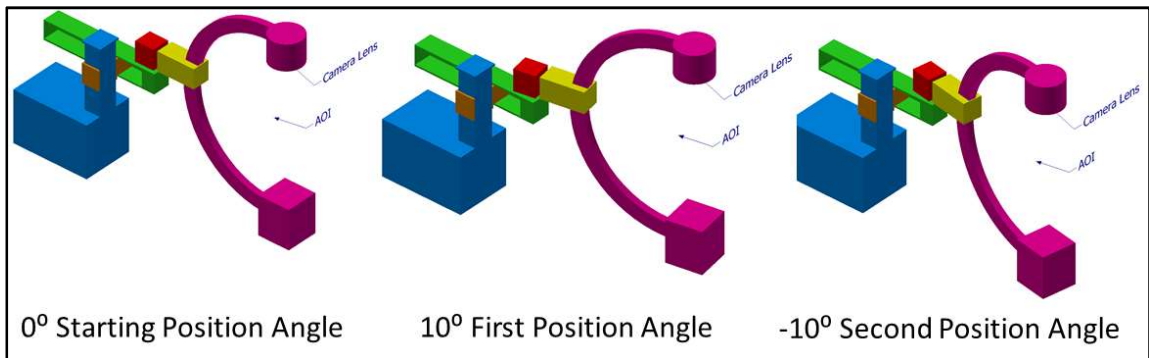


Figure 58. Wig-Wag Test Positions and Procedure

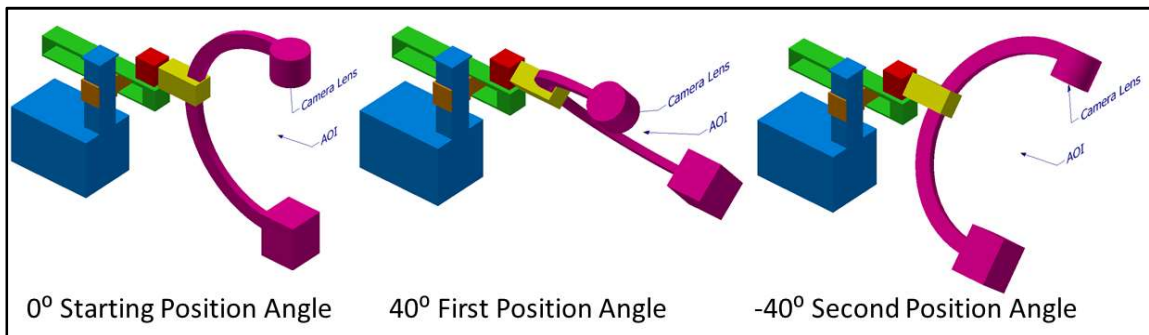


Figure 59. Tilt Test Position and Procedure

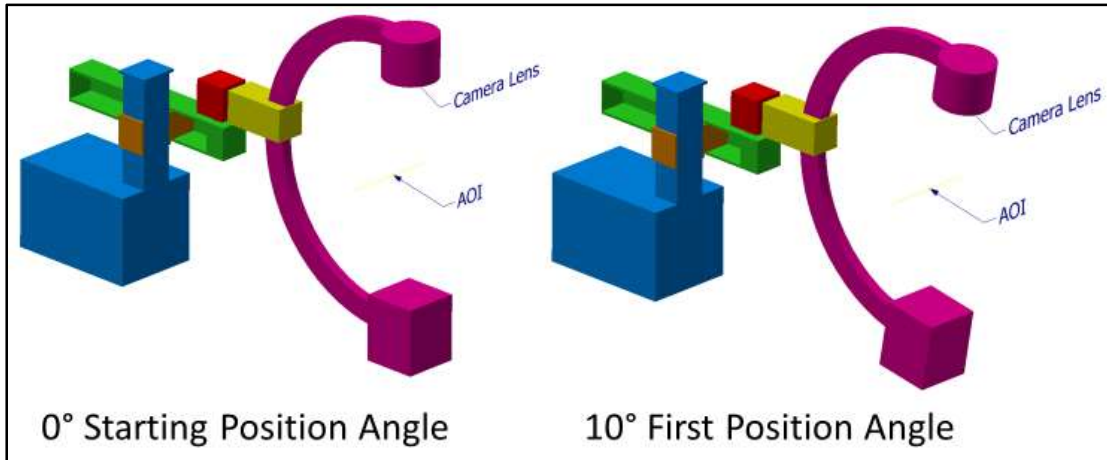


Figure 60. Orbital Test Poisons and Procedure

#### 4.2.2 Vicon Data Acquisition

Vicon, a reliable and diverse data acquisition system, can be used for multiple tests and multiple data types. However, as previously explained, Vicon was only used to acquire the cartesian coordinates of select markers placed on the C-Arm. By limiting the dependence of Vicon to provide additional functions, the overall speed of the testing and data feedback is reduced. Figure 61 shows exactly what data points Vicon uses for the testing of the CAP and how Vicon processes the testing procedure.

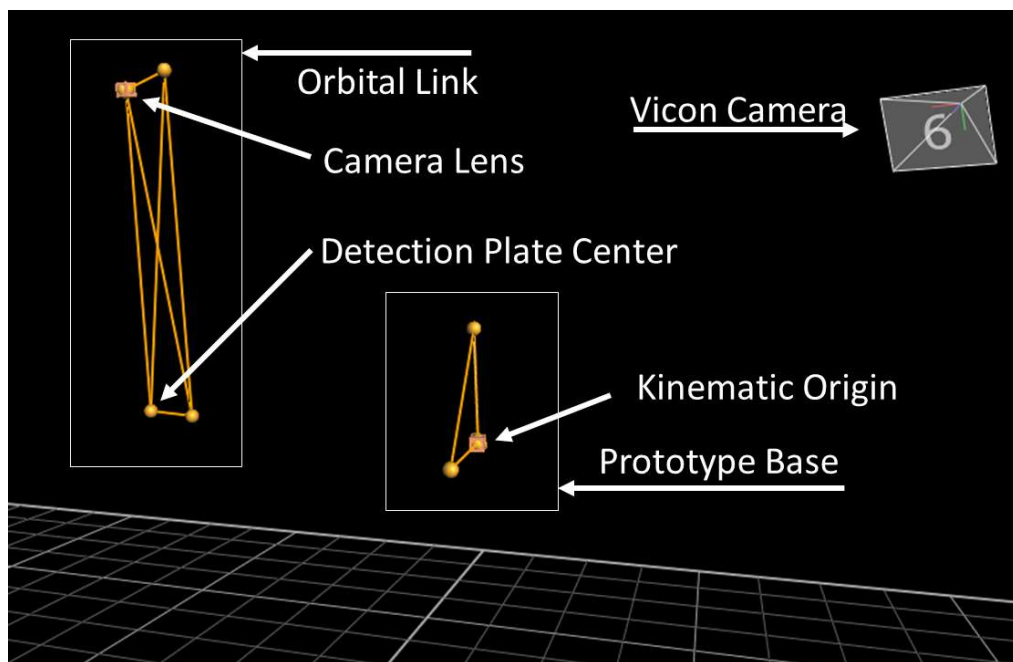


Figure 61. Vicon Data Acquisition of Markers Placed on Prototype

From Figure 61, a few things are important to note and understand. The prototype base is marked using three markers, but only the cartesian coordinates of the kinematics origin marker is used. The other two markers in the prototype base section are used to calculate the orientation of the prototype with respect to the Vicon global origin. Additionally, the Vicon interpretation of the orbital link does not need to be geometrically accurate if the camera lens and detection plate center markers are placed correctly on the prototype. Two additional markers were placed on the orbital link to allow for a ridged body interpretation. It is important to remember that the AOI is a marker-less calculated point. The cartesian coordinates of the AOI are interpolated between the camera lens and the detection plate center using the midpoint formula in Equation 3.

## 5.1 Key Results

### 5.1.1 Vicon Raw Data

During the Vicon testing procedure, the data acquired was converted to MATLAB arrays for mathematical and visual processing. The cartesian coordinates of the camera lens and the calculated AOI during each joint testing are graphed in the figures.

Figure 62 shows the path and positions the camera lens takes during the Vicon testing of the wig-wag joint. The wig-wag Joint was at zero degrees during the start position. When the joint was moved to a positive 10 degrees position, the first point was recorded. Lastly, the wig-wag joint was moved to -10 degrees resulting in the second point for this test. The shape of the path is also intuitive with the expected movements.

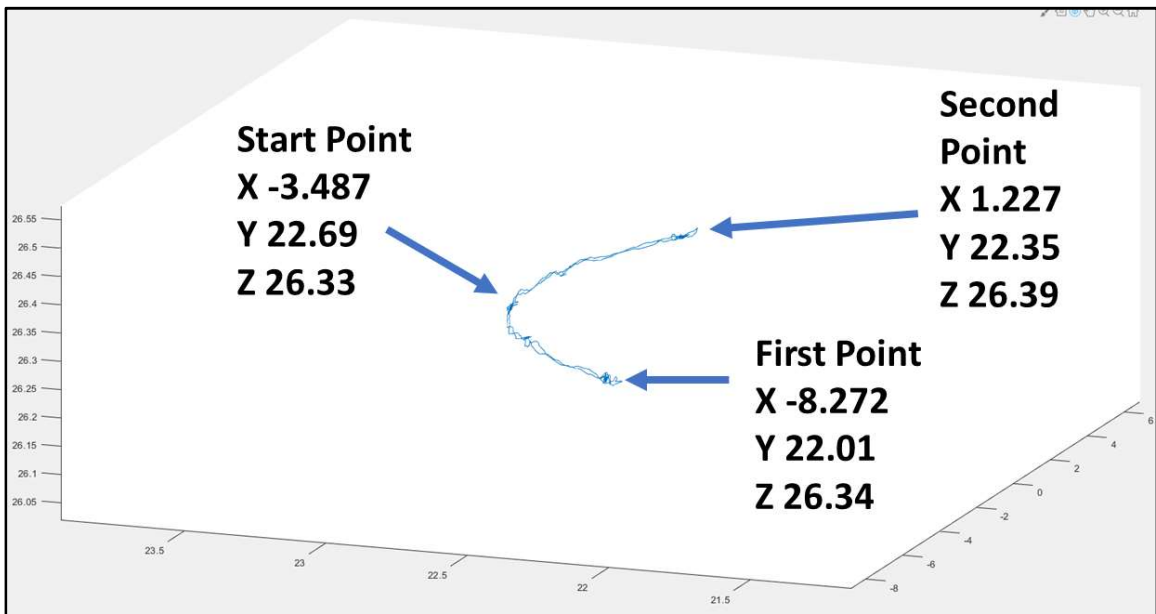


Figure 62. Wig-Wag Testing Coordinates of the Camera Lens

Figure 63 shows the interpolated AOI path and positions during the wig-wag testing of the C-Arm. The values of this point are interpolated by finding the midpoint between the camera lens and the detection plate. At zero degrees, the starting point was recorded. Then, at 10 degrees, wig-wag movement resulted in the first point. Finally, the second point correlated with a wig-wag angle of -10 degrees. The path that the AOI follows during the wig-wag testing is also intuitive with what is expected out of such movement.

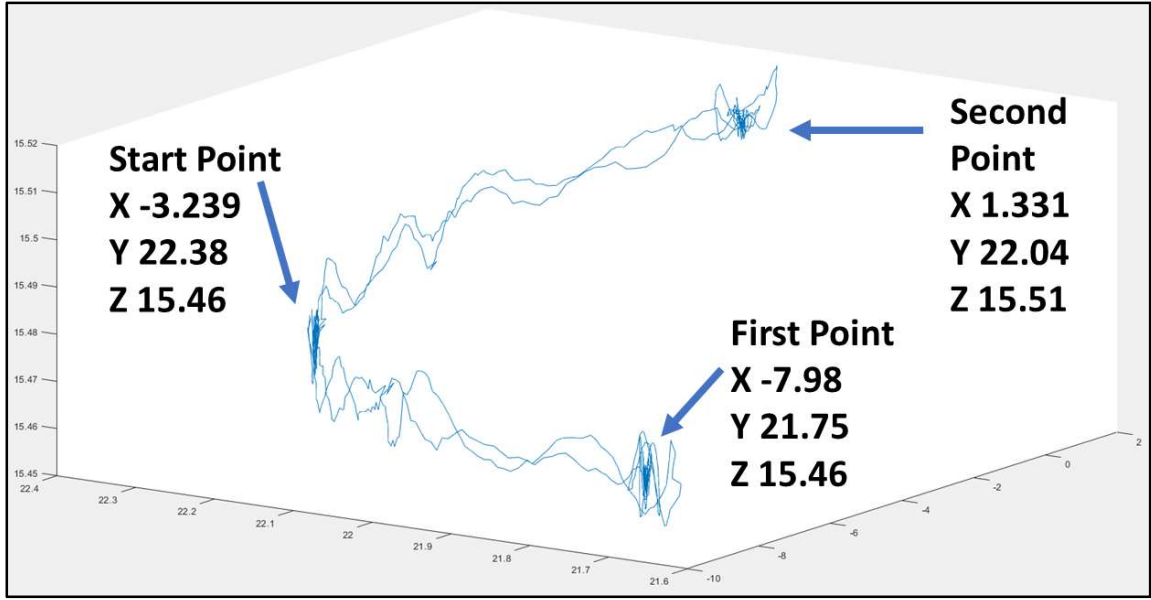


Figure 63. Wig-Wag Testing Coordinates of AOI

Figure 64 shows the path and position of the camera lens during the tilt testing procedure. At the beginning, the tilt angle of zero degrees resulted in the start point for this test. Then, the tilt angle was set to 40, resulting in the first point for the camera lens. Finally, the tilt angle was set to a complementary -40 degrees, providing a second point.

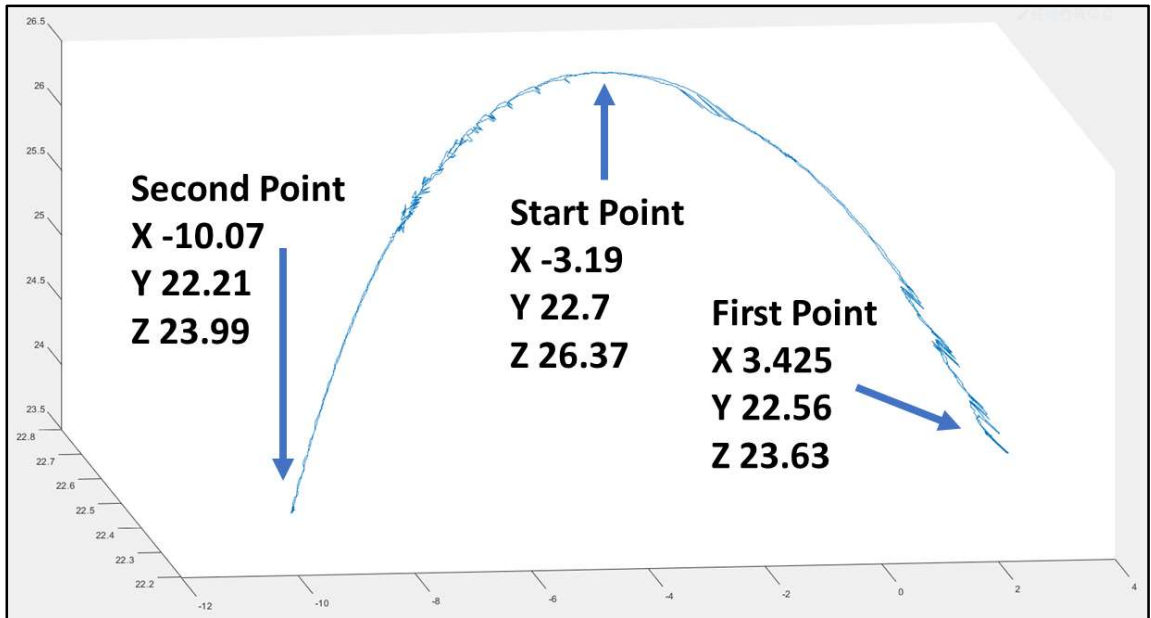


Figure 64. Tilt Testing Coordinates of Camera Lens



Figure 65 shows the path of the AOI during the tilt test. It is important to note, that if all Vicon markers were placed perfectly, and no mechanical error existed in the physical prototype, the AOI should be ideally stationary during tilt movements. However, because of vibration, mechanical inaccuracies, and Vicon marker errors, the AOI is not perfectly still during the movements from starting point to second point. The interpolated AOI path and position of however are in a small proximity and can be considered still.

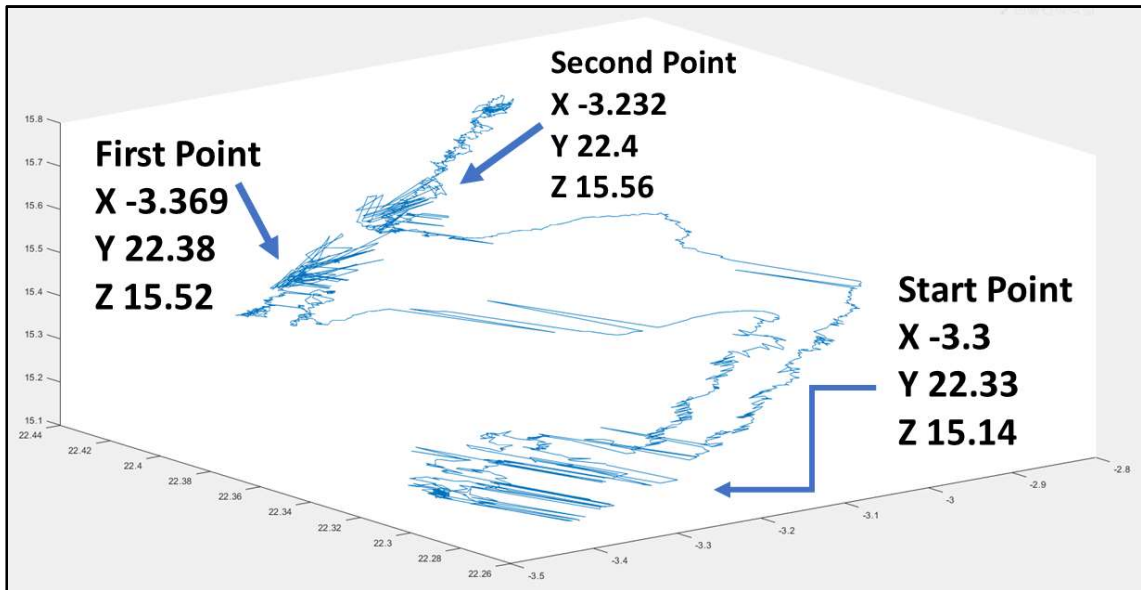


Figure 65. Tilt Test Coordinates of AOI

Figure 66 shows the camera lens movement and positions as the orbital angle was moved from the starting position of zero degrees to a first position of 10 degrees. For the orbital movement, no second position was tested. The starting point and the first point are labeled with their respective cartesian coordinates.

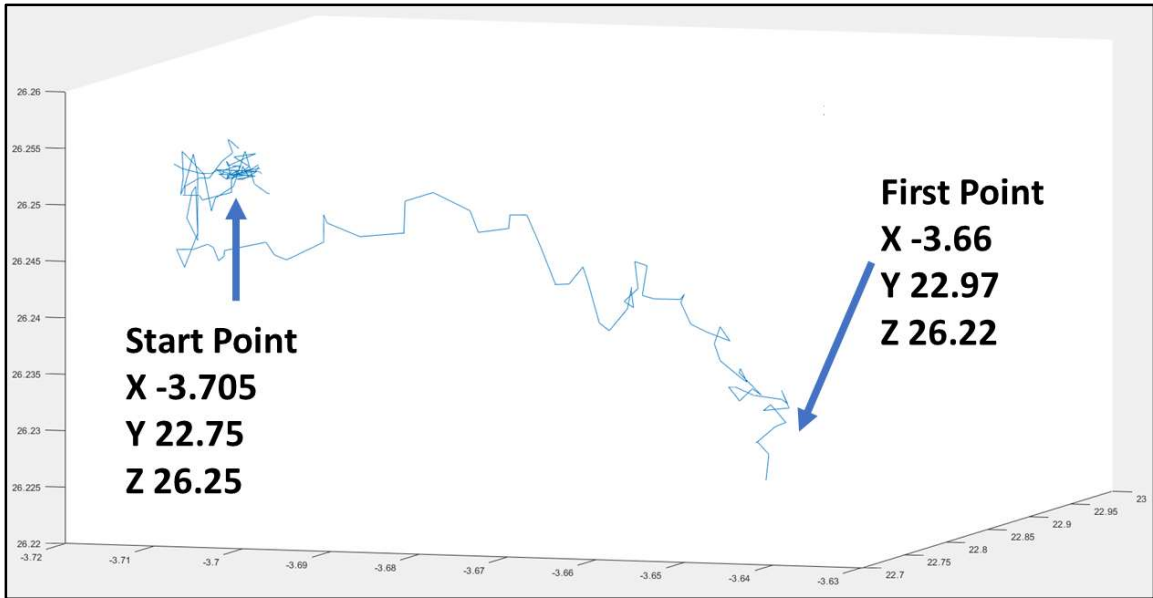


Figure 66. Orbital Test Coordinates of Camera Lens

Ideally, during the orbital movement of the CAP, the AOI remains still and does not move. However, due to mechanical slack, less than perfect marker placement and vibrations, the AOI is not perfectly still as can be seen in Figure 67. Because the movement of the interpolated AOI is small, the point can be considered still for this practical application.

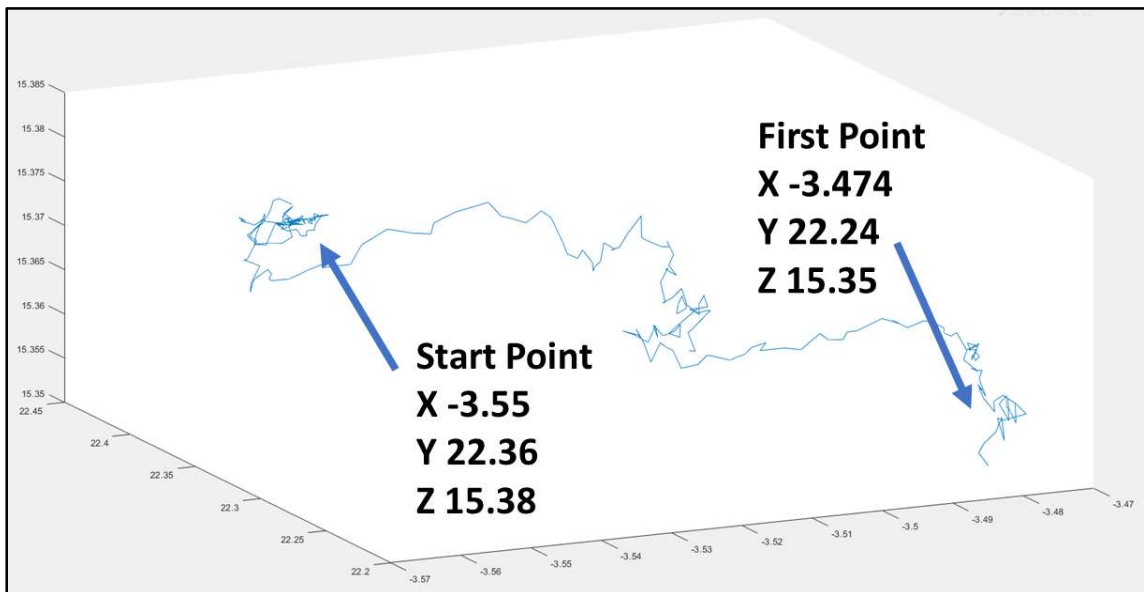


Figure 67. Orbital Test Coordinates of AOI

### 5.1.2 Data Comparison and Analysis

After the raw data had been compiled, it was organized for comparison. A table was created that compared the extracted Vicon coordinates for the camera lens and the AOI to the predicted kinematic values. The difference in those values was compared and recorded as the “Test Difference”. These values can be seen in Table 1. Table 1 shows the values for all three tested joints, wig-wag, tilt, and orbital. Each joint is analyzed based on two critical locations: the lens and the AOI. The most left set of columns, labeled Test Vicon Results, contains the acquired Vicon test position while the center set of columns, labeled Test Kinematic, shows the calculated points provided by the theoretical kinematic model. The set of columns to the right, labeled Difference, shows the calculated differences between those two previous values.

Table 1. Vicon Cartesian Test Points Comparison to Theoretical Kinematic Values

Wig-Wag Test Vicon Results :Lens			Wig-Wag Test Kinematic :Lens			Wig-Wag Test Difference :Lens			
Start Point	First Point	Second Point	Start Point	First Point	Second Point	Start Point	First Point	Second Point	
X	-3.487	-8.272	1.227	-3.246	-7.117	0.6246	0.241	1.155	0.6024
Y	22.69	22.01	22.35	22.81	22.48	22.48	0.12	0.47	0.13
Z	26.33	26.34	26.39	27.15	27.15	27.15	0.82	0.81	0.76
Wig-Wag Test Vicon Results :AOI			Wig-Wag Test Kinematics :AOI			Wig-Wag Test Difference :AOI			
Start Point	First Point	Second Point	Start Point	First Point	Second Point	Start Point	First Point	Second Point	
X	-3.239	-7.98	1.331	-3.246	-7.117	0.6246	0.007	0.863	0.7064
Y	22.38	21.75	22.04	22.81	22.48	22.48	0.43	0.73	0.44
Z	15.46	15.46	15.51	15.4	15.4	15.4	0.06	0.06	0.11
Tilt Test Vicon Results: Lens			Tilt Test Kinematics: Lens			Tilt Test Difference: Lens			
Start Point	First Point	Second Point	Start Point	First Point	Second Point	Start Point	First Point	Second Point	
X	-3.19	-10.07	3.425	-3.246	-10.8	4.305	0.056	0.73	0.88
Y	22.7	22.21	22.56	22.81	22.81	22.81	0.11	0.6	0.25
Z	26.37	23.99	23.63	27.15	24.4	24.4	0.78	0.41	0.77
Tilt Test Vicon Results: AOI			Tilt Test Kinematics: AOI			Tilt Test Difference: AOI			
Start Point	First Point	Second Point	Start Point	First Point	Second Point	Start Point	First Point	Second Point	
X	-3.3	-3.369	-3.232	-3.246	-3.246	-3.246	0.054	0.123	0.014
Y	22.33	22.38	22.4	22.81	22.81	22.81	0.48	0.43	0.41
Z	15.14	15.52	15.56	15.4	15.4	15.4	0.26	0.12	0.16
Orbital Test Vicon Results: Lens			Orbital Test Kinematic: Lens			Orbital Test Difference: Lens			
Start Point	First Point	Second Point	Start Point	First Point	Second Point	Start Point	First Point	Second Point	
X	-3.705	-3.66	-	-3.246	-3.246	-	0.459	0.414	-
Y	22.75	22.97	-	22.81	24.86	-	0.06	1.89	-
Z	26.25	26.22	-	27.15	26.97	-	0.9	0.75	-
Orbital Test Vicon Results: AOI			Orbital Test Kinematics: AOI			Orbital Test Difference: AOI			
Start Point	First Point	Second Point	Start Point	First Point	Second Point	Start Point	First Point	Second Point	
X	-3.55	-3.474	-	-3.246	-3.246	-	0.304	0.228	-
Y	22.36	22.24	-	22.81	22.81	-	0.45	0.57	-
Z	15.38	15.35	-	15.4	15.4	-	0.02	0.05	-
All units are in inches									

Once the difference in the physical test lens and AOI positions in comparison to the calculated theoretical kinematic positions was found, a simple error analysis was performed. This analysis provides the average error in repositioning of the camera lens and of the AOI. These results are in Table 2 below and show the average error in repositioning for each joint at the lens and the AOI.

Table 2. Average Repositioning Error

Parameters	Average Error	
	Value	Unit
Average Lens Repositioning Error for Wig-Wag	0.6	$in^3$
Average AOI Repositioning Error for Wig-Wag	0.4	$in^3$
Average Lens Repositioning Error for Tilt	0.5	$in^3$
Average AOI Repositioning Error for Tilt	0.2	$in^3$
Average Lens Repositioning Error for Orbit	0.7	$in^3$
Average AOI Repositioning Error for Orbit	0.3	$in^3$
Average Repositioning Error for the Entire System	0.4	$in^3$

## 5.2 Discussion

### 5.2.1 Task 1: Virtual Platform and GUI

The VP, consisting of the CVP and the GUI, was successfully designed and fully developed. The VP, once tested and validated, became the groundwork for the development of the kinematic model. In addition, with the applications of different control systems to the VP, data was gathered to aid in the design decision of the CAP such as motor selection.

Although very basic, the GUI developed for the manipulation of the VP was successful. The GUI included all the elements required for the complete manipulation of the C-Arm virtual model in the VP. However, more useful live data could be extracted from the background calculations and displayed in the GUI. This could allow users to better understand the forces, torques, and velocities required to maneuver a real C-Arm in a timely manner.

### 5.2.2 Task 2: Kinematic Modeling

The forward kinematics of general C-Arm models were developed using the DH parameters. These universal parameters were chosen because of how common they are in other real work applications. This will allow for future users to apply the forward

kinematic model to other C-Arm models no matter the different individual dimension. As long as the offsets are correctly measured and implemented, this forward kinematics model should be universal. After development, the forward kinematic model was converted into MATLAB script and integrated with the CAP. The developed forward kinematic model was tested and validated using the VP and through the Vicon testing, both with successful results.

The inverse kinematics made use of simple trigonometry and algebra to provide output joint values for the CAP. A total of four different scenarios were needed to create a properly functioning inverse kinematic model that controlled the CAP's AOI. It was determined that automatically repositioning the AOI using the inverse kinematics and manually controlling the camera lens would result in the fastest repositioning method.

### **5.2.3 Task 3: Physical Prototype**

The CAP is an original small-scale robotic C-Arm. The prototype was successfully designed and manufactured using as many standard parts as possible. To produce custom parts, only three different aluminum stocks were used. A total of five components required custom CNC manufacturing. After the prototype was fully designed and manufactured, it was connected to the GUI through the developed kinematic model. Next the performance of the prototype was validated by integrating it with Vicon. The main purpose of the CAP is to provide a physical base where students and educators can apply various theories to help improve the performance of the C-Arm.

### **5.2.4 Task 4: Integration with Vicon**

The CAP was integrated with Vicon with ease. Select markers were placed on critical points whose coordinates needed to be known for proper repositioning calculations. One marker was placed directly onto the kinematic origin of the CAP. This was done to convert the global coordinates of all markers to the local coordinates needed for proper repositioning and testing analysis. Additional markers were placed on the camera lens and the detection plate center. Using linear interpolation, the coordinates for the AOI were calculated. The integration model and integration procedures for the CAP can also be applied to other C-Arm models.

### **5.2.5 Testing Results**

The CAP provided very promising results. In order to acquire good results through Vicon testing, the GUI, C-Arm virtual model, kinematic model, and the CAP all had to work properly in synchronization. Therefore, by acquiring the expected results, we can be reassured that all four tasks/subsystems work with one another properly. The testing was done to one joint at a time to keep procedures as simple as possible. The positions of two points on the CAP, the camera lens and the AOI, were recorded during the testing procedures. These two recorded point coordinates were compared to the theoretical coordinates of the same points calculated by the kinematic model. The difference between theoretically calculated points and those provided by Vicon are on average 0.4 inches cubed. These results are reasonable and ensure that the entire integrated repositioning system works well.

## Chapter 6: Concluding Remarks

### 6.1 Closure

The C-Arm is one of the most important surgical tools because it provides surgeons the ability to take X-ray imaging during surgery on demand. In a handful of spinal surgical procedures, the C-Arm needs to be moved out of the way to make room for other equipment and maneuvers. Then, for validation of those procedures, the C-Arm needs to be repositioned to its original position. While the C-Arm's simple and manually maneuverable design works well in most uses, the C-Arm is difficult to accurately reposition manually. The difficulty in accurate repositioning comes with many downsides, including excessive radiation exposure to the patient and operating staff, increased risk of infection, longer time under anesthesia, and increased surgery cost. While different solutions to C-Arm repositioning have been proposed, most are not feasible enough to be implemented on a mass scale or only work within strict limits.

To develop a simple repositioning system that works universally and without restriction, the C-Arm was integrated with Vicon motion capture system, allowing surgery personal to have feedback of current positions of the C-Arm relative to its previous positions. To complete the objective of automatic repositioning, first a set of tasks needed to be completed. These first included the development of a virtual prototype maneuvered by a GUI inside a VP. The second task consisted of developing a complete forward and inverse kinematic model of the C-Arm and integrating the kinematics into the GUI. Thirdly, a fully functioning robotic C-Arm prototype was developed that was programmed to be moved in synchronization with the VP. Finally, the fourth task was to integrate the C-Arm robotic prototype with Vicon to allow for the digital cartesian feedback into the kinematic program.

After the completion of all four tasks, the integrated robotic C-Arm was tested by comparing its actual Vicon marker positions to the automatically calculated kinematic values. The results were promising and showed that the C-Arm camera lens and the AOI could be repositioned within an average error margin of less than  $\frac{1}{2}$  inches cubed. This relatively small error is in part due to the inaccurate marker placements, and the physical size of the markers themselves. However, to overcome this relatively small average error in repositioning, future work is needed.

## 6.2 Implications and Expected Outcomes

This novel approach manages to reach its objective of accurate repositioning the C-Arm and still manages to avoid all restrictions that have kept similar ideas from being implemented. By applying this system, we move significantly closer to the goal of autonomous X-ray imaging during surgery. It is expected that all, if not most, surgical centers that already use motion capture during surgery will implement and use the proposed methods of repositioning developed in this thesis. If successful in those cases, a larger spread of motion capture integration with medical imaging devices can also be expected. By doing so, surgeries that rely on accurate C-Arm repositioning will benefit from significantly shorter repositioning time and radiation exposure to patients, and surgical personnel will also decrease. This, in fact, will have the chain reaction of reducing surgery cost and surgery risk such as infections and anesthesia complications.

## 6.3 Future Work

One of the next important steps for the continuation of the C-Arm repositioning project will be the development of obstacles in the repositioning program. For example, how can a robot arm move itself from one cartesian space point to another and still consider the physical limitation of its joints? In addition, no-go regions might also exist, where the robot arm must avoid a physical obstacle or barrier. In the case of the C-Arm, the obstacles are the patient and the operating table. These kinds of scenarios place challenges for path planning, where the route from one point to the next is never a straight line. Solutions to these kinds of problems have been proposed by J.T. Schwarz and M. Sharir, where attempts were made to find the shortest robotic path between two points while avoiding obstacles. Figure 68 shows an example problem where the shortest path between point  $x$  and  $y$  was calculated all while avoiding four separate obstacles. [39]

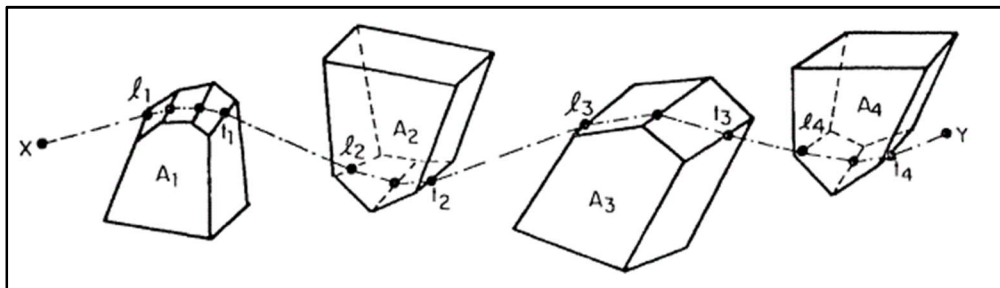


Figure 68. Motion Planning Algorithm Example Problem [39]



Furthermore, the inverse kinematic model of the CAP needs to be further developed to include the position of the camera lens. With this addition to the kinematics, repositioning could be applied not only to the AOI but also to the orientation of the point. This could lead to better repositioning.

Finally, a secondary repositioning method needs to be developed that will allow for the small angle adjustments. Once the C-Arm or a physical prototype is repositioned using the Vicon integration method of this thesis, small errors in reposition most likely still exist. A secondary repositioning method that uses artificial intelligence and image processing could through analysis of imaging detect the small errors in repositioning. After these error values are found, projective transformations can be found, and adjustment signals can be produced. These adjustment signals could then be sent to the kinematic model of the C-Arm to make small angle adjustments to ensure repositioning perfection. Such a secondary system can be seen in Figure 69 below. A full diagram of the first and second step repositioning vision can be found in Figure 28 in the beginning of Chapter 3.

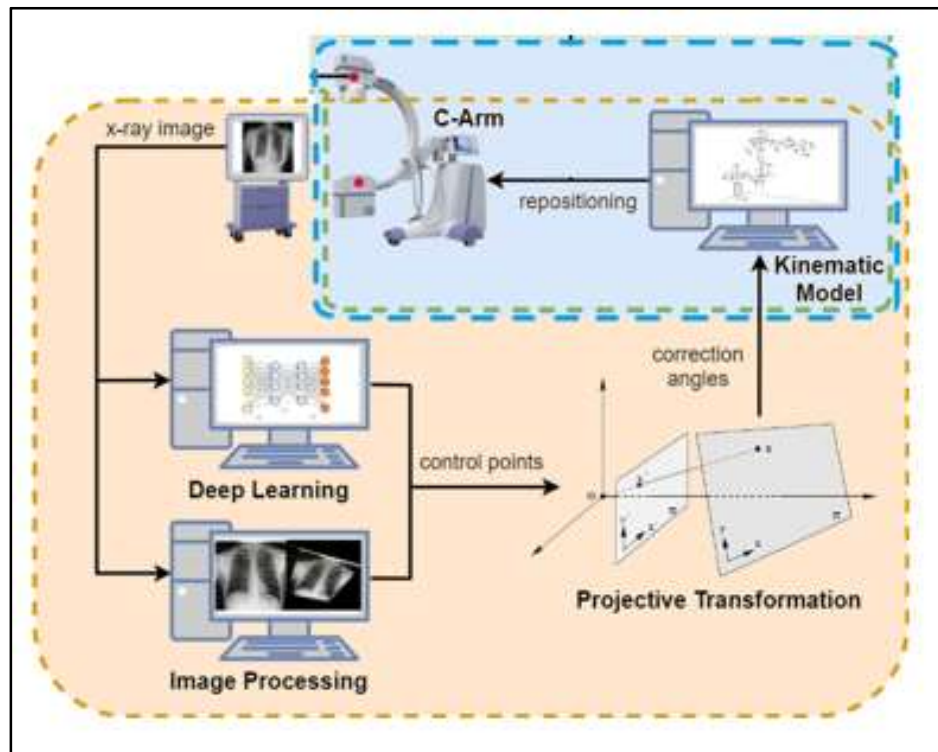


Figure 69. Second Step of Automatic C-Arm Repositioning Goal

## References

- [1] Bluestone Diagnostics, "GE OEC 9800 PLUS MOBILE C-ARM," General Electric Company, 2019. [Online]. Available: <https://bluestonediagnostics.com/product/ge-oec-9800-c-arm/>. [Accessed 17 3 2019].
- [2] General Electric Company, "OEC 9900 Elite Mobile C-arm," General Electric, 2018. [Online]. Available: [http://africa.gehealthcare.com/en/products/categories/surgical\\_imaging/oec\\_c-arms/oec\\_9900\\_elite](http://africa.gehealthcare.com/en/products/categories/surgical_imaging/oec_c-arms/oec_9900_elite). [Accessed 17 3 2019].
- [3] Elizabeth W. Riser, Rupen Desai, Sarah A. Byrd, Harrison Farber, Deborah Chi, Cary S. Idler, Robert E. Isaacs, "C-Arm Positioning Is a Significant Source of Radiation in Spine Surgery," *Spine*, vol. 42, no. 9, pp. 707-710, 2017.
- [4] "Siemens-healthineers.com," Siemens, 2019. [Online]. Available: <https://www.siemens-healthineers.com/en-us/surgical-c-arms-and-navigation>. [Accessed 07 May 2019].
- [5] Philips Electronics Company, "History of X-ray," [Online]. Available: [https://www.philips.com/consumerfiles/newscenter/main/shared/assets/Downloadablefile/FACT\\_SHEET\\_X-ray\\_history.pdf](https://www.philips.com/consumerfiles/newscenter/main/shared/assets/Downloadablefile/FACT_SHEET_X-ray_history.pdf). [Accessed 21 03 2019].
- [6] J. Hofman, "The art of medical imaging: Philips and the evolution of medical X-ray technology," in *Medicalmundi*, 2010.
- [7] Z. Shao, "Virtual Reality Aided Positioning of Mobile C-Arms for," *Advances in Mechanical Engineering*, vol. 2014, no. 25 June 2014, pp. 5-12, 2014.
- [8] S. C. Leschka, "C-arm cone beam computed tomography needle path overlay for image-guided procedures of the spine and pelvis," *Neuroradiology*, pp. 5-7, April 2011.
- [9] H. Xiao, "RGBD Camera Integration into Camera Augmented Mobile C-arm (CamC)," 2015.
- [10] N. Navab, "Camera Augmented Mobile C-Arm (CAMC): Calibration, Accuracy Study, and Clinical Applications," *IEEE Transactions on Medical Imaging*, vol. 29, no. No.7, p. 1414, 2010.

- [11] P. Azad, "Combining Appearance-based and Model-based Methods for Real-Time Object Recognition and 6D Localization," in *International Conference of Intelligent Robotics and Systems*, Beijing, China, 2006.
- [12] Alireza Yazdanshenas, Emilli Morrison, Chung-Hyun Goh, Janet K. Allen, Farrokh Mistree, "Repositioning Method of C-Arm Using Motion Capture on the Virtual Reality Platform," in *IASTEM International*, Seoul, South Korea, 2018.
- [13] E. Marinetto, "Optical Tracking System Interaction into IORT Treatment Planning System," in *Mediterranean Conference of Medical and Biological Engineering and Computing*, Madrid, Spain, 2013.
- [14] N. Navab, "Visual Servoing for Intraoperative Positioning and Repositioning of Mobile C-arms," in *MICCAI*, Munich, Germany, 2006.
- [15] M. Unberath, "Augmented reality-based feedback for technician-in-the-loop C-arm repositioning," *Healthcare Technology Letters*, vol. 5, no. 5, pp. 143-147, 2018.
- [16] Z. Shao, "Virtual Reality Aided Mobile C-arm Positioning for Image-Guided Surgery," University of Tennessee, Knoxville, Tennessee, 2013.
- [17] C. Schaller, "Inverse C-arm Positioning for interventional procedures using real-time body part detection," in *ResearchGate*, Erlangen, Germany, 2009.
- [18] O. J. Bott, "Use of a C-Arm Fluoroscopy Simulator to Support Training in Intraoperative Radiography," *Informatics in Radiology*, vol. 31, no. May-June 2011, pp. 2-10, 2011.
- [19] P. Stefan, "A Mixed-Reality Approach to Radiation-Free Training of C-arm Based Surgery," in *International Conference of Medical Image Computing and Computer-Assisted Intervention*, Munich, Germany, 2017.
- [20] Tiago Leal Ghezzi, Oly Campos Corleta, "30 Years of Robotic Surgery," *World Journal of Surgery*, no. 16 May 2016, pp. 2550-2557, 2016.
- [21] Z. B. Serdar Kucuk, *Robot Kinematics: Forward and Inverse Kinematics*, Germany: Web of Science, 2006.
- [22] A. Pott, "Arm Algorithm for Real-time Forward Kinematics of Cable-Driven Parallel Robots," *Advances in Robot Kinematics: Motion in arm and Machine*, no. 2010, pp. 529-530, 2010.

- [23] Ana C. Majarena, Jorge Santolaria, David Samper, Juan J. Aguilar, "An Overview of Kinematic and Calibration Models Using Internal/External Sensors or Constraints to Improve the Behavior of Spatial Parallel Mechanisms," *Sensors*, vol. 10, no. November 16 2010, pp. 10256-10297, 2010.
- [24] C. G. Atkeson, "Learning Arm Kinematics And Dynamics," Massachusetts Institute of Technology, Cambridge, Massachusetts, 1989.
- [25] Hadi El Daou, K. C. Geoffrey, Richard Van Arkel, Jonathan Jeffers, Ferdinando Rordriguez Y Baena, "Robotic Hip Joint Testing: Developmental and Experimental Protocols," *Medical Engineering and Physics*, vol. 63, no. 2019, pp. 57-62, 2019.
- [26] J. M. Selig, *Introduction to Robotics*, Hemel Hempstead: Prentice Hall, 1992.
- [27] P. Corke, *Robotics, Vision and Control*, Berlin: Springer, 2011.
- [28] Rostislav Vasilchenko, Fedor Simankin, Grigorii Ziyakeav, Arkadiy Simankin, "Kinematics of the orbital movement of a digital X-ray scanner of annular pipe seams," *International Forum for Young Scientist*, vol. 158, no. MATEC Web Conf, 2018.
- [29] R. K. Serkan Dereli, "IW-PSO Approach to the Inverse Kinematics Problem Solution of a 7-DOF Serial Robot Manipulator," *Sigma Journal of Engineering and Natural Sciences*, vol. 36, no. 1, pp. 77-85, 2018.
- [30] Ahmed Khalifa, Mohamed Fanni, Ahmed Ramadan, Ahmed Abo-Ismael, "New Quadrotor Manipulation System: Inverse Kinematics, Identification and RC-Based Control," *International Journal of Recent Advances in Mechanical Engineering*, vol. 4, no. 3, pp. 39-58, 2015.
- [31] De Xu, Carlos A. Acosta, Calderon, John Q. Gan, Huosheng Hu, "An Analysis of the Inverse Kinematics for a 5-DOF Manipulator," *International Journal of Automation and Computing*, vol. 2, no. 2005, pp. 114-124, 2005.
- [32] "cnsoyo.com," CNSOYO, 2014. [Online]. Available: [http://www.cnsoyo.com/?gclid=CjwKCAjwwtTmBRBqEiwA-b6c\\_60yDw4Ox3-XRbRokI5SiC\\_mN7RLChTlxpsnVDPnAowJ2Q7IVN2sGBoCz1YQAvD\\_BwE](http://www.cnsoyo.com/?gclid=CjwKCAjwwtTmBRBqEiwA-b6c_60yDw4Ox3-XRbRokI5SiC_mN7RLChTlxpsnVDPnAowJ2Q7IVN2sGBoCz1YQAvD_BwE). [Accessed 10 05 2019].
- [33] Adso Fernandez-Baena, Antonio Susin, Xavier Llgadas, "Biomechanical Validation of Upper-Body and Lower-Body Joint Movements of Kinectic Motion Capture Data

- for Rehabilitation Treatments," in *International Conference on Intelligent Networking and Collaborative Systems*, Bucharest, Romania, 2012.
- [34] John Andrew Berton, Kai-Lin Chuang, "Effects of Very High Frame Rate Display in Narrative CGI Animation," in *International Conference Information Visualisation (IV)*, Lisbon, Portugal, 2016.
- [35] Shaima Al Habsi, Maha Shehada, Marwah Abdoon, Ahmed Mashood, Hassan Noura, "Intergration of Vicon Camera System for Indoor Flight of a Parrot AR Drone," in *Internatonal Symposium on Mechatronics and its Applications*, Sharjah, United Arab Emirates, 2015.
- [36] Andrew Chan, Janelle Aguillon, Doug Hill, Edmond Lou, "Precision and accuracy of consumer-grade motion tracking system for pedicle screw placement in pediatric spinal fusion surgery," *Medical Engineeing and Physics*, vol. 46, pp. 33-43, 2017.
- [37] J. M. Donald, "Indoor Flight of AR Drone 2.0 UAV in Vicon Motion Capture System," University of New South Wales, Canberra, 2017.
- [38] Patric Eichelberger, Matteo Ferraro, Ursina Minder, Trevor Denton, Angela Blasimann, Fabian Krause, Heiner Baur, "Analysis of Accuracy in Optical Motion Capture- a protocol for laboratory setup evaluation," *Journal of Biomechanics*, vol. 49, pp. 2085-2088, 2016.
- [39] J. T. Schwartz, M. Sharir, "Motion Planning and Related Geometric Algorithms in Robotics," in *International Congress of Mathematics*, Berkley, California, 1986.

Appendix A: C-Arm Virtual Prototype & Virtual Platform CAD Models

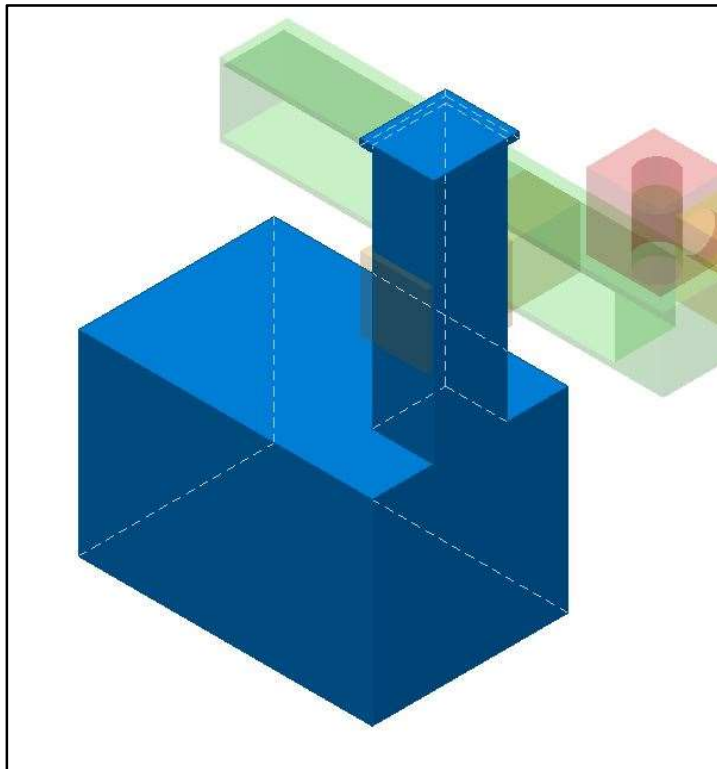


Figure 70. Virtual C-Arm Base

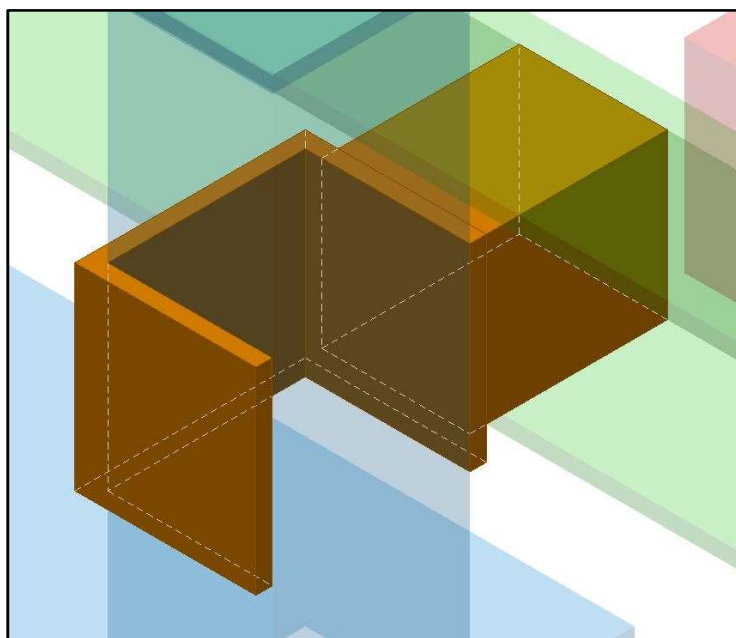


Figure 71. Vertical Translation Joint

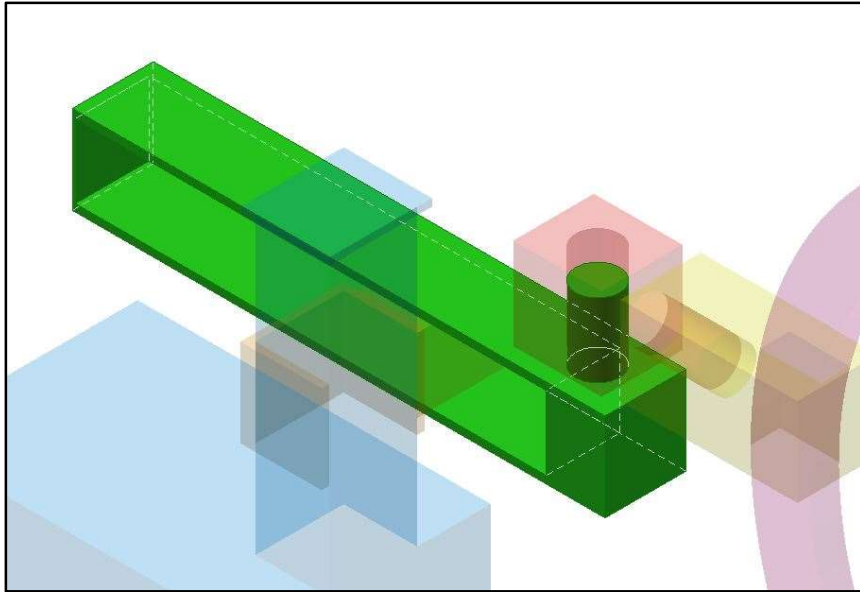


Figure 72. Horizontal Translational Joint

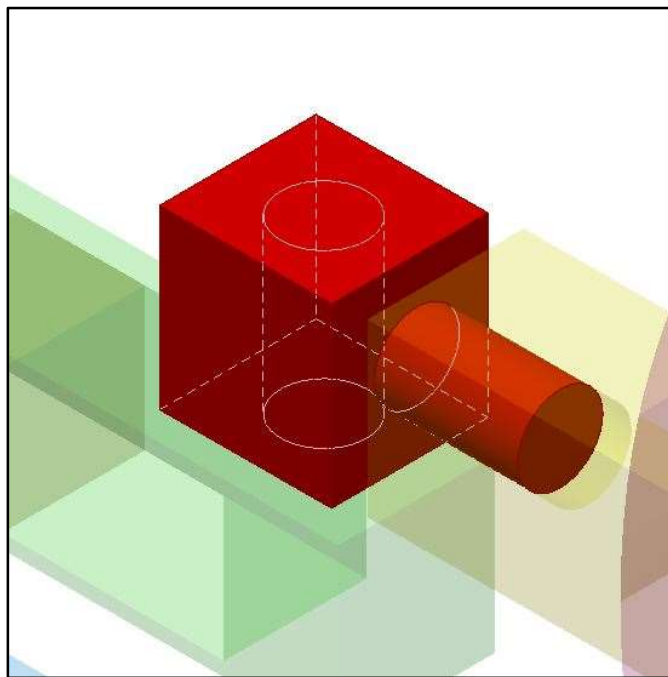


Figure 73. Wig-Wag Link

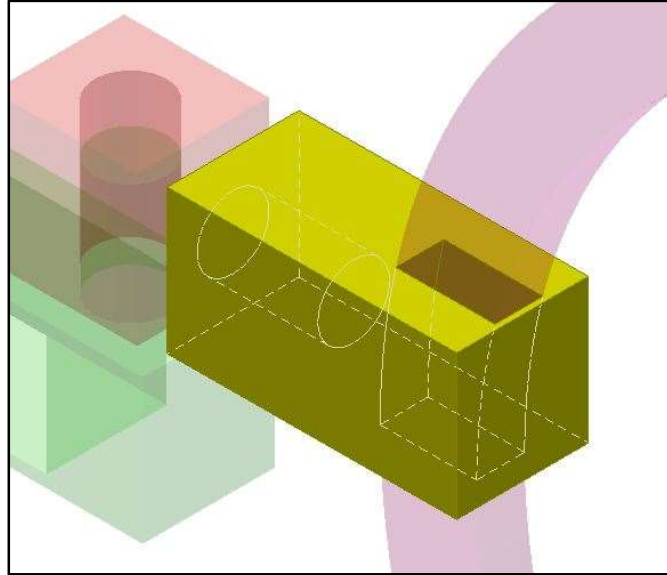


Figure 74. Tilt Link

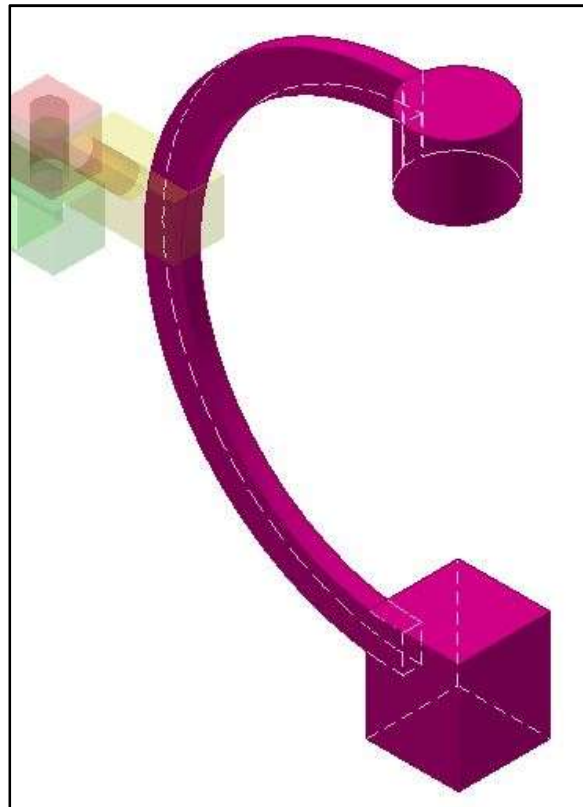


Figure 75. Orbital Link



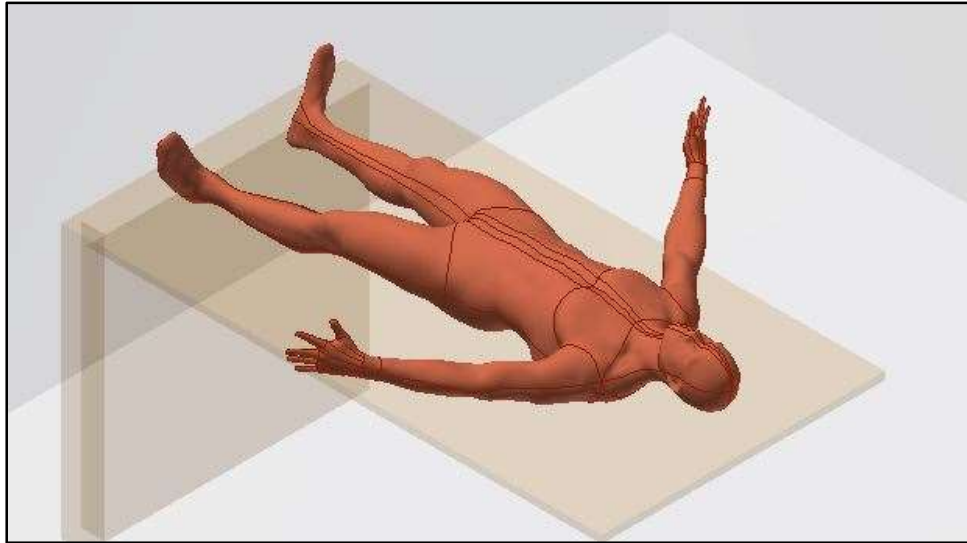


Figure 76. Humanoid Shape

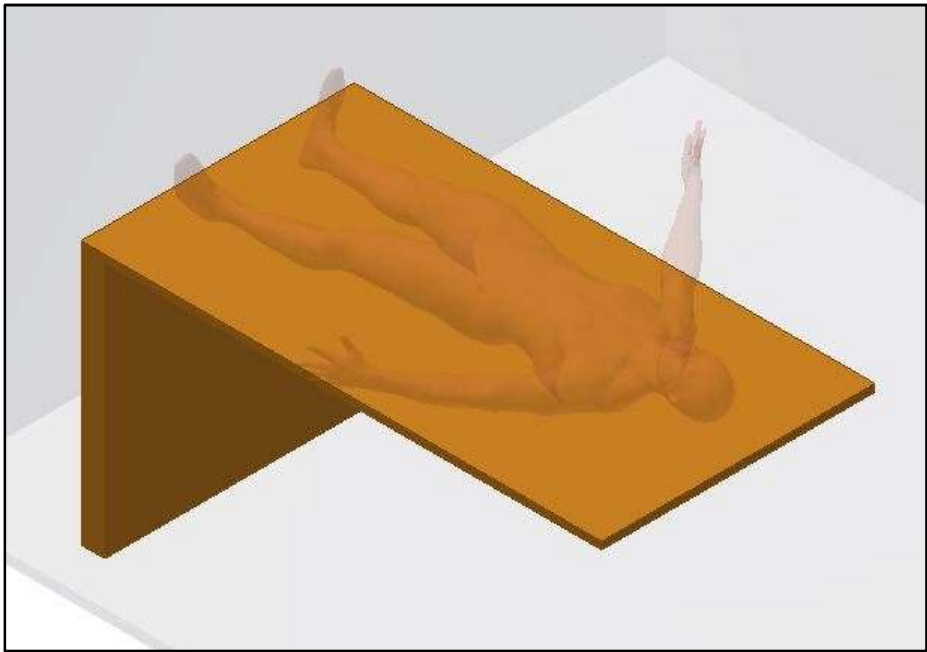


Figure 77. Operation Table

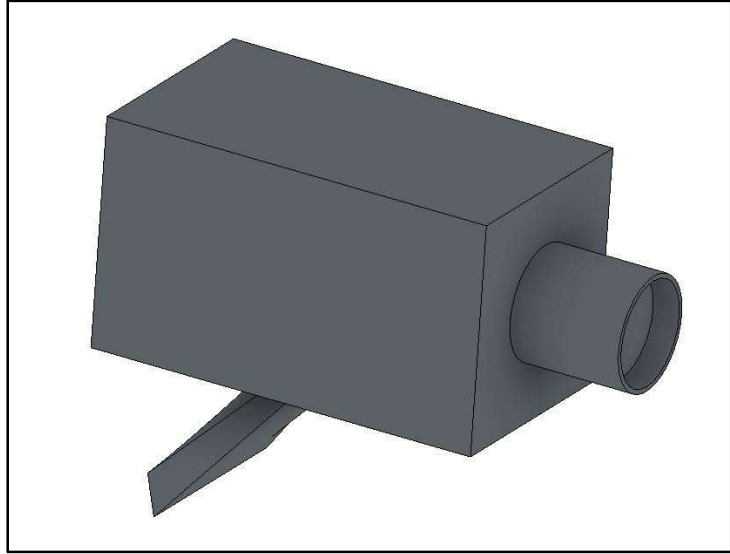


Figure 78. Vicon Motion Capture Camera

## Appendix B: Simulink Models

### C-Arm Virtual Platform Simulink Subsystems

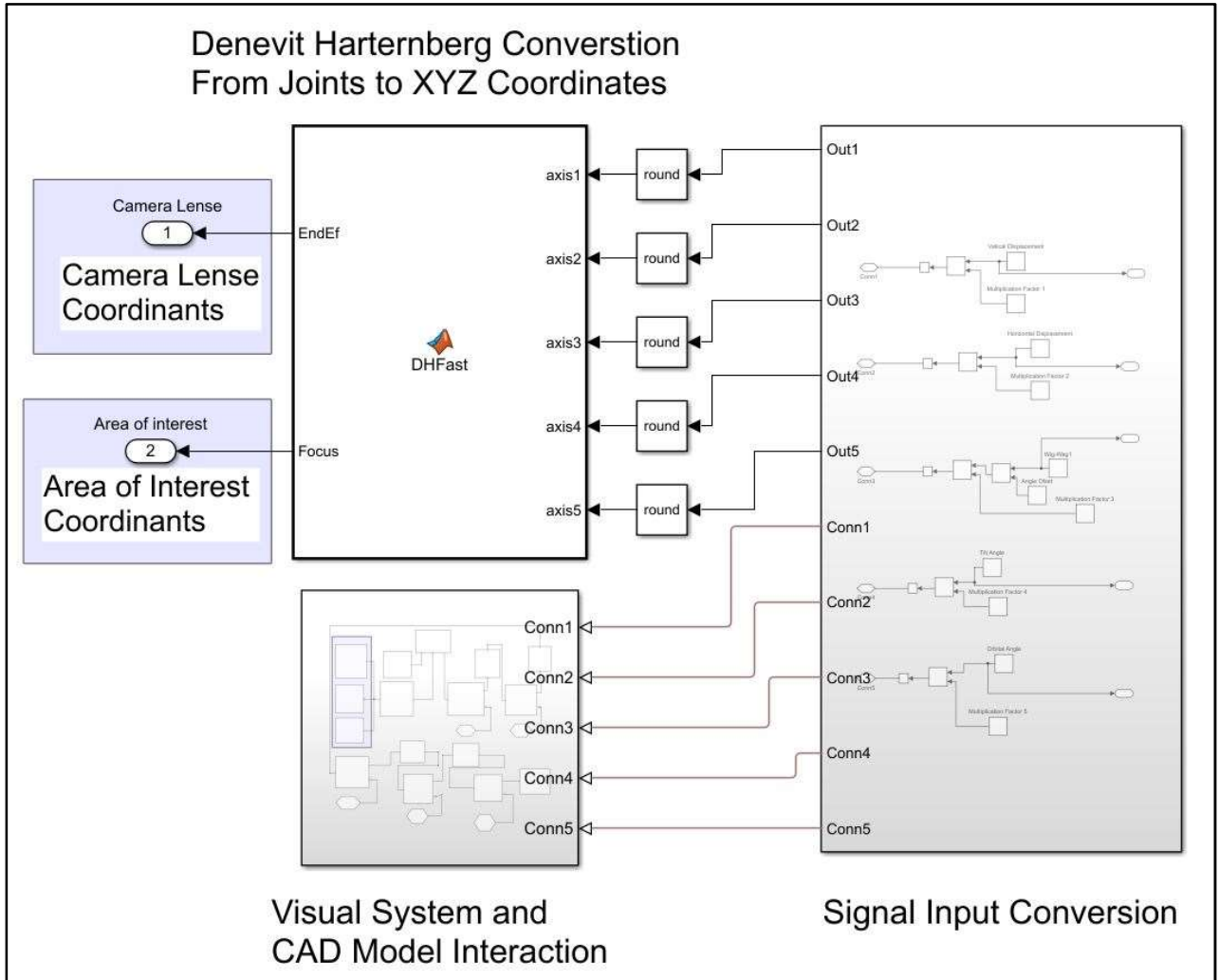


Figure 79. GUI Virtual Model Background Calculations

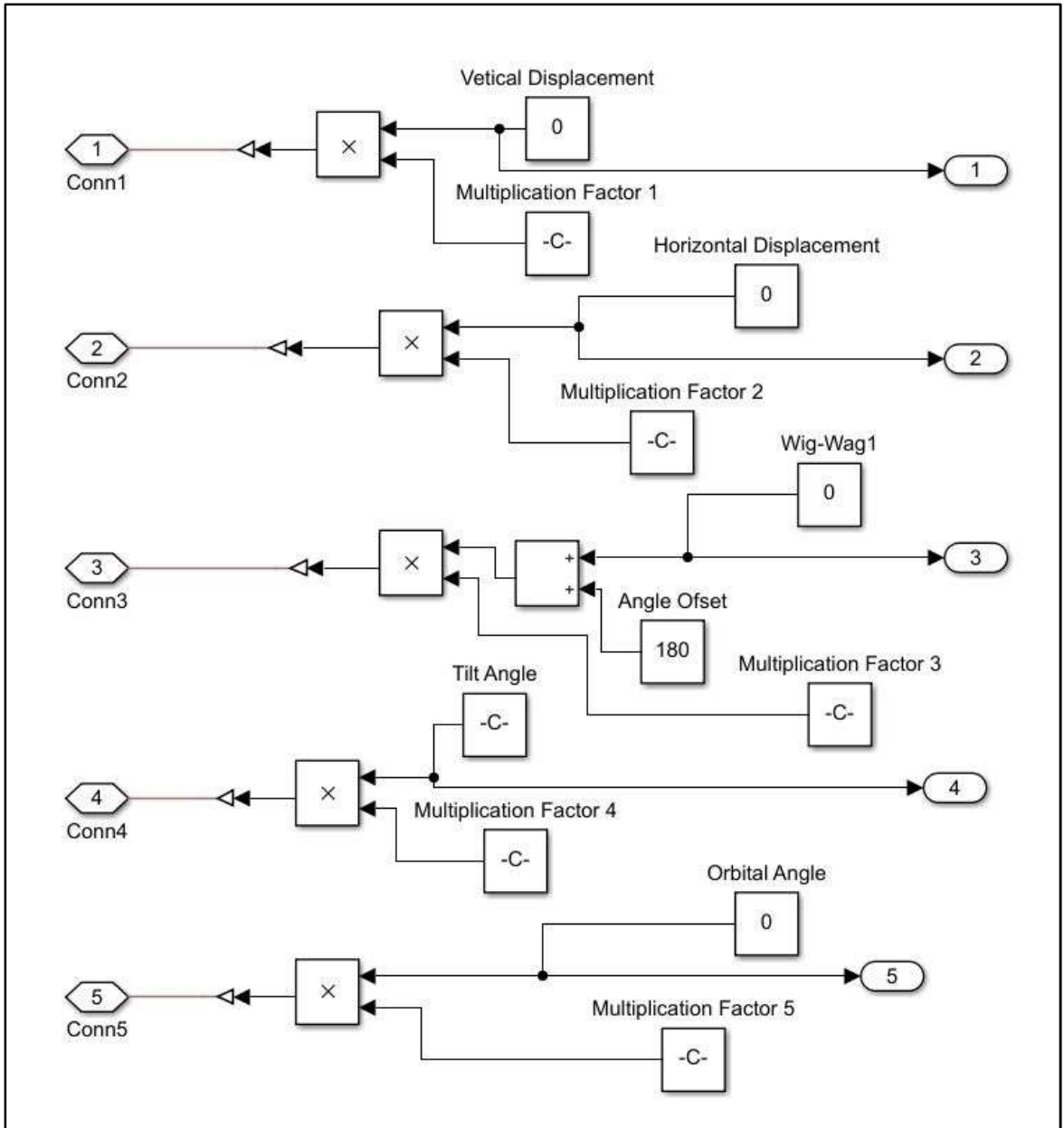


Figure 80. GUI Signal Input Conversion

# C-Arm Physical Prototype Simulink Subsystems

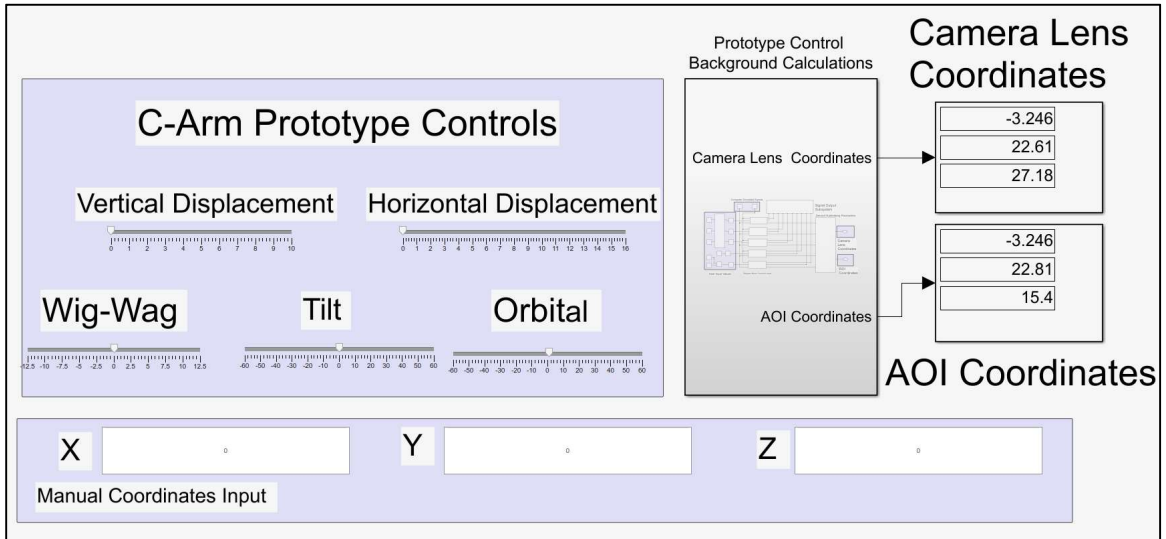


Figure 81. GUI for C-Arm Prototype (all joints set to zero)

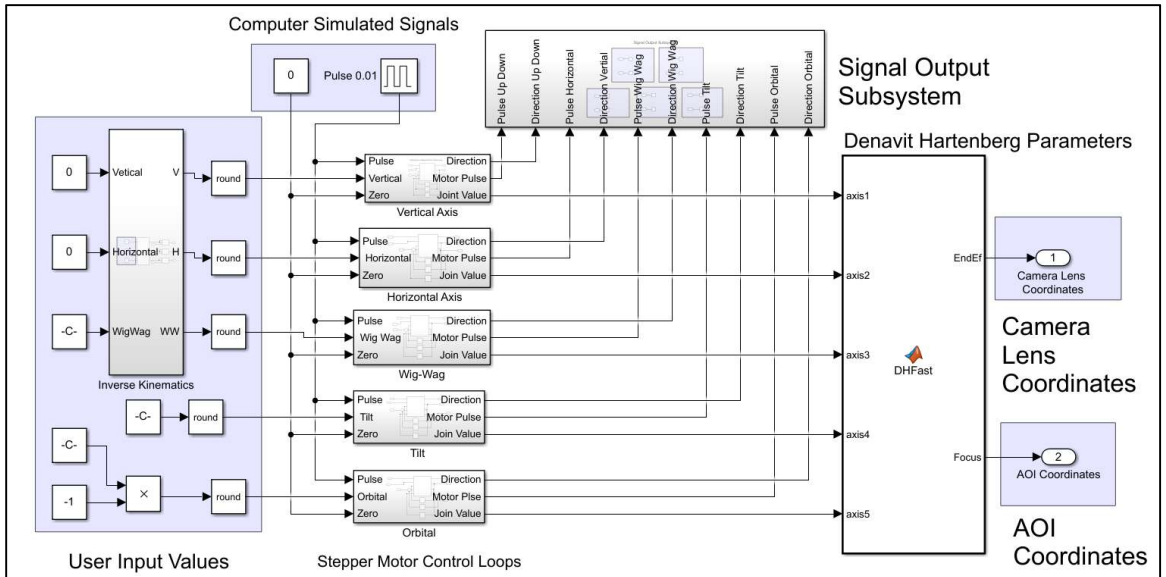


Figure 82. C-Arm Prototype GUI Background Computations

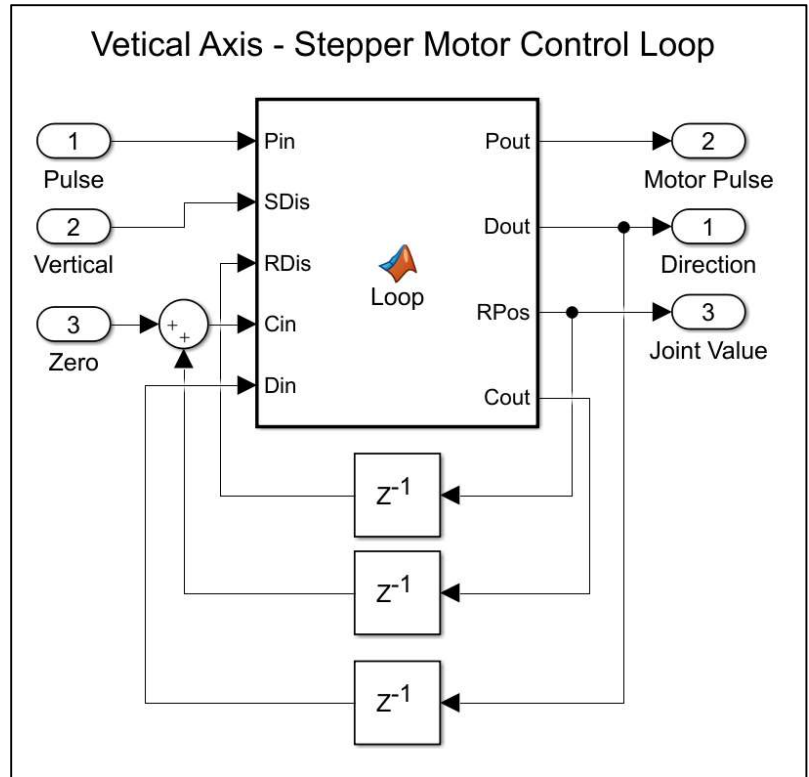


Figure 83. Stepper Motor Control Loop (vertical axis used as an example)

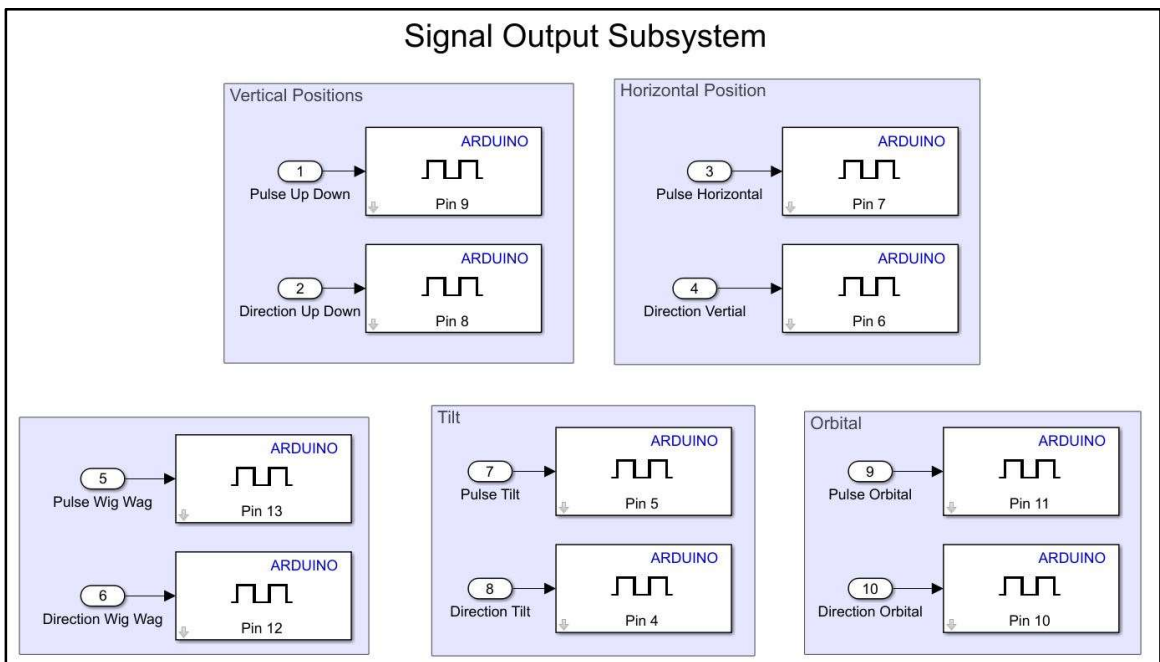


Figure 84. Signal Output Subsystem to Arduino

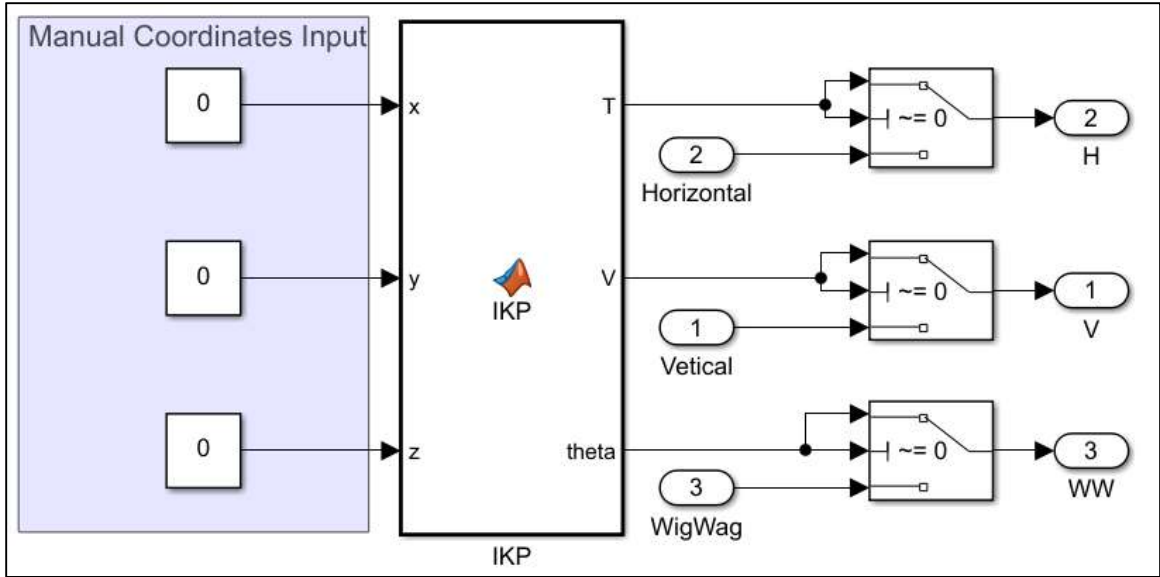


Figure 85. Inverse Kinematics Subsystem

## Appendix C: MATLAB Computer Code

### User defined function block “Vertical Axis- Stepper Motor Control Loop”

This function block script and all other function blocks for the “Stepper Motor Control Loops” convert the GUI input values to motor signals for the Arduino Mega and movement values used in the “Denavit Hartenberg Parameters” block.

```
function [Pout,Dout,RPos,Cout] =Loop(Pin,SDis,RDis,Cin,Din)

% Initial Values set for Pout and for RPos

Pout=0;
RPOs=0;

% If conditions checking the input of the GUI and determining the
% direction the stepper motor must turn to reach is desired position.
% This loop also checks if the motor must move at by asking if the
% prototype has reached its desired position already or not.

if SDis<RDis && Pin==1
    Cin=Cin-1;
    Din=1;
    Pout=Pin;

elseif SDis>RDis && Pin==1
    Cin=Cin+1;
    Din=0;
    Pout=Pin;

elseif SDis==RDis
    Cin=Cin;
    Din=Din;

else

end

RPos=Cin*0.00019685
Cout=Cin;
Dout=Din;
end

% 0.00019685 is the conversion factor specified by a different value to
% each of the five stepper motors. These conversion factors specify
% how much robotic movement the stepper motor produces with each step
% these movements are in inches for the translational joints and in
%degrees for rotational joints
```



## User defined function block “Denavit Hartenberg Parameters”

This function block script uses the DH Parameters and the DH Transformation Matrix to convert the GUI specified movements of each joint to output x,y,z coordinates. In this scrip the coordinates for the AOI and the Camera Lens are Produced.

```
%Denavit Hartenberg Parameter Calculations

function [EndEf, Focus] =DHFast(axis1, axis2, axis3, axis4, axis5)

% angles of joint movement (rotation about the z axis) in deegree
% provided by GUI input.

T0=0;
T1=0;
T2=0;
T3=axis3*pi/180;
T4=(axis4-90)*pi/180;
T5=axis5*pi/180;

% translations of each joint, in inches, along the z axix
% provided by GUI input and by physical robot constants.

S0=0;
S1=15.4+axis1
S2=0.525+axis2
S3=0;
S4=22.29;
S5=0;

% degrees offset of each joint along the x-axis.
% All these values are constants and do not change.

Ao0=0;
Ao1=-90*pi/180;
Ao2=90*pi/180;
Ao3=-90*pi/180;
Ao4=90*pi/180;
Ao5=0;

% translational offset of joints on the x axis in inches.
% All these values are constants and od not change.

O0=0;
O1=-3.246;
O2=0;
O3=0;
O4=0;
O5=11.78;

% Calculated joint states using Denevit Hartenberg matrix.
```

```
% All Previously gathered parameters T,S,A, O values will be placed in
% the following.
```

```
J0=[1 0 0 0;0 1 0 0;0 0 1 0;0 0 0 1];
J1=[cos(T1) -sin(T1)*cos(Ao1) sin(T1)*sin(Ao1) O1*cos(T1);sin(T1)
cos(T1)*cos(Ao1) -cos(T1)*sin(Ao1) O1*sin(T1);0 sin(Ao1) cos(Ao1) S1;0
0 0 1];
J2=[cos(T2) -sin(T2)*cos(Ao2) sin(T2)*sin(Ao2) O2*cos(T2);sin(T2)
cos(T2)*cos(Ao2) -cos(T2)*sin(Ao2) O2*sin(T2);0 sin(Ao2) cos(Ao2) S2;0
0 0 1];
J3=[cos(T3) -sin(T3)*cos(Ao3) sin(T3)*sin(Ao3) O3*cos(T3);sin(T3)
cos(T3)*cos(Ao3) -cos(T3)*sin(Ao3) O3*sin(T3);0 sin(Ao3) cos(Ao3) S3;0
0 0 1];
J4=[cos(T4) -sin(T4)*cos(Ao4) sin(T4)*sin(Ao4) O4*cos(T4);sin(T4)
cos(T4)*cos(Ao4) -cos(T4)*sin(Ao4) O4*sin(T4);0 sin(Ao4) cos(Ao4) S4;0
0 0 1];
J5=[cos(T5) -sin(T5)*cos(Ao5) sin(T5)*sin(Ao5) O5*cos(T5);sin(T5)
cos(T5)*cos(Ao5) -cos(T5)*sin(Ao5) O5*sin(T5);0 sin(Ao5) cos(Ao5) S5;0
0 0 1];
```

```
% Calculated Transformation of each joint. These Transformations
% contain the x,y,z, coordinates and the roll, pitch, and yaw for each
% Joint.
```

```
T0=J0;
T1=J0*J1;
T2=T1*J2;
T3=T2*J3;
T4=T3*J4;
EE=T4*J5;
```

```
% extracted z,y,z coordinates of each joint.
```

```
Joint1=T1(1:3,4);
Joint2=T2(1:3,4);
Joint3=T3(1:3,4);
Focus=T4(1:3,4);
EndEf=EE(1:3,4)
```

## User Defined Block IDK for the calculation of the Inverse Kinematics

```
function [T,V,theta] = IKP(x,y,z)

% conditon set for the use of forwardk kinematics

if x==0 && y==0 && z==0
    theta=0
    V=0
    T=0
else

    %vertical calculation (z)

    V=z-15.4;
    if V<0
        V=0;
    else
    end

    % horizontal and depth calculations(X,Y)
    % base on all four different cases

    if x< -3.246
        t=(-1)*asin((x+3.246)/22.296);
        theta=t*180/pi
        b=cos(t)*22.29;
        T=y-b-0.525;

        if T<0
            T=0
        else
        end

    elseif x<0 && x>-3.246
        a=3.246+x;
        t=(-1)*asin(a/22.29);
        theta=t*180/pi
        b=cos(t)*22.29;
        T=y-b-0.525;

        if T<0
            T=0
        else
        end

    elseif x>0
        a=x+3.246;
        t=(-1)*asin(a/22.29);
        theta=t*180/pi
        b=cos(t)*22.29;
        T=y-b-0.525;
    else
    end
end
```

```

a=0;
b=22.29;
theta=0;
T=y-b-0.525;

if T<0
    T=0
else
end
end
end

end

```

## Vicon Data Processing MATLAB Code

This script uses the collected data from the Vicon markers placed on the CAP. To produce the results and graphs that show the difference between the Kinematic model and the actual CAP Movements.

### Wig-Wag Test

```

%wig-wag Test

%read data
Orgin=table2array(WigWagTest(:,1:3));
Lens=table2array(WigWagTest(:,4:6));
Detector=table2array(WigWagTest(:,7:9));

% tranform to local coordinants
Lens=Lens-Orgin;
Detector=Detector-Orgin;

%calculate Area of Interest
Area=(Lens+Detector)/2

% convert form mm to inches
Lens=Lens*0.0393701;
Area=Area*0.0393701;

% Normalize coordinants and apply offset
Lens=[(Lens(:,1)-1)*-1 Lens(:,2)*-1 Lens(:,3)+3];
AOI=[(Area(:,1)-1)*-1 Area(:,2)*-1 Area(:,3)+3];

% show s
figure(1)
plot3(Lens(:,1),Lens(:,2),Lens(:,3))

figure(2)
plot3(AOI(:,1),AOI(:,2),AOI(:,3))

```

## Tilt Test

```
% Tilt Test

% acquire Data
Orgin=table2array(TiltTest(:,1:3));
Lens=table2array(TiltTest(:,4:6));
Detector=table2array(TiltTest(:,7:9));

% tranform to local coordinants
Lens=Lens-Orgin;
Detector=Detector-Orgin;

%calculate Area of Interest
Area=(Lens+Detector)/2

% convert form mm to inches
Lens=Lens*0.0393701;
Area=Area*0.0393701;

% Normalize coordinants and apply offset
Lens=[(Lens(:,1)-1)*-1 Lens(:,2)*-1 Lens(:,3)+3];
AOI=[(Area(:,1)-1)*-1 Area(:,2)*-1 Area(:,3)+3];

% show figures
figure(1)
plot3(Lens(:,1),Lens(:,2),Lens(:,3))

figure(2)
plot3(AOI(:,1),AOI(:,2),AOI(:,3))
```

## Orbital Test

```
% orbit Test

% acquire Data
Orgin=table2array(OrbTest(:,1:3));
Lens=table2array(OrbTest(:,4:6));
Detector=table2array(OrbTest(:,7:9));

% tranform to local coordinants
Lens=Lens-Orgin;
Detector=Detector-Orgin;

%calculate Area of Interest
Area=(Lens+Detector)/2

% convert form mm to inches
Lens=Lens*0.0393701;
Area=Area*0.0393701;

% Normalize coordinants and apply offset
Lens=[(Lens(:,1)-1)*-1 Lens(:,2)*-1 Lens(:,3)+3];
```

```
AOI=[(Area(:,1)-1)*-1 Area(:,2)*-1 Area(:,3)+3];
```

```
% show figures
```

```
figure(1)
```

```
plot3(Lens(:,1),Lens(:,2),Lens(:,3))
```

```
figure(2)
```

```
plot3(AOI(:,1),AOI(:,2),AOI(:,3))
```

## Appendix D: G-Code Used in CNC

**(Start: BASE FRAME-ZERO)**

(T1 D=0.375 CR=0. - ZMIN=-0.125 - FLAT  
 END MILL)  
 G90 G94 G91.1 G40 G49 G17  
 G20  
 G28 G91 Z0.  
 G90

(2D POCKET1)

M5  
 M9  
 T1 M6  
 S800 M3  
 G54  
 M9  
 G0 X1. Y-3.5717  
 G43 Z0.6 H1  
 Z0.2  
 G1 Z0.1594 F40.  
 Z-0.125 F10.  
 X1.0155 F12.  
 G2 X1.0283 Y-3.5845 I0. J-0.0128  
 G1 Y-4.3155  
 .  
 .  
 .  
 .

G2 X1.6125 Y-3.175 I0. J-0.1875  
 G1 Y-4.2062  
 G0 Z0.6  
 M9  
 G28 G91 Z0.  
 G28 X0. Y0.  
 M30

**(End: BASE FRAME-ZERO)**

**(Start: BASE PLATE 1)**

(T1 D=0.25 CR=0. - ZMIN=-0.5015 - FLAT  
 END MILL)  
 G90 G94 G91.1 G40 G49 G17  
 G20  
 G28 G91 Z0.  
 G90

(2D ADAPTIVE13)

M5  
 M9  
 T1 M6  
 S1000 M3

G54  
 M9  
 G0 X0.887 Y1.375  
 G43 Z0.6 H1  
 Z0.125  
 G1 Z0.1 F3.  
 Z-0.2  
 X0.8859 Y1.374  
 X0.8844 Y1.3741

.  
 .  
 .  
 .  
 X1.2387 Y1.371 Z-0.4912  
 X1.238 Y1.369 Z-0.4878  
 X1.2375 Y1.3676 Z-0.4842  
 X1.2372 Y1.3668 Z-0.4804  
 X1.2371 Y1.3665 Z-0.4765  
 G0 Z0.6  
 M9  
 G28 G91 Z0.  
 G28 X0. Y0.  
 M30

**(End: BASE PLATE 1)**

**(Start: LARGE SIDE PLATE 8)**

(T2 D=0.25 CR=0. - ZMIN=-0.235 - FLAT  
 END MILL)  
 G90 G94 G91.1 G40 G49 G17  
 G20  
 G28 G91 Z0.  
 G90

(DRILL5)

M5  
 M9  
 T2 M6  
 S5000 M3  
 G54  
 M8  
 G0 X7.8 Y1.78  
 G43 Z0.6 H2  
 Z0.2  
 G98 G81 X7.8 Y1.78 Z-0.205 R0.2 F13.3  
 Y2.7805  
 X3.725 Y4.14  
 X2.3399 Y4.1065  
 X0.975 Y3.565  
 X0.3 Y2.26

X0.975 Y0.975  
 X2.3421 Y0.4315  
 X3.725 Y0.4  
 G80  
 Z0.6  
  
 (2D ADAPTIVE1)  
 S2000 M3  
 M9  
 G0 X3.0604 Y2.3271  
 Z0.6  
 Z0.1  
 G3 X3.296 Y2.297 Z0.0342 I0.1178 J-0.015  
 F5.  
 X3.0604 Y2.3271 Z-0.0316 I-0.1178 J0.015  
 .  
 .  
 .

X3.4603 Y2.5838 Z-0.2213  
 X3.4589 Y2.5844 Z-0.2177  
 X3.458 Y2.5848 Z-0.2139  
 X3.4578 Y2.5849 Z-0.21  
 G0 Z0.6  
 M9  
 G28 G91 Z0.  
 G28 X0. Y0.  
 M30  
**(End: LARGE SIDE PLATE 8)**

**(Start: SMALL SIDE PLATE-16)**  
 (T2 D=0.25 CR=0. - ZMIN=-0.25 - FLAT  
 END MILL)  
 G90 G94 G91.1 G40 G49 G17  
 G20  
 G28 G91 Z0.  
 G90

(DRILL2)  
 M5  
 M9  
 T2 M6  
 S200 M3  
 G54  
 M9  
 G0 X2.2563 Y0.8813  
 G43 Z0.6 H2

Z0.2  
 .  
 .  
 .  
 X3.5875 Y3.088  
 X4.131 Y1.7212  
 X4.1698 Y0.3395  
 G80  
 Z0.6  
 M9  
 G28 G91 Z0.  
 G28 X0. Y0.  
 M30  
**(End: SMALL SIDE PLATE-16)**

**(Start: TILT BASE 19)**  
 (T1 D=0.5625 CR=0. - ZMIN=-0.48 - FLAT  
 END MILL)  
 (2D ADAPTIVE3)  
 M5  
 M9  
 T1 M6  
 S1000 M3  
 G54  
 M9  
 G0 X4.414 Y1.1383  
 Z0.15  
 G3 X4.3057 Y1.6616 Z0.1207 I-0.0542  
 J0.2616 F3.  
 X4.414 Y1.1383 Z0.0914 I0.0542 J-0.2616  
 X4.3057 Y1.6616 Z0.0621 I-0.0542 J0.2616  
 X4.414 Y1.1383 Z0.0328 I0.0542 J-0.2616  
 X4.627 Y1.4 Z0.02 I-0.0542 J0.2616  
 X4.7076 Y1.7059 Z-0.4519

.  
 .  
 .  
 X4.7053 Y1.7073 Z-0.4466  
 X4.7035 Y1.7084 Z-0.4411  
 X4.7022 Y1.7092 Z-0.4354  
 X4.7014 Y1.7097 Z-0.4296  
 X4.7012 Y1.7099 Z-0.4238  
 G0 Z0.6  
 M9 G28 G91 Z0.  
 G28 X0. Y0. M30  
**(End: TILT BASE 19)**



## Appendix E: Purchased Standard and Stock Parts

4/20/2019

6061 Aluminum with Certification, 1/2" Thick x 3" Wide | McMaster-Carr

**McMASTER-CARR.**

6061 Aluminum with Certification  
1/2" Thick x 3" Wide

9872T119



Material	6061 Aluminum
Shape	Sheet and Bar
Thickness	1/2"
Thickness Tolerance	-0.009" to 0.009"
Tolerance Rating	Standard
Width	3"
Width Tolerance	-0.034" to 0.034"
Length Tolerance	-1" to 1"
Yield Strength	35,000 psi
Fabrication	Extruded
Temper	T6511
Heat Treatment	Hardened
Hardness	Brinell 95 (Soft)
Certification	Material Certificate with Traceable Lot Number and Test Report
Heat Treatable	Yes
Appearance	Plain
Temperature Range	-320° to 300° F
Specifications Met	ASTM B221
Aluminum Performance Properties	Corrosion Resistant, Easy to Machine, Easy to Weld
Straightness Tolerance	Not Rated
Elongation	12.5%
Material Composition	
Aluminum	95.1-98.2%
Chromium	0.4-0.8%
Copper	0.05-0.4%
Iron	0-0.7%
Magnesium	0.8-1.2%
Manganese	0-0.15%

**McMASTER-CARR.****6061 Aluminum with Certification**

1/4" Thick x 4" Wide

9872T68

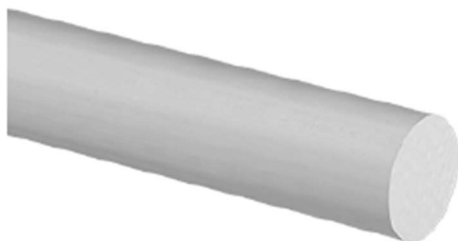


Material	6061 Aluminum
Shape	Sheet and Bar
Thickness	1/4"
Thickness Tolerance	-0.012" to 0.012"
Tolerance Rating	Standard
Width	4"
Width Tolerance	-0.034" to 0.034"
Length Tolerance	-1" to 1"
Yield Strength	35,000 psi
Fabrication	Extruded
Temper	T6511
Heat Treatment	Hardened
Hardness	Brinell 95 (Soft)
Certification	Material Certificate with Traceable Lot Number and Test Report
Heat Treatable	Yes
Appearance	Plain
Temperature Range	-320° to 300° F
Specifications Met	ASTM B221
Aluminum Performance Properties	Corrosion Resistant, Easy to Machine, Easy to Weld
Straightness Tolerance	Not Rated
Elongation	12.5%
Material Composition	
Aluminum	95.1-98.2%
Chromium	0.4-0.8%
Copper	0.05-0.4%
Iron	0-0.7%
Magnesium	0.8-1.2%

**McMASTER-CARR.****6061 Aluminum Rod with Certification**

2-1/4" Diameter

1615T34

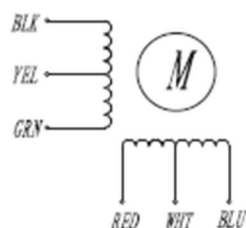


Material	6061 Aluminum
Shape	Rod and Disc
Shape Type	Rods
Diameter	2 1/4"
Diameter Tolerance	-0.034" to 0.034"
Tolerance Rating	Standard
Yield Strength	35,000 psi
Fabrication	Extruded
Temper	T6511
Heat Treatment	Hardened
Hardness	Brinell 95
Hardness Rating	Soft
Certification	Material Certificate with Traceable Lot Number and Test Report
Heat Treatable	Yes
Appearance	Plain
Temperature Range	-320° to 300° F
Specifications Met	ASTM B221
Aluminum Performance Properties	Corrosion Resistant, Easy to Machine, Easy to Weld
Straightness Tolerance	Not Rated
Elongation	12.5%
Material Composition	
Aluminum	95.1-98.2%
Chromium	0.4-0.8%
Copper	0.05-0.4%
Iron	0-0.7%
Magnesium	0.8-1.2%
..	- - - - -

## HIGH TORQUE HYBRID STEPPING MOTOR SPECIFICATIONS

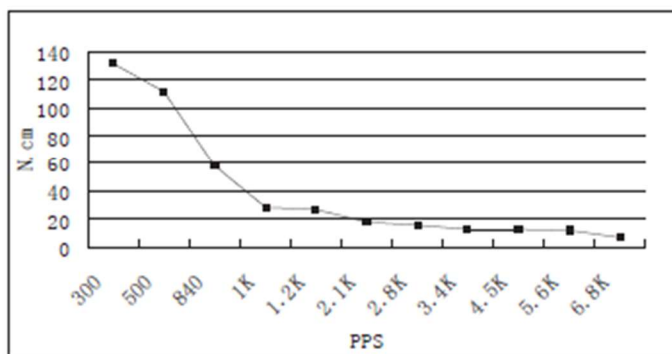
General specifications		Electrical specifications	
Step Angle (°)	1.8	Rated Voltage (V)	8.6
Temperature Rise (°C)	80 Max (rated current, 2 phase on)	Rated Current (A)	1.0
Ambient Temperature (°C)	-20 ~ +50	Resistance Per Phase ( $\pm 10\%$ $\Omega$ )	8.6
Number of Phase	2	Inductance Per Phase ( $\pm 20\%$ mH)	14
Insulation Resistance (M $\Omega$ )	100 Min (500VDC)	Holding Torque (N.cm)	135
Insulation Class	Class B		
Max. radial force (N)	75 (20mm from the flange)		
Max. axial force (N)	15		

● Wiring Diagram :

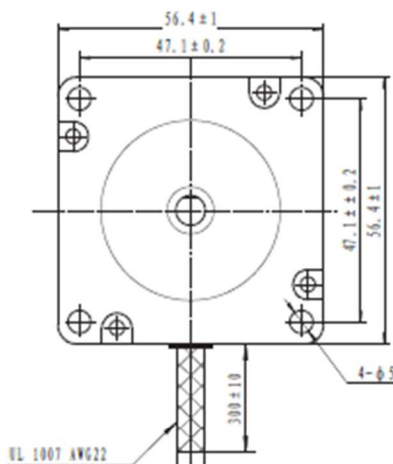
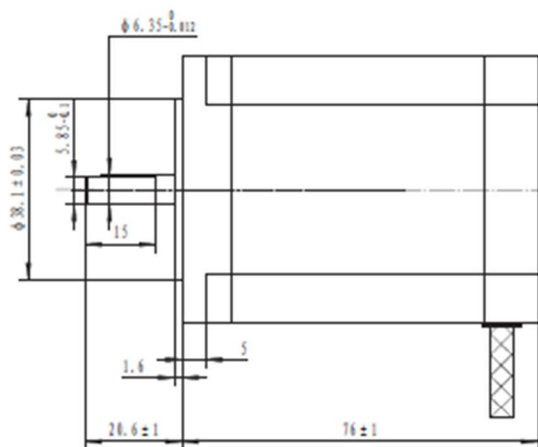


● Pull out torque curve :

VOLTAGE: 30VDC, CONSTANT CURRENT: 1.0A, HALF STEP



● Dimensions:  
(unit:mm)

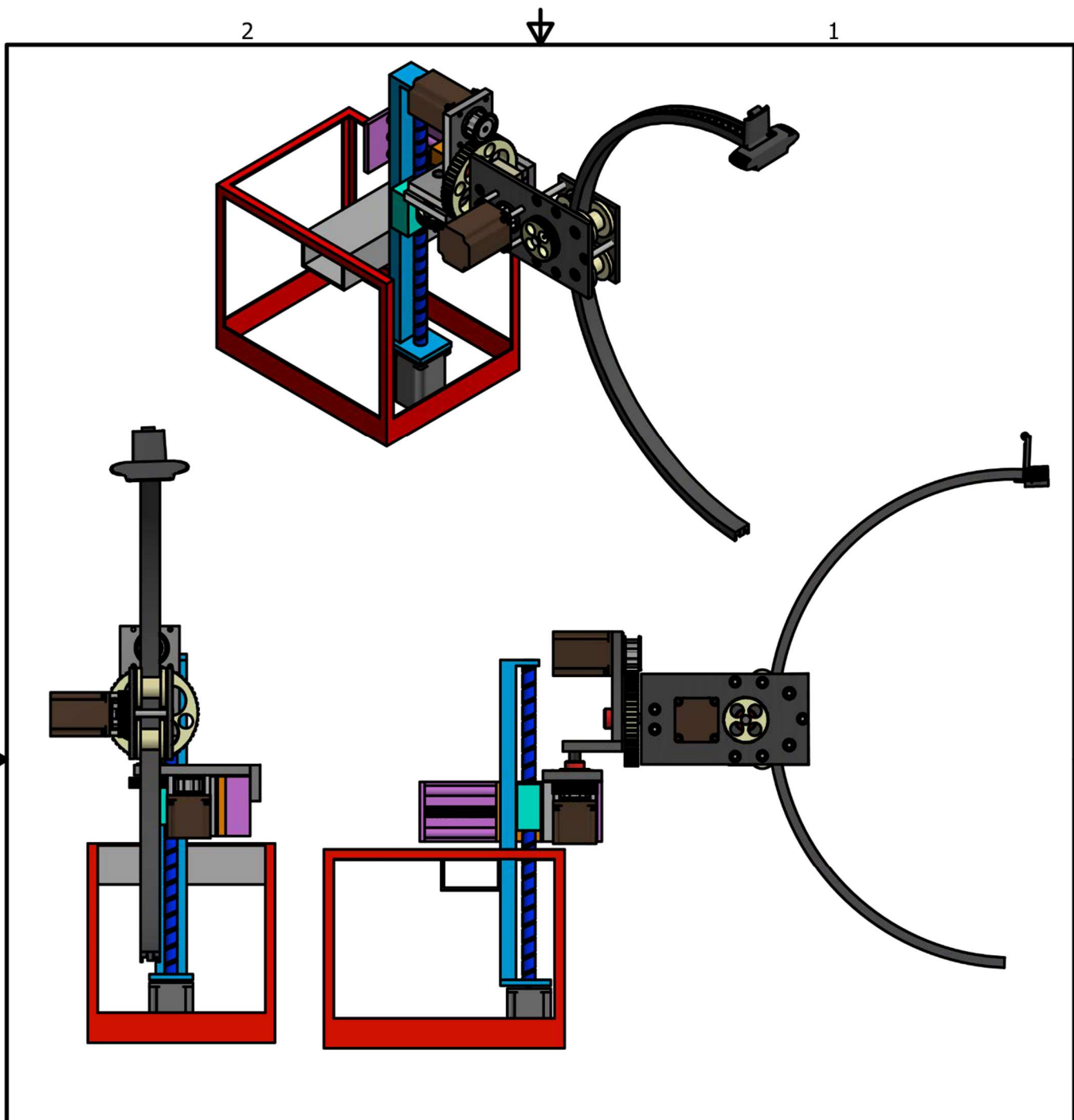


REV	REVISIONS	DESCRIPTION	BY	DATE	SY57STH76-1006A	TECHNICAL CONDITIONS
DRAW	2013/02/19					
CHECK						
APPROVE						

## Appendix F: C-Arm Prototype Engineering Drawings

Only important assembly views and those parts that were manufactured in the machine shop using CNC are included in this appendix. All dimensions are in inches.

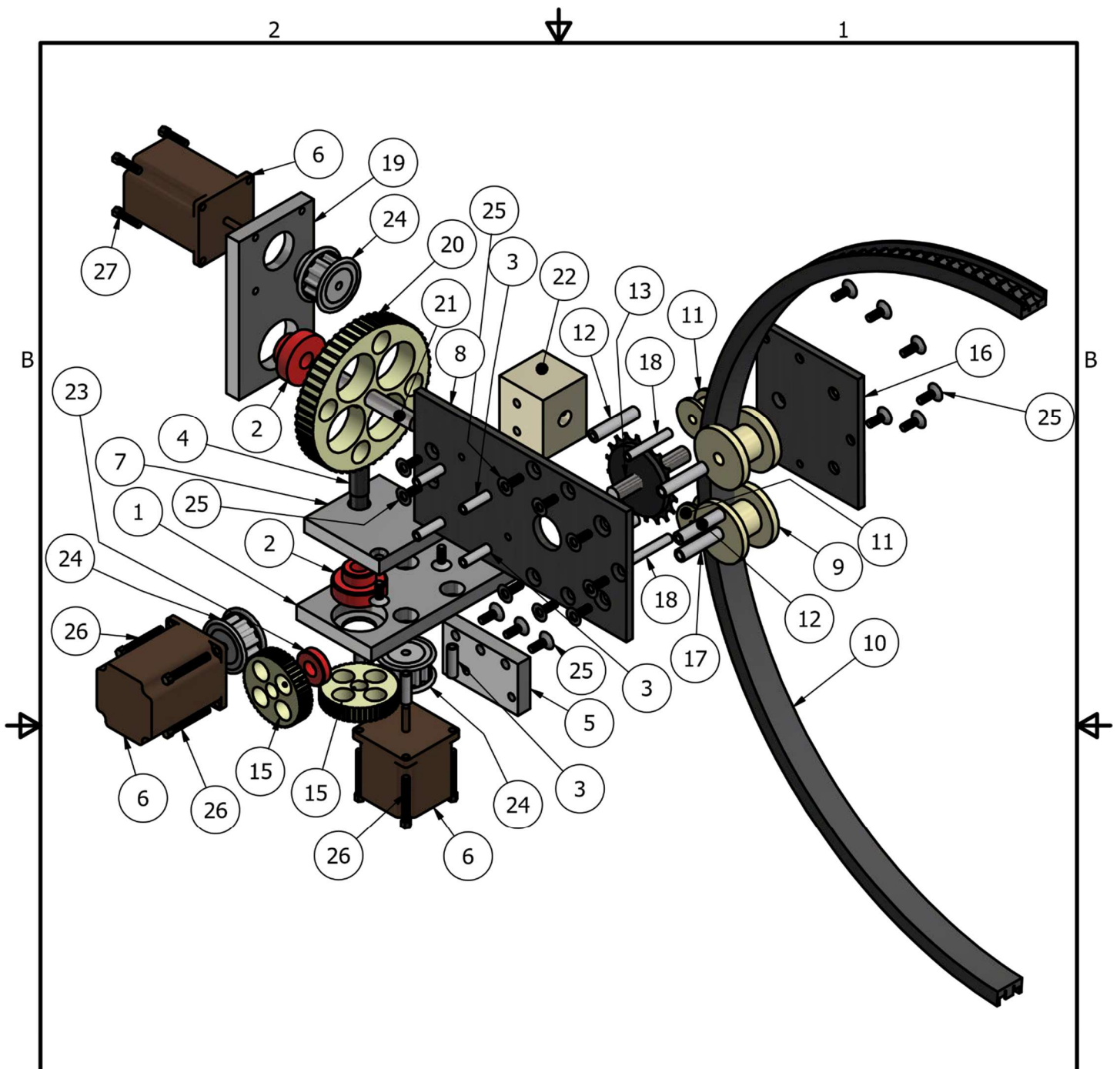
PARTS LIST			
ITEM	QTY	PART NUMBER	DESCRIPTION
1	1	Base Plate	needs to be machined
2	2	Axel Bearing	purchased standard bearing low rpm
3	8	Spacer-Stepper Motor	
4	1	Vertical Shaft	needs to be machined
5	1	Plate Mound	conects to liniar actuators
6	3	Stepper Motor	standard Nema 23
7	1	Spin Plate	
8	1	Large Side Plate	manufactured using CNC
9	2	Big Roller	3D printed
10	1	Orbital Link	performes orbital motion
11	2	Small Roller	3D printed
12	3	Plate Spacer	coneects plates firmly
13	1	Sproket Shaft	converts torque
14	1	Bicycle Sproket	2.5 inch pitch diameter
15	2	Pulley Sproket-Small	by 4th axis machining
16	1	Small Side Plate	manufactured using CNC
17	2	Big Roller Shaft	inserts into Big Roller
18	2	Small Roller Shaft	
19	1	Tilt Base	needs to be machined
20	1	Sproket Pulley - Large	3D printed or machined
21	1	Horizontal Shaft	needs to be strong
22	1	Conector Block	rechtengular prisim
23	1	Baring Orbital	bought standard part
24	1	Small Pulley	bought standard part
25	23	Cap Screw	1/2"-13 Flat Head
26	8	Stepper Motor Screw	1"
27	4	Stepper Motor Screw Short	3/4"



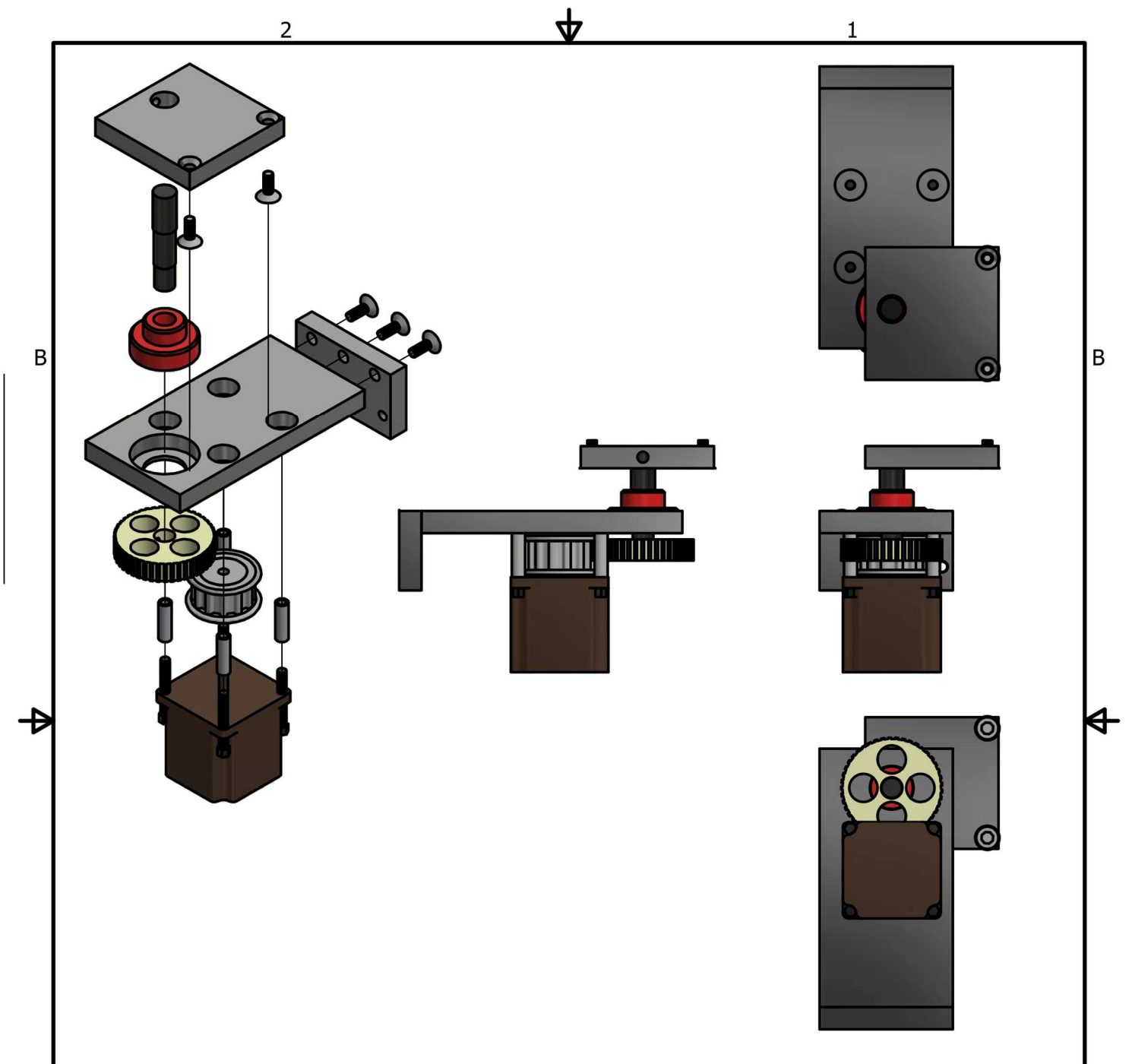
A	DRAWN	4/11/2019	University of Texas at Tyler COE			A
	Alireza Yazdanshenas					
	CHECKED		TITLE			
	QA		C-Arm Prototype Full Assembly			
	MFG					
APPROVED		SIZE	DWG NO	REV		
		A	C-Arm Prototype			
		SCALE	1/7	SHEET 1 OF 1		

2

1

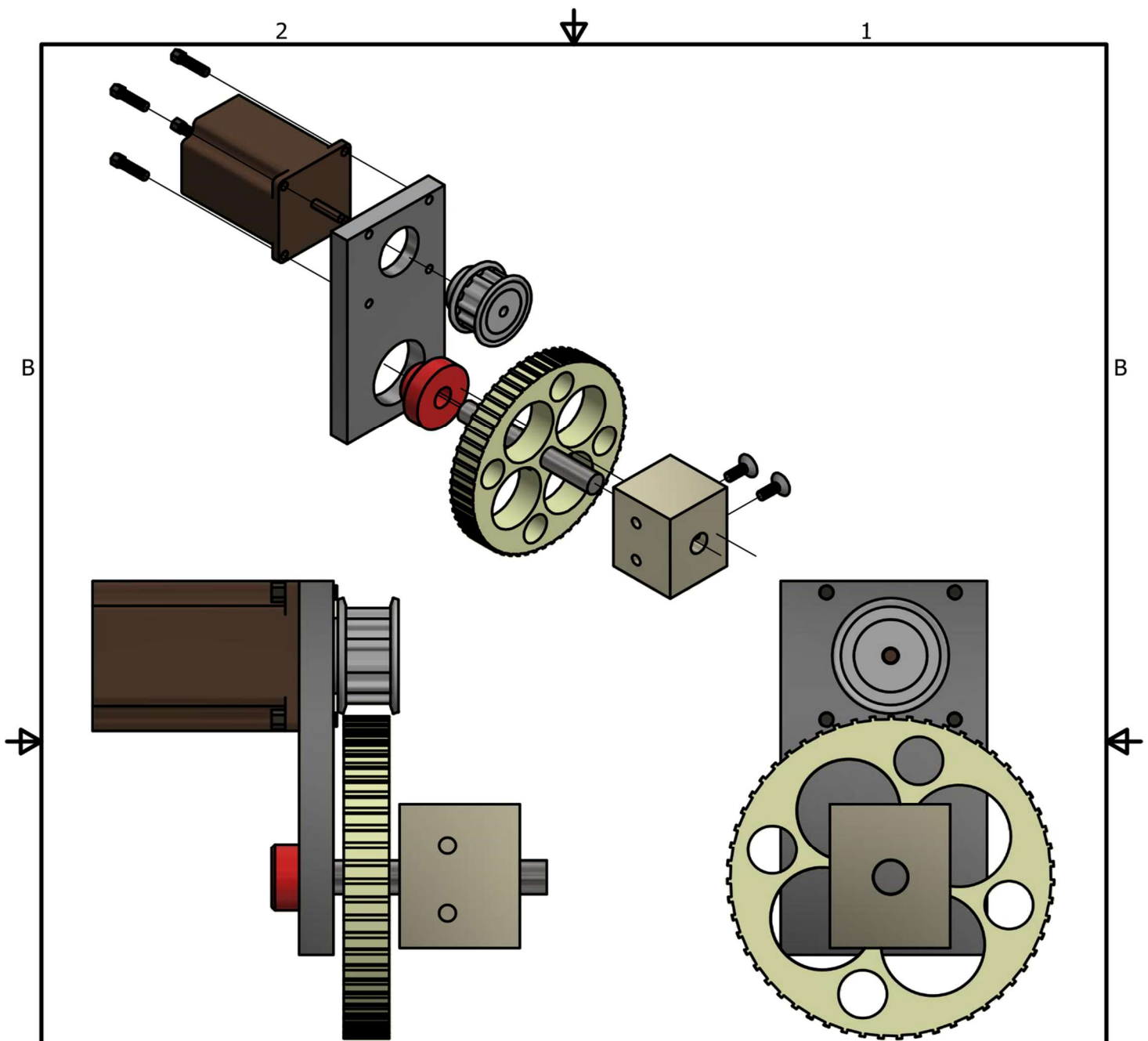


A	DRAWN	Alireza Yazdanshenas	4/12/2019	University of Texas at Tyler COE			A
	CHECKED			TITLE			
	QA			C-Arm Custom Parts			
	MFG			SIZE			
	APPROVED			DWG NO			
				A	C-Arm Custom Parts Color	REV	
				SCALE	1/3.8	SHEET 1 OF 2	

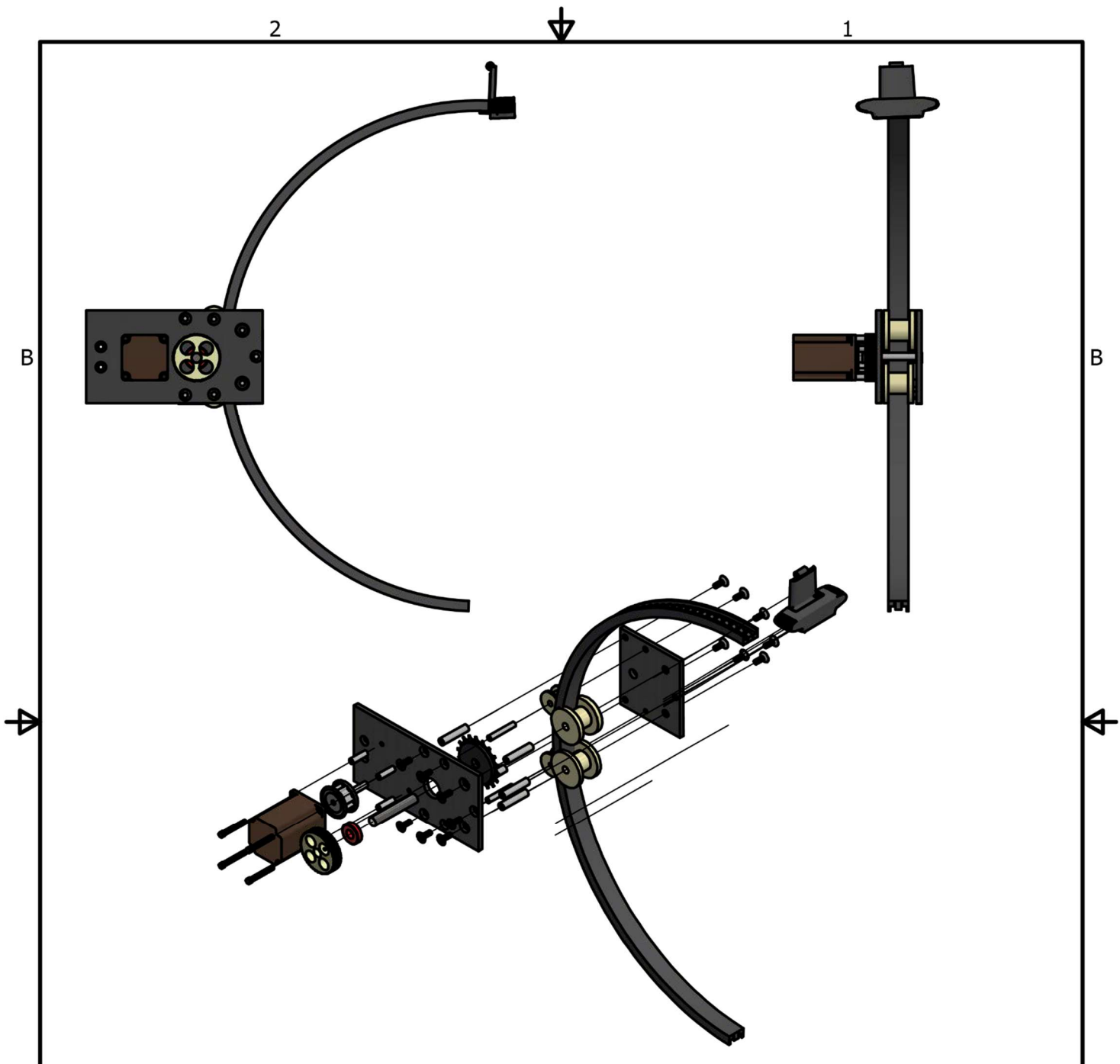


A	DRAWN	Alireza Yazdanshenas	4/12/2019	University of Texas at Tyler COE		
	CHECKED					
	QA			TITLE Wig Wag Mechanism		
	MFG					
	APPROVED					
	SIZE	A	DWG NO	WigWag Mechanism Color View	REV	
	SCALE	1 / 3	SHEET 1 OF 1			





A	DRAWN	Alireza Yazdanshenas	4/12/2019	University of Texas at Tyler COE			A		
	CHECKED			TITLE					
	QA			Tilt Mechanism					
	MFG								
	APPROVED								
				SIZE	A	DWG NO	Tilt Mechanism Color View	REV	
				SCALE	1/3	SHEET 1 OF 1			

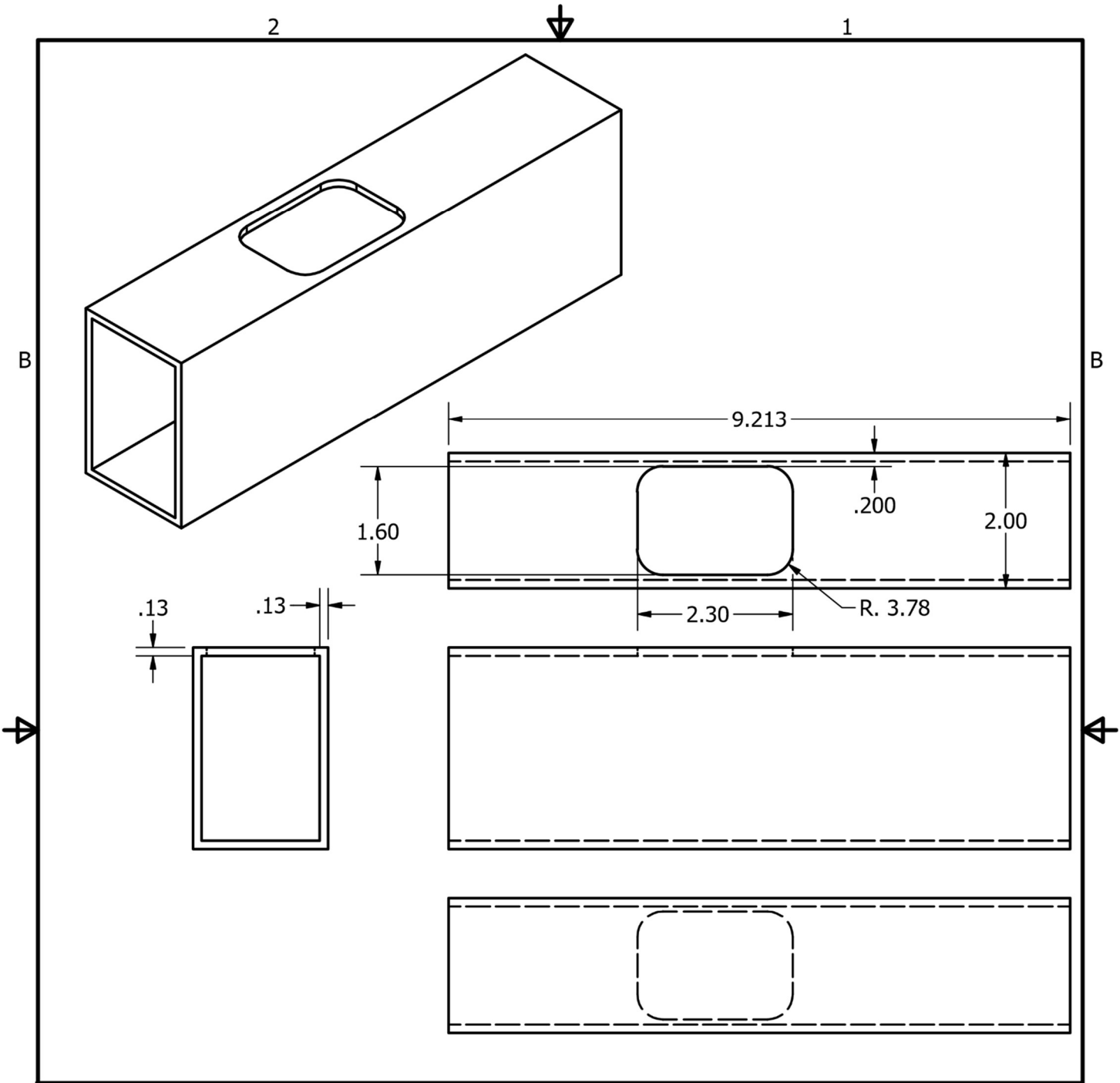


A	DRAWN	Alireza Yazdanshenas	4/11/2019	University of Texas at Tyler COE			A
	CHECKED						
	QA	TITLE					
	MFG	Orbital Mechanism					
	APPROVED						
		SIZE		DWG NO		REV	
		A		Orbital Mechanism			
		SCALE	1/6.5	SHEET 1 OF 2			

2

1

1

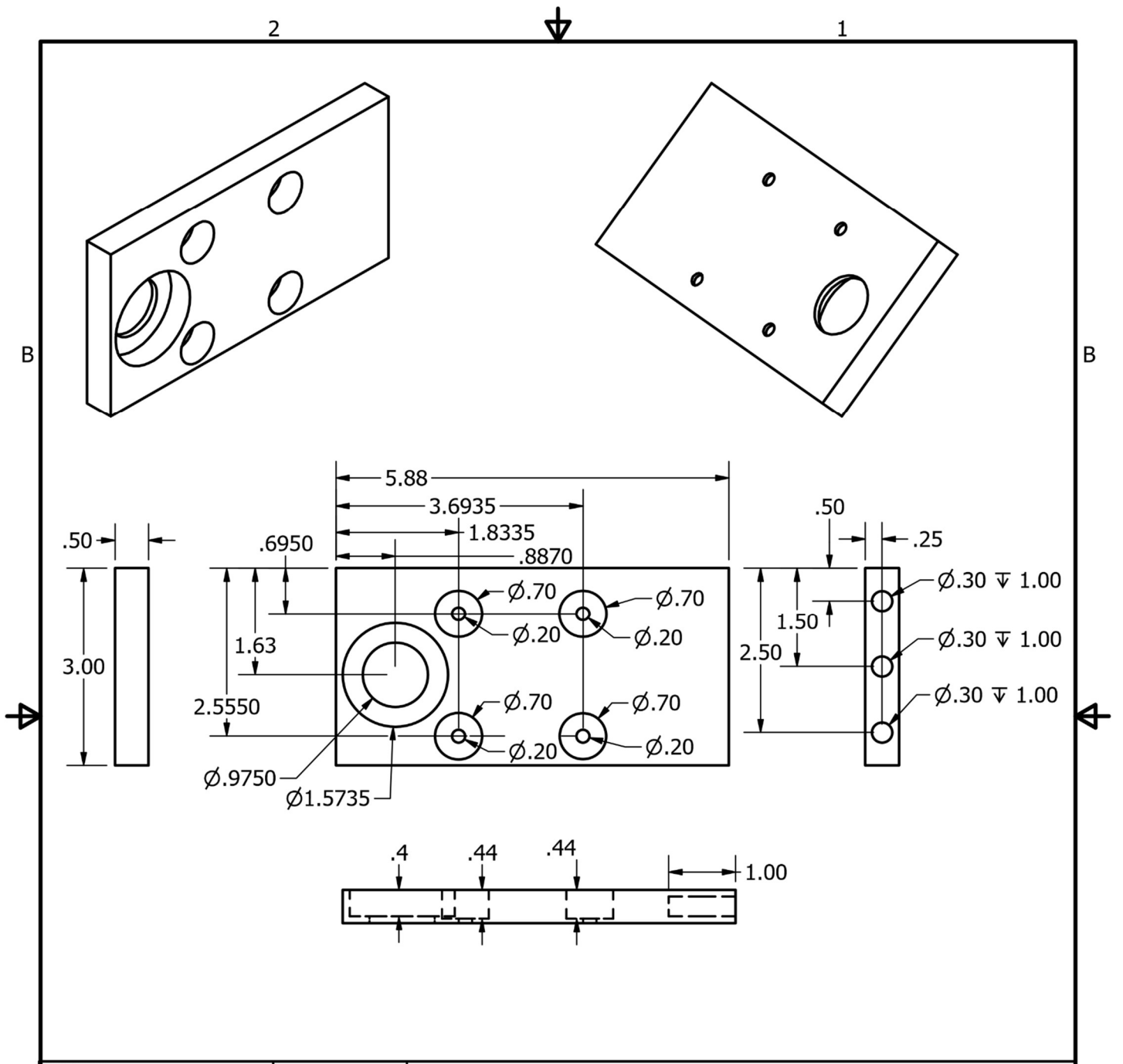


A	DRAWN	4/10/2019	University of Texas at Tyler COE		
	Alireza Yazdanshenas				
	CHECKED		TITLE		
	QA		Base Frame		
	MFG				
	APPROVED				
			SIZE	DWG NO	REV
			A	Zero	
			SCALE	1/2	SHEET 1 OF 1

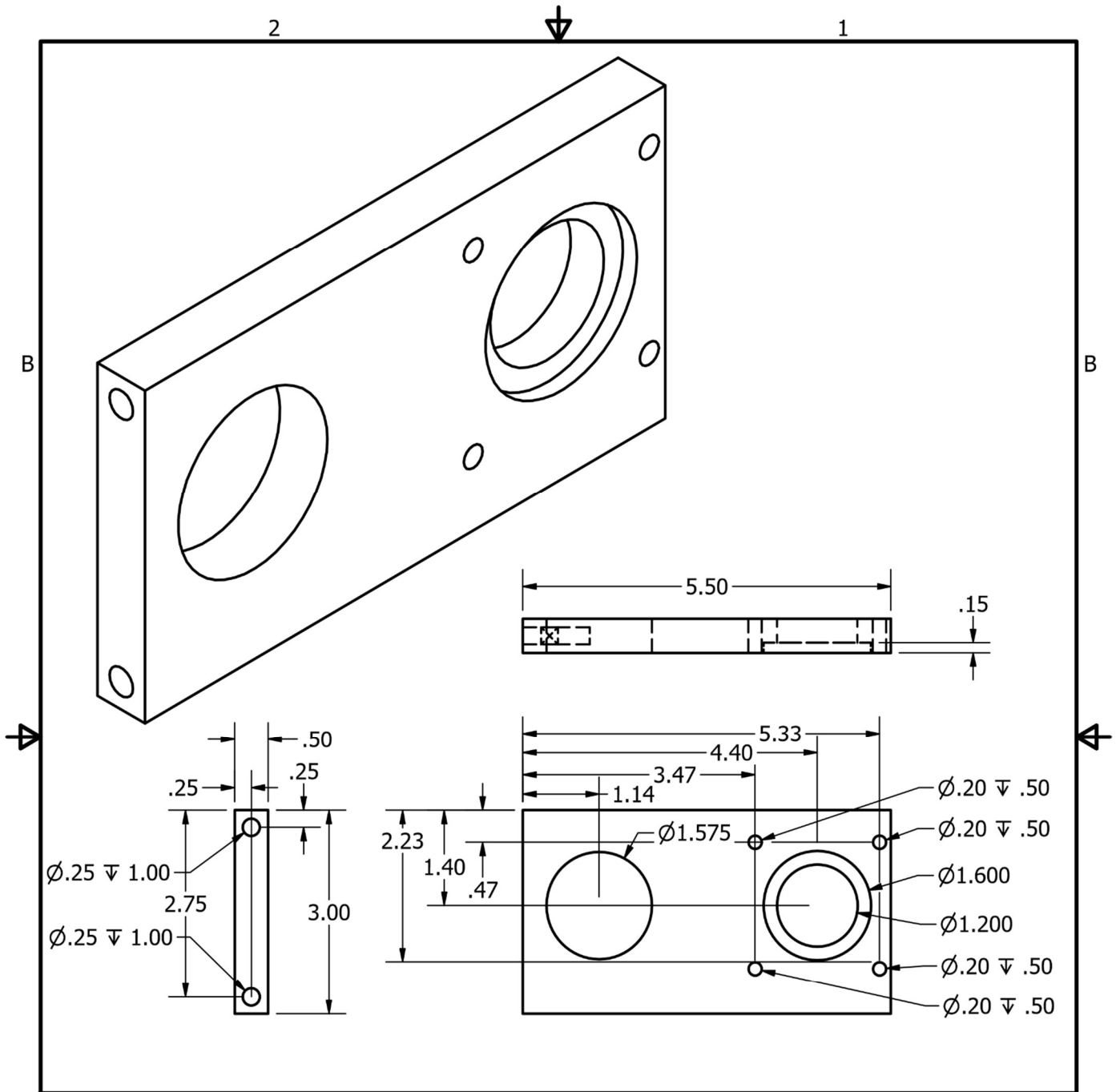
2



1



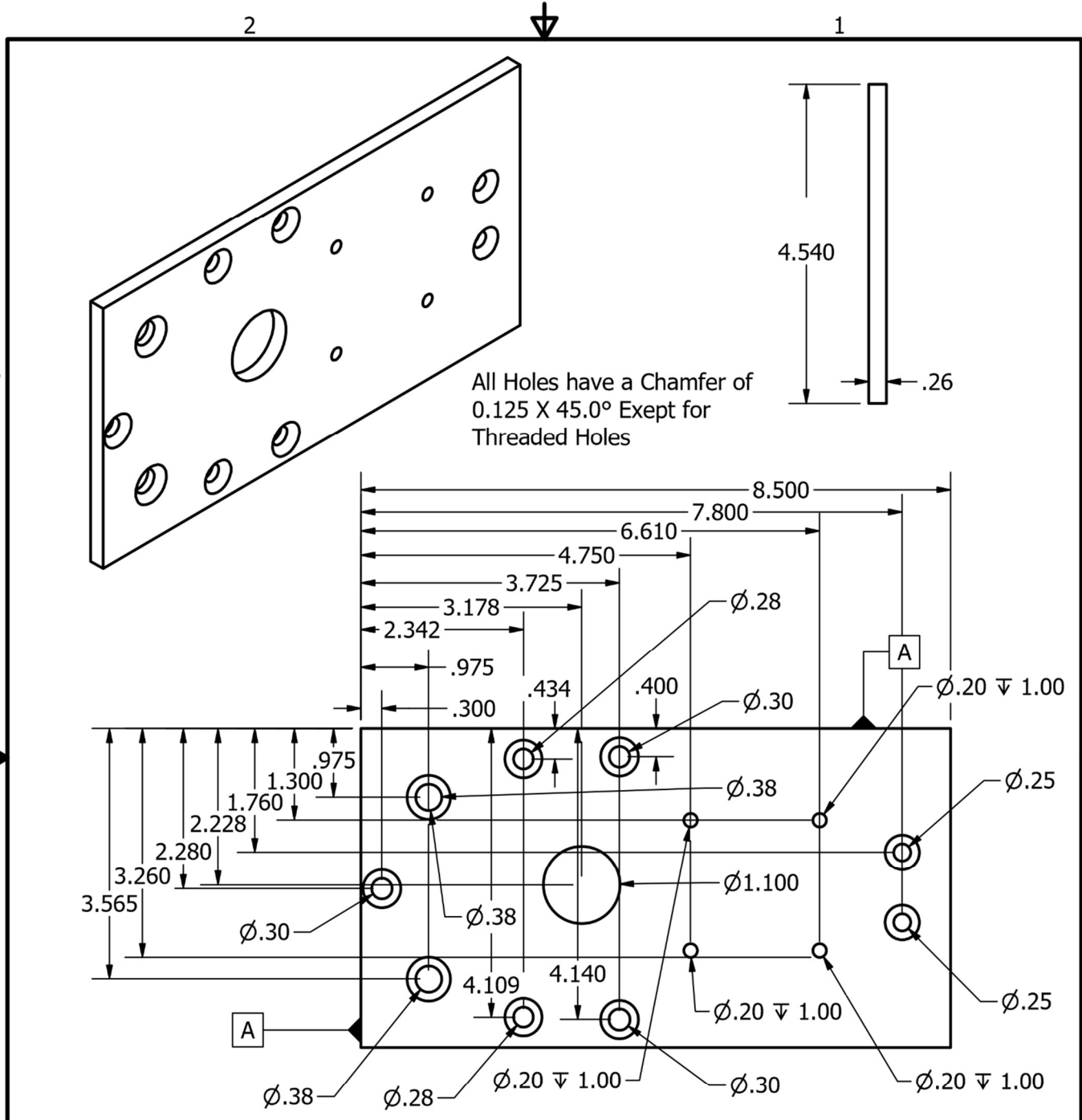
A	DRAWN	4/10/2019	University of Texas at Tyler COE		
	CHECKED				
	QA		TITLE		
	MFG		Base Plate		
	APPROVED		SIZE	DWG NO	REV
	A	1			
	SCALE	1 / 2	SHEET 1 OF 1		



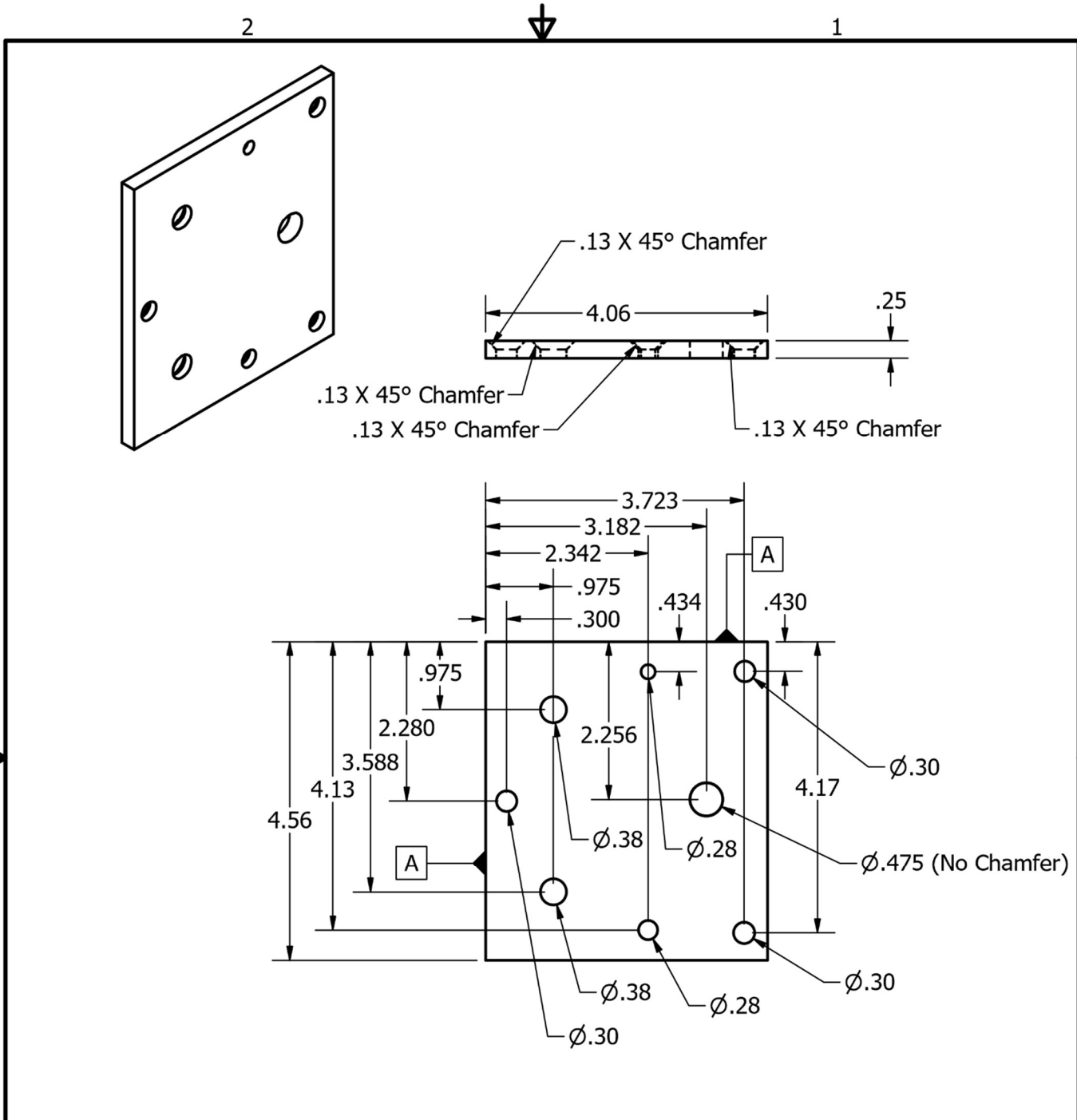
A	DRAWN	Alireza Yazdanshenas	4/10/2019	University of Texas at Tyler COE		
	CHECKED					
	QA			TITLE		
	MFG			Tilt Base		
	APPROVED			SIZE	DWG NO	REV
			A	19		
			SCALE	1 : 1	SHEET 1 OF 1	

2

1



DRAWN	Alireza Yazdanshenas	4/11/2019	University of Texas at Tyler COE		
	CHECKED				
QA			TITLE		
MFG			Large Side Plate		
APPROVED					
			SIZE	DWG NO	REV
			A	8	
			SCALE	SHEET 1 OF 1	
			1 / 2		



A	DRAWN	Alireza Yazdanshenas	4/11/2019	University of Texas at Tyler COE			A
	CHECKED						
	QA			TITLE			
	MFG			Small Side Plate			
	APPROVED						
				SIZE	DWG NO	REV	
				A	16		
				SCALE	1 / 2	SHEET 1 OF 1	